JOURNAL OF MASS SPECTROMETRY
J. Mass Spectrom. 2008; **43**: 1581–1617
Published online 14 October 2008 in Wiley InterScience
(www.interscience.wiley.com) DOI: 10.1002/jms.1480

JMS

SPECIAL FEATURE: PERSPECTIVE

Analysis of flavonoids: Tandem mass spectrometry, computational methods, and NMR

Raymond March[a]* and Jennifer Brodbelt[b]

[a] Department of Chemistry, Trent University, Ontario, Canada
[b] Department of Chemistry, University of Texas, Texas, USA

Received 18 March 2008; Accepted 9 July 2008

Due to the increasing understanding of the health benefits and chemopreventive properties of flavonoids, there continues to be significant effort dedicated to improved analytical methods for characterizing the structures of flavonoids and monitoring their levels in fruits and vegetables, as well as developing new approaches for mapping the interactions of flavonoids with biological molecules. Tandem mass spectrometry (MS/MS), particularly in conjunction with liquid chromatography (LC), is the dominant technique that has been pursued for elucidation of flavonoids. Metal complexation strategies have proven to be especially promising for enhancing the ionization of flavonoids and yielding key diagnostic product ions for differentiation of isomers. Of particular value is the addition of a chromophoric ligand to allow the application of infrared (IR) multiphoton dissociation as an alternative to collision-induced dissociation (CID) for the differentiation of isomers. CID, including energy-resolved methods, and nuclear magnetic resonance (NMR) have also been utilized widely for structural characterization of numerous classes of flavonoids and development of structure/activity relationships.

The gas-phase ion chemistry of flavonoids is an active area of research particularly when combined with accurate mass measurement for distinguishing between isobaric ions. Applications of a variety of *ab initio* and chemical computation methods to the study of flavonoids have been reported, and the results of computations of ion and molecular structures have been shown together with computations of atomic charges and ion fragmentation. Unambiguous ion structures are obtained rarely using MS alone. Thus, it is necessary to combine MS with spectroscopic techniques such as ultraviolet (UV) and NMR to achieve this objective. The application of NMR data to the mass spectrometric examination of flavonoids is discussed.

Supporting information may be found in the online version of this article.

KEYWORDS: flavonoids; flavonoid glycosides; metal complexation; tandem mass spectrometry; electrospray ionization; chemical computation; nuclear magnetic resonance spectroscopy

INTRODUCTION

Every one of the thousands of members of the class of phytochemicals known as flavonoid[1] possesses a basic C_{15} phenyl-benzopyrone skeleton modified with differing numbers and positions of substituents, including hydroxyl, methoxyl, and glycosyl groups. Glycosidic moieties are attached *via* either an O atom (–*O*–) or a skeletal C atom (–*C*–). The enormous array of unique structures, many of which are isomers, poses an important analytical challenge, especially given that the biological activities and chemopreventive properties of flavonoids correlate with specific structural features. The study of the flavonoids has been confined largely to their distribution in the plant kingdom, elucidation of their structures, and the pathways by which they are synthesized. Flavonoids are found primarily in petals, the foliage of trees and bushes, and are distributed widely in the edible parts of plants. Plants synthesize flavonoids and secondary metabolites for protection against pathogens and herbivores. It has been estimated that of the approximately 10^9 tons of growth each year, roughly 2% is due to the formation of flavonoids. The predominant form of naturally occurring flavonoids in plants is that of a flavonoid glycoside. Flavonoids and isoflavonoids may be of ecotoxicological importance because they are present in the heartwood of tree species used for wood pulp[2,3] and are found in a variety of fruits and vegetables. Flavonoids are of environmental significance because several

*Correspondence to: Raymond March, Department of Chemistry, Trent University, Ontario, Canada. E-mail: rmarch@trentu.ca

JMS

flavonoid aglycons (flavonoid glycosides that have lost the sugar or glycan moiety) are known to be biologically active[4] while some isoflavones are also phytoestrogens[5,6] that have radical scavenger[7,8] and anticarcinogenic[9,10] activities. Because of their antioxidant and anticancer properties flavonoids present in foodstuffs, herbal medicines,[11] and preventative therapeutics[9] have received much attention recently. Various biological activities of polyphenols such as antioxidative activity, free radical scavenging capacity, coronary heart disease prevention and anticancer activity have been studied extensively.[12,13]

Within the past few years, it has become clear that flavonoids are now in the public purview principally through their association with the Mediterranean diet. In response to enhanced public interest in heart-healthy eating plans, the Mediterranean diet that incorporates olive oil, red wine, vegetables, fruit, and other characteristic components of the traditional cooking style of countries bordering the Mediterranean Sea, has been promoted. The advocacy of red wine consumption is based on the flavonoids contained therein and their antioxidant properties.[14,15]

The general structure of this review is an examination of the metal complexation of flavonoids, chemistry of flavonoids, and of mass spectrometric analytical methods that have been developed for the determination of flavonoids and flavonoid glycosides. Complementary to mass spectrometric determinations is the utilization of nuclear magnetic resonance (NMR) spectrometry for structure determination. The enormous task of compiling NMR data for the flavonoids has, perhaps, been simplified modestly by the development of a predictive tool for assessing ^{13}C NMR chemical shifts of flavonoids. Cuyckens and Claeys have recently reviewed the role of mass spectrometry (MS) in the structural analysis of flavonoids.[16]

Flavonoid is a collective noun given to several classes of structurally similar, naturally occurring compounds. The major classes are flavones, isoflavones, flavans, anthocyanins, proanthcyanidins, flavanones, chalcones, and aurones; the basic structures of flavanones, flavones, and isoflavones are shown in Scheme 1.

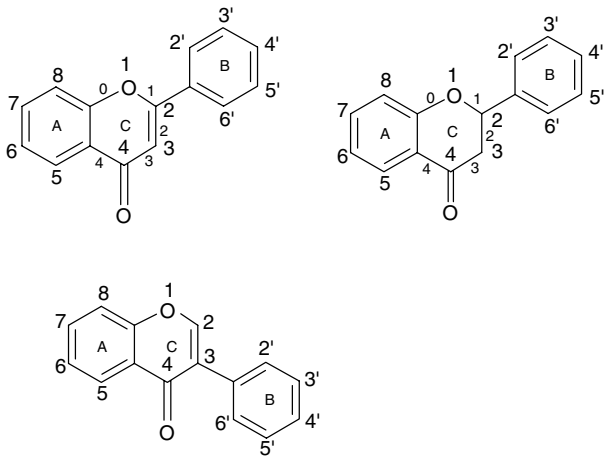

Scheme 1. Structures and numbering schemes: (a) flavones; (b) flavanones; and (c) isoflavones.

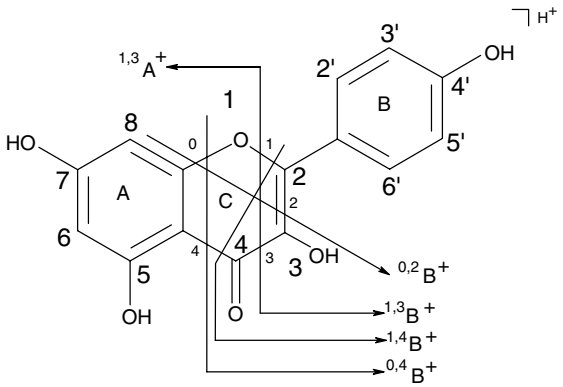

Scheme 2. Structure of protonated kaempferol, nomenclature and principal fragmentations.

A systematic ion nomenclature for flavonoid aglycons has been proposed[17] that is conceptually similar to that introduced for the description of carbohydrate fragmentations in product ion mass spectra of glycoconjugates.[18] This nomenclature is illustrated in Scheme 2 with reference to the fragmentation of protonated kaempferol.

A wide range of flavonoids and flavonoid glycosides are discussed here, and a number of representative structures are shown in Fig. 1. In the tandem mass spectrometric examination of protonated, metal complexed, and deprotonated flavonoid glycoside molecules, many types of product ions can be formed. While the systematic ion nomenclature shown in Scheme 1 is adequate for the identification of product ions from flavonoid aglycons (without added sugar), an additional form of nomenclature is required for the identification of product ions from flavonoid glycosides. The additional nomenclature, illustrated in Scheme 3, was proposed by Domon and Costello[18] and adapted by Claeys and coworkers.[19]

METAL COMPLEXATION OF FLAVONOIDS FOR STRUCTURAL CHARACTERIZATION

Collision-induced dissociation (CID) has proven to be the most important tool for the elucidation of flavonoid structures. CID of deprotonated flavonoids has been reported for a variety of applications and has been successful for providing key information about the basic flavonoid skeletons.[16,17,20–36] As CID of deprotonated flavonoid glycosides results primarily in loss of the attached sugars, product ion mass spectra may not permit differentiation of groups of isomers.

A common fragmentation process of the deprotonated molecule, $[M - H]^-$, of a flavonoid glycoside is the loss of the glycan residue (162 Da for a flavonoid glucoside) to form the Y_o^- ion. Hvattum reported the observation from $[M - H]^-$ (m/z 447) of quercitrin (5,7,3′,4′-tetrahydroxyflavone-3-*O*-rhamnose) of the aglycone fragment (Y_o^-) at m/z 301 and the radical aglycone anion $(Y_o - H)^{-\bullet}$ at m/z 300.[37] Subsequently, Hvattum and Ekeberg[29] reported on the ability of flavonoid glycosides to generate both negative ion collision-induced heterolytic and homolytic cleavage. The relative abundance ratio of the radical aglycone to the aglycone product ion increased with increasing collision

DOI: 10.1002/jms

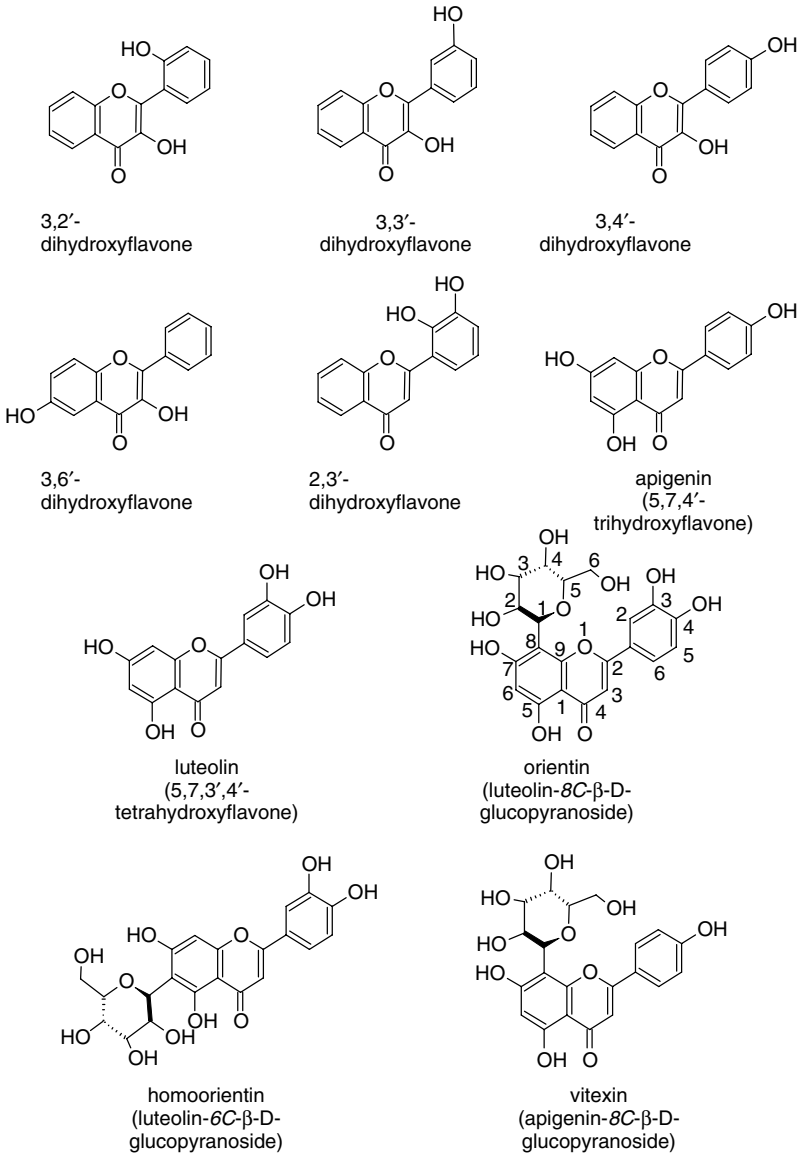

Figure 1. Structures of some of the flavonoids discussed in this review. The numbering scheme is shown for orientin.

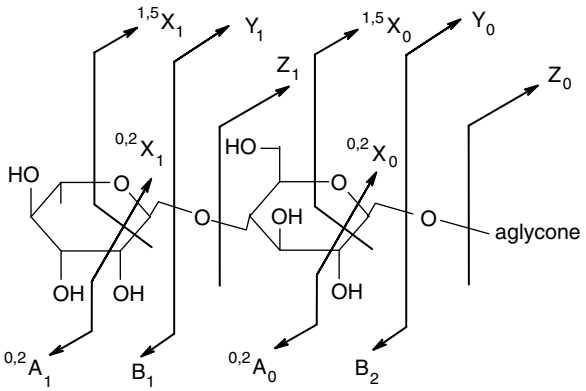

Scheme 3. Carbohydrate ion nomenclature according to Domon and Costello (Ref. 18) and adapted by Claeys and coworkers (Ref. 17).

energy and with the degree of hydroxylation in the B-ring. Furthermore, the nature and position of flavonoid glycosylation affected fragmentation to the radical aglycone. For genistein-7-*O*-glucoside, the intensity ratio of the $(Y_o - H)^{-\bullet}$: Y_o^- ions increases with collision energy.[38]

Protonated flavonoids generally afford more distinctive fragmentation patterns than do deprotonated flavonoids, but the ionization efficiencies of flavonoids in the positive mode are often rather low because flavonoids are acidic, not basic, compounds. Metal complexation is an alternative ionization mode which has been explored extensively in the past decade for analysis of flavonoids.[39–52] Implementation of metal complexation is straightforward: a metal salt is added to a flavonoid solution prior to electrospray ionization (ESI). Metal complexation results typically in larger ion abundances than those obtained upon protonation or deprotonation of flavonoids, thus enhancing detection sensitivity, in addition to yielding a greater number of structurally diagnostic product ions upon CID. Absolute ion abundances and the resulting dissociation patterns of the flavonoids can be enhanced further by incorporation of an auxiliary chelating ligand into the complexes. This latter approach is accomplished by addition of an auxiliary

DOI: 10.1002/jms

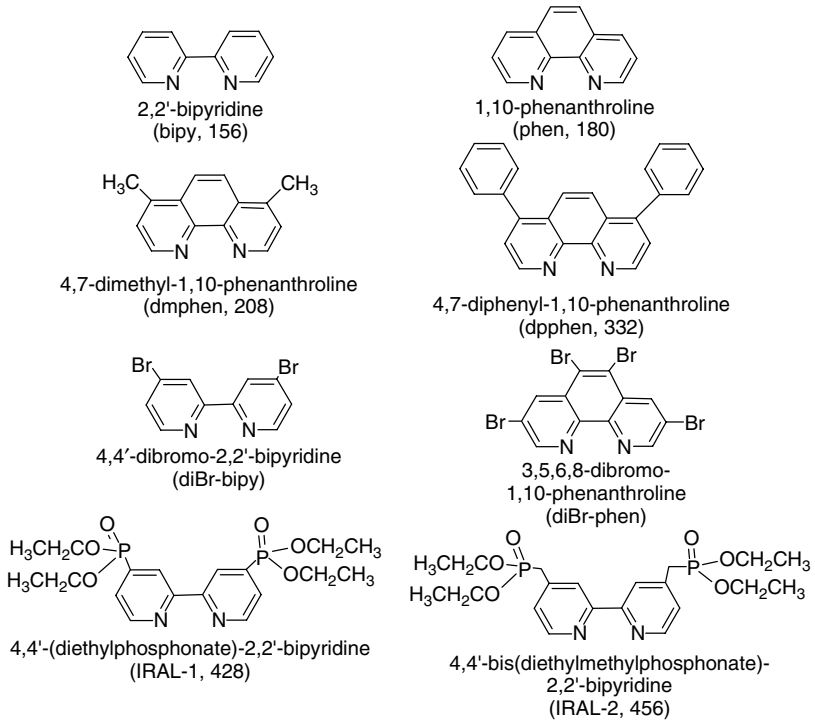

Figure 2. Structures of auxiliary chelating ligands (molecular weight).

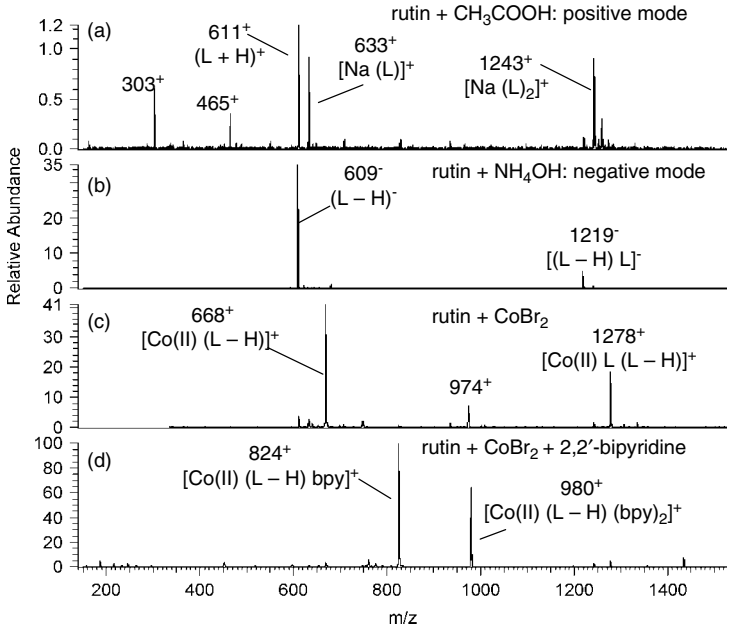

Figure 3. Electrospray ionization mass spectra of rutin obtained in four ionization modes. (a) Positive mode upon addition of acetic acid, (b) negative mode upon addition of ammonium hydroxide, (c) cobalt complexation upon addition of CoBr2 and (d) cobalt complexation with the auxiliary ligand, 2,2′-bipyridine. The vertical scales reflect the relative abundances (Ref. 39).

ligand to the flavonoid/metal salt solution prior to ESI-MS. The ease of varying the metal (e.g. Co, Ni, Cu, Mg, Ca, Ag, Al) and the auxiliary ligand (e.g. 2,2′-bipyridine, 1,10-phenanthroline, etc.; refer Fig. 2) affords a great degree of 'tunability' for this ionization strategy, in the sense that both the ion abundances and the nature of the CID patterns vary as a function of the metal and auxiliary ligand. A variety of examples of the metal complexation approach and its application for the elucidation of flavonoid structures and differentiation of isomers is described in the following sections.

A comparison of the types and relative abundances of ions generated from four ESI modes is shown in Fig. 3 for rutin, a flavone.[39] In positive ESI mode, both protonated and sodium-cationized species are observed with relatively modest abundances (Fig. 3(a)). Deprotonated rutin is the dominant ion detected in the negative ESI mode (Fig. 3(b)) with significantly greater signal-to-noise than observed

DOI: 10.1002/jms

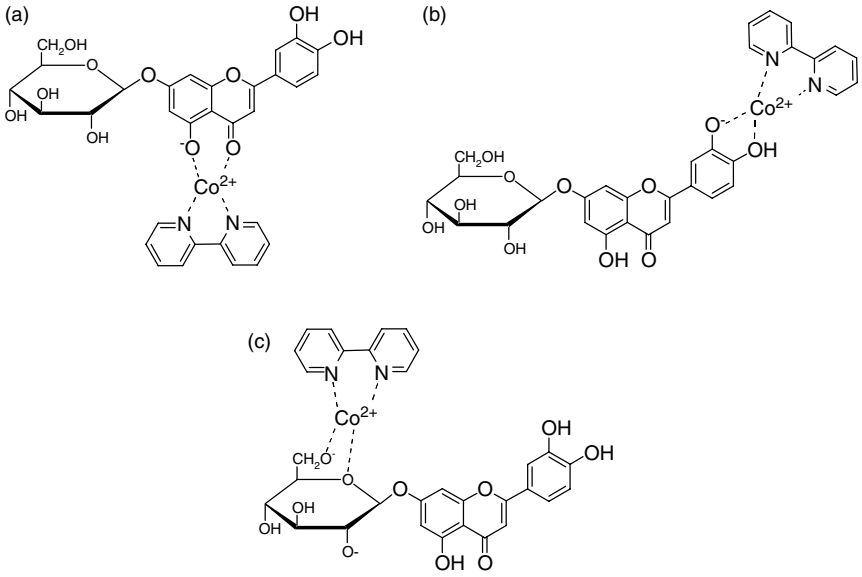

Figure 4. Proposed structures for [Co(II) (L − H) bpy]+ complexes (Ref. 42).

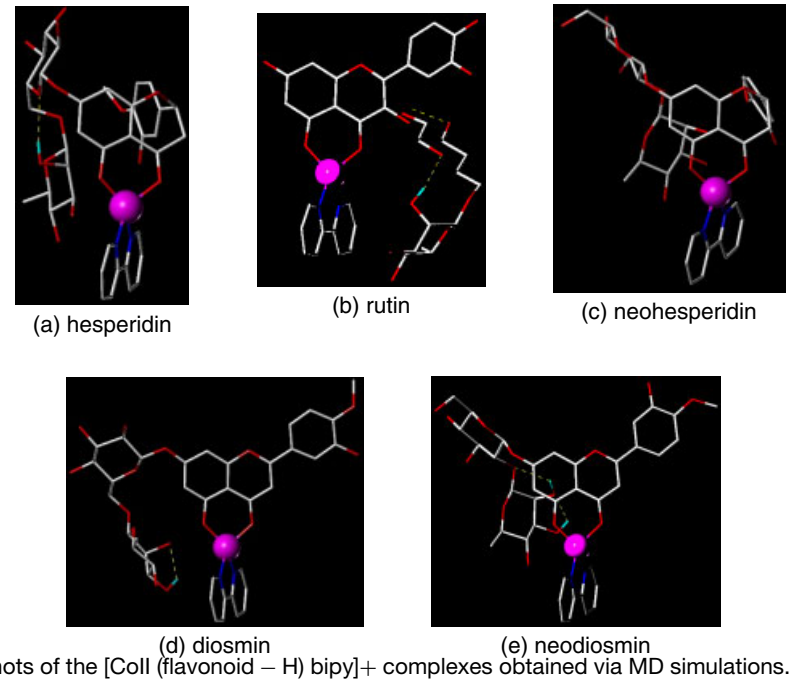

Figure 5. The last snapshots of the [CoII (flavonoid − H) bipy]+ complexes obtained via MD simulations. Hydrogen bonds are shown as dashed lines and cobalt is shown as a ball (Ref. 44).

in the positive ESI mass spectrum. Addition of $CoBr_2$ to the rutin solution (with the metal salt and flavonoid at approximately equimolar concentrations) leads to the formation of singly charged metal complexes containing one metal and a deprotonated flavonoid, $[Co(II) + (rutin - H)]^+$, or one metal and both a deprotonated flavonoid and a neutral flavonoid, $[Co(II) + (rutin - H) + rutin]^+$ (Fig. 3(c)). Upon addition of an auxiliary chelating ligand to the solution, singly charged complexes containing a metal, a deprotonated flavonoid, and the auxiliary ligand, [Co(II) + (flavonoid − H) + 2, 2-bipyridine]$^+$, are detected (Fig. 3(d)). Ion abundances are greatest for this last spectrum in Fig. 3, and this trend in the types of complexes and their relative abundances is similar for solutions containing other flavonoids, other metals, and other auxiliary ligands. As evident in Fig. 3(c) and (d), the ESI mass spectra are easy to interpret and relatively simple, and the dominant metal complexes have abundances that make them amenable to subsequent characterization by CID.

Metal complexes of the type [M(II) + (flavonoid − H) + 2, 2′-bipyridine]$^+$ have proven to be the most versatile for characterization of flavonoid structures, as detailed *via* various examples described later in this review.[39–42,44,47–51] Possible structures for the [Co(II) + (flavonoid − H) + 2, 2-bipyridine] complexes are shown in Fig. 4, with several arrangements shown to illustrate different possible coordination sites that may occur under different

DOI: 10.1002/jms

JMS

ESI and CID conditions. Energy-minimized structures calculated from molecular dynamics simulations are shown in Fig. 5 for five flavonoids.[44] All the structures obtained from the molecular modeling show the metal ion coordinated to the ketone group and adjacent deprotonated phenolic oxygen (5-OH position) of the flavonoid aglycone. The most favorable coordination geometry of the complexes has a plane-angle of about 62°, which means that the deprotonated flavonoid and 2,2′-bipyridine do not reside in the same plane. Moreover, the disaccharide folds toward the metal ion that is chelated by oxygen atoms on the A- and C-rings for several of the flavonoid complexes, a feature most pronounced for the rutinoside flavonoids. Flavanones generally are predicted to form more compact complexes than the corresponding flavones because the flavanones have a flexible single bond rather than a double bond between C2 and C3. Although the molecular modeling specifically supports the proposed structure shown in Fig. 4(a), those in Fig. 4(b) and (c), in which the metal is coordinated to the B-ring or the disaccharide group, are alternatives that may be produced upon ESI, or may occur especially upon rearrangement of the energy-minimized structures during subsequent energization in CID experiments.

Differences in the CID patterns due to the nature of the precursor ions (i.e. deprotonated flavonoids versus metal complexes) are illustrated in Figs 6 and 7 for three isomers: hesperidin, neohesperidin, and rutin (all of molecular weight 610).[40] A single dominant product ion (m/z 301) is observed from the CID of the deprotonated flavonoids due to the loss of the disaccharide part. In contrast,

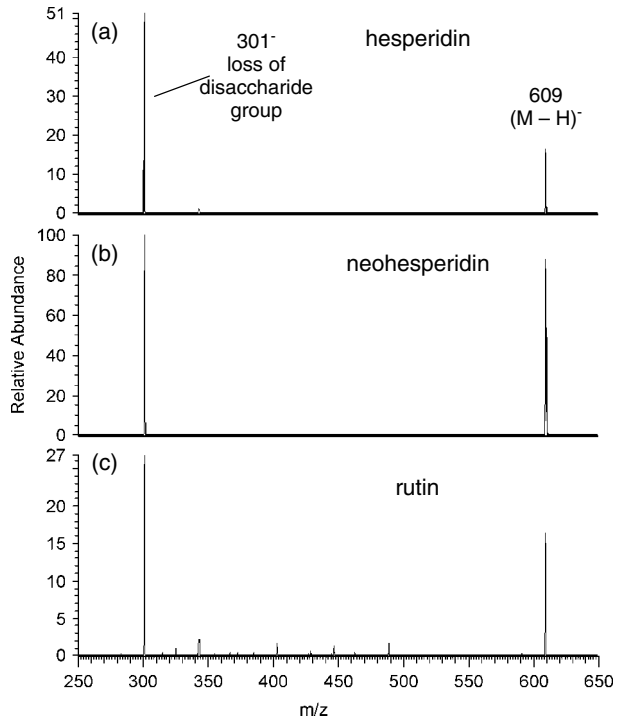

Figure 6. CID mass spectra of three deprotonated flavonoids: (a) Hesperidin, (b) neohesperidin, and (c) rutin.

CID of the cobalt complexes, $[(\mathrm{Co(II)} + (\mathrm{flavonoid} - \mathrm{H}) + 2,2\text{-bipyridine}]^+$, yields a greater array of product ions. In general, there are four dominant fragmentation pathways of the flavonoid diglycoside complexes: loss of a single

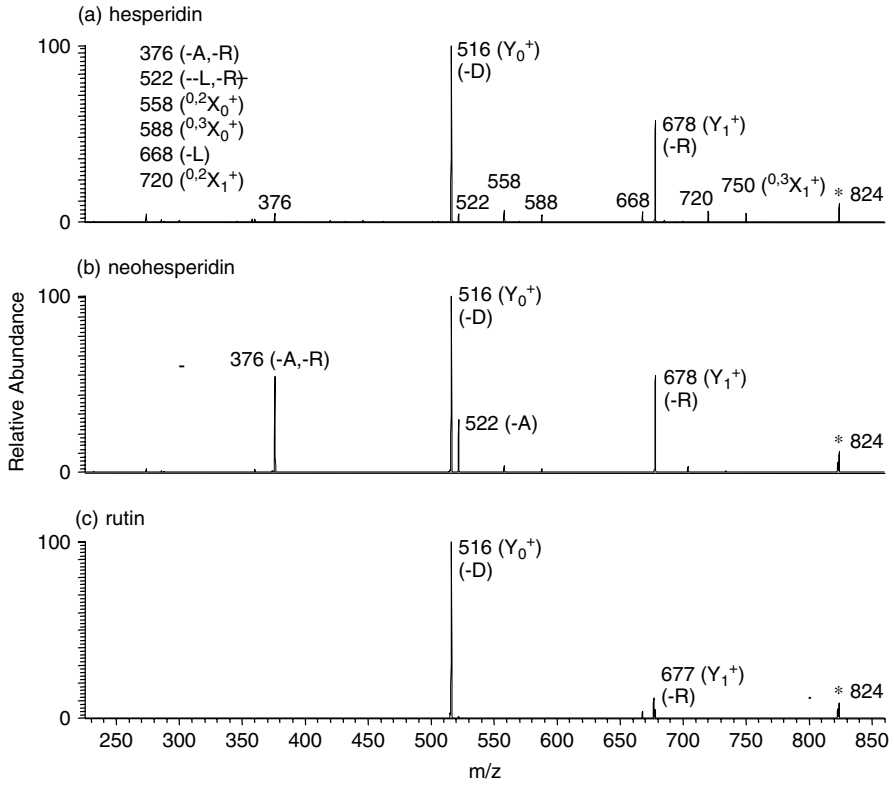

Figure 7. Representative CID mass spectra of the [CoII (L − H) bipy]+ complexes of hesperidin, neohesperidin, and rutin. The parent complex ions are labeled with asterisks. The loss of the aglycon portion is indicated by −A, the loss of the rhamnose residue is indicated by −R, and the loss of the disaccharide moeity is indicated by −D.

DOI: 10.1002/jms

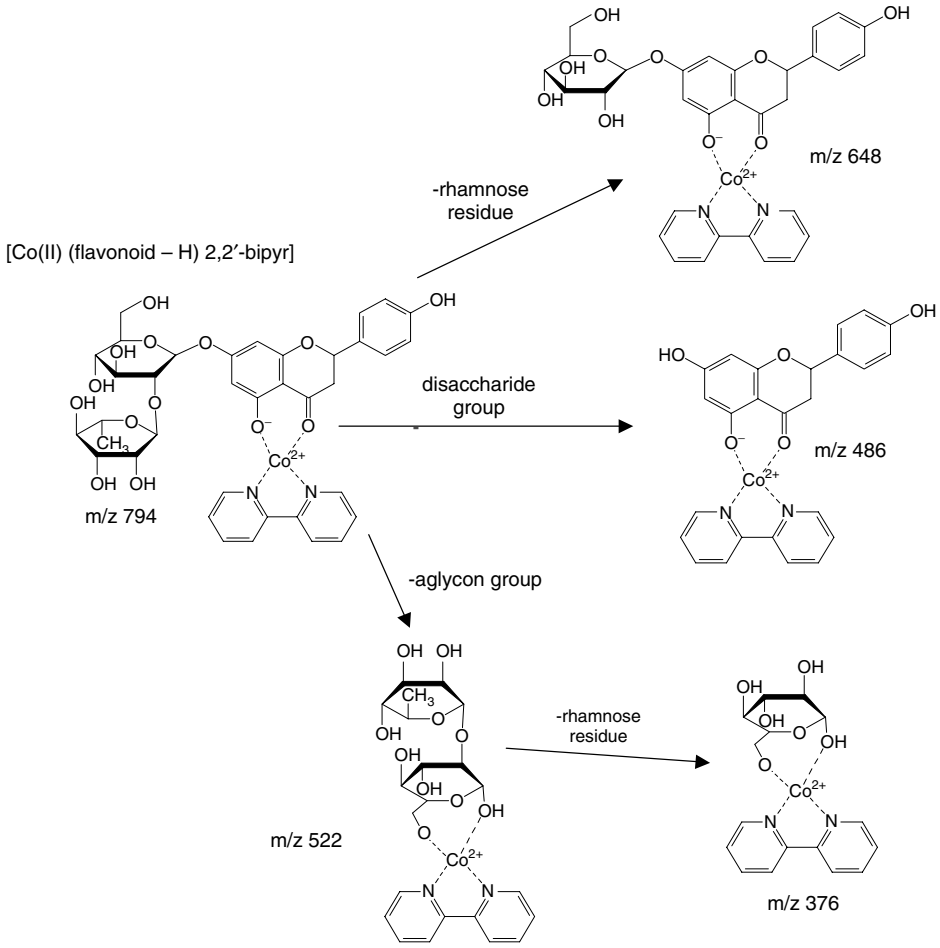

Scheme 4. Dissociation pathways of [M(II) (flavonoid − H) 2, 2′-bipyridine]$^{+}$ complexes.

sugar residue (e.g. rhamnose, −R), elimination of the entire disaccharide moiety (−D), loss of the aglycon part (−A), and elimination of both the aglycon and rhamnose parts, (−A, −R). Each isomer has a unique CID pattern that allows it to be distinguished readily from the others. Some of the possible structures of the resulting CID product ions are illustrated in Scheme 4. The losses of the rhamnose moiety or the entire disaccharide moiety can be easily rationalized based on simple cleavage in conjunction with a single hydrogen migration. The dissociation pathway that entails the loss of the aglycon part (i.e. the lower pathway in Scheme 4) is less straightforward because clearly the metal ion and auxiliary chelating ligand cannot remain coordinated to the keto oxygen and phenolic 5-oxygen atom of the core flavonoid as shown in the precursor complex. These product ions must involve either migration of the metal to the disaccharide portion of the flavonoid during collisional activation or initial coordination of the metal by the disaccharide moiety of the flavonoid in solution or during subsequent ESI. Observation of these types of product ions in the CID mass spectra of the metal complexes offers supporting evidence for some of the more unusual structures proposed in Fig. 4. Given that some of the energy-minimized structures determined from molecular modeling (Fig. 5) showed extensive folding of the flavonoids and intramolecular interactions of the disaccharide portion with the metal center, it is not surprising that the complexes may dissociate via elimination of the entire aglycon portion with retention of the metal by the glycoside moiety of the flavonoid.

The metal ion plays a significant role in the complexation process and subsequent dissociation of the complexes,[40,42] as illustrated in Fig. 8 as well as in later examples. Figure 8 shows the CID mass spectra obtained for complexes containing rhoifolin and 2,2′-bipyridine, and one of three different transition metals. The Cu(II) and Ni(II) complexes exhibit similar fragmentation patterns, with the single dominant pathway being the elimination of the disaccharide moiety. In contrast, the CID mass spectrum for the analogous Co(II) complex reveals two additional product ions, one attributed to the loss of the rhamnose moiety and the other due to the loss of the rhamnose moiety in conjunction with the aglycon part. For characterization of rhoifolin, the Co(II) complex provides the most diagnostic fragmentation pattern. The comparison in Fig. 8 conveys the importance of the metal ion in influencing the dissociation pathways of the metal complexes, due to either changes in coordination geometries or differences in the critical energies of the various pathways.

Another factor that influences the fragmentation patterns of the metal complexes, and thus offers a way to 'tune' the CID behavior is the nature of the auxiliary chelating ligand.[42] The examples shown in Figs 7 and 8 illustrate product ion mass spectra of complexes that incorporated 2,2′-bipyridine as the auxiliary chelating ligand. To date,

DOI: 10.1002/jms

JMS

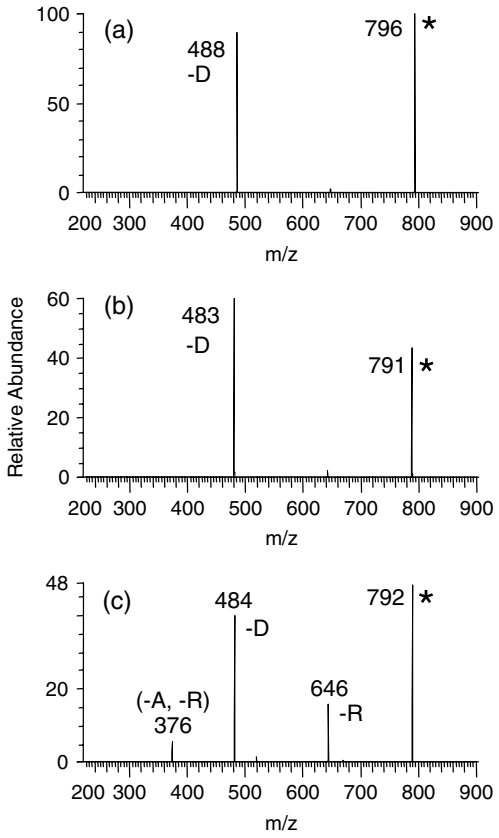

Figure 8. CID mass spectra for [M(II) (rhoifolin − H) 2,2′-bipyridine] complexes where M is (a) Cu, (b) Ni, and (c) Co. The parent ions are indicated by asterisks. The loss of the aglycon portion is indicated by −A, the loss of the rhamnose residue is indicated by −R, and the loss of the disaccharide moiety is indicated by −D.

2,2′-bipyridine has proven to be one of the most versatile, robust chelating ligands in numerous flavonoid applications. However, one could envision that the properties of the auxiliary chelating ligand, such as its metal binding affinity and steric bulk, could have an impact on the complexation efficiency of the flavonoids and the resulting fragmentation patterns. An example that illustrates this latter point is shown in Fig. 9 for complexes containing rhoifolin, Co(II), and one of five different pyridyl-based chelating ligands (2,2′:6′,2″-terpyridine, 2,2′-bipyridine, 1,10-phenanthroline, 4,7-dimethyl-1,10-phenanthroline, and 4,7-diphenyl-1,10-phenanthroline).[42] The relative abundances of the three major product ions, ones attributed to cleavage of the rhamnose moiety (−R), elimination of the disaccharide part (−D), and loss of both the rhamnose moiety and the aglycon part (−R, −A), vary depending on the auxiliary chelating ligand. The third fragmentation pathway is not observed for the complex containing 2,2′:6′,2″-terpyridine which may be due to the extremely high metal binding affinity of this pyridyl ligand which alters the balance of the binding interactions between the cobalt ion, the flavonoid, and the auxiliary ligand, thus suppressing the dual losses of the rhamnose moiety and the aglycon part.

An example of how the use of metal complexation enhances the differentiation of isomers is shown in Fig. 10 for vitexin and isovitexin, two flavonol monoglycosides.[42] The product ion mass spectra of the deprotonated isomers show dissociation by losses of 120 and 90 Da due to cross-ring sugar cleavages (corresponding to the $^{0,2}X_0^+$ and $^{0,3}X_0^+$ product ions, respectively, labeled in Fig. 10). These product ion mass spectra are not substantially different, and the differentiation of the isomers would rely on only the variation in the relative abundances of the same two product ions. The [Co(II) + (flavonoid − H) + 2, 2′-bipyridine]$^+$ complexes dissociate by a greater array of diagnostic pathways, including several cross-ring cleavages (CRCs) (losses of 90 Da or 120 Da) and dehydration (Fig. 10(c) and (d)). Proposed pathways which summarize the diverse array of fragmentation pathways for the [Co(II) (vitexin − H) + 2, 2-bipyridine]$^+$ complex and are supported by MS^n experiments are shown in Scheme 5. These pathways include the loss of the terminal sugar (A), which is most prevalent for the *O*-glucosides, a CRC resulting in a loss of 120 Da (B), and another CRC resulting in a loss of 90 Da (C).

Pyridyl ligands serve as excellent auxiliary ligands in the flavonoid/metal complexes because of their ability to chelate metal ions *via* their nitrogen atoms. Modification of the size, polarizability, and number of electron-releasing or electron-withdrawing substituents of the auxiliary ligands influences their metal binding interactions which, in turn, may be translated into variations in the resulting fragmentation pathways of the flavonoid/metal complexes. Just as the pyridyl ligands possessing different alkyl substituents changed the distribution of fragment ions for the rhoifolin complexes in Fig. 9, using pyridyl ligands with electron-withdrawing halogen substituents provides another way to influence the fragmentation routes.[50] As reported in one recent study,[50] the product ion mass spectra of metal complexes containing each of 12 isomers of 7-*O*-flavonoid diglycosides and auxiliary ligands containing bromo substituents were analyzed. Figure 11 shows the product ion mass spectra for a series of cobalt/isorhoifolin complexes, each containing one of six different auxiliary ligands. The product ion mass spectra have significant differences in the relative abundances of specific fragment ions, as well as the presence of new diagnostic fragment ions as the identity of the auxiliary ligand changes. The relative abundances of two key fragment ions, one due to the elimination of the rhamnose moiety (−R) and the other due to the loss of the disaccharide part (−D), vary significantly for the series of product ion mass spectra. Moreover, for those complexes containing phenanthroline auxiliary ligands, the ratio of (−R)/(−D) increases as the degree of bromination increases (Fig. 11(b–e)). The abundances of the two product ions stemming from CRCs (X_1 (−74 Da, labeled with a square) and X_2 (−104 Da, labeled with a circle)) change substantially. These latter CRC pathways are summarized in Scheme 6. The use of auxiliary ligands that contained electron-withdrawing substituents proved to be particularly useful for differentiation of flavone and flavanone disaccharides with 1 → 2 and 1 → 6 linkages. The types of fragment ions observed for all the cobalt complexes containing four bromophenanthroline ligands and each of the flavonoids are summarized in Table 1. The characteristic fragmentation pathways include the loss of the rhamnose part (−R), the

DOI: 10.1002/jms

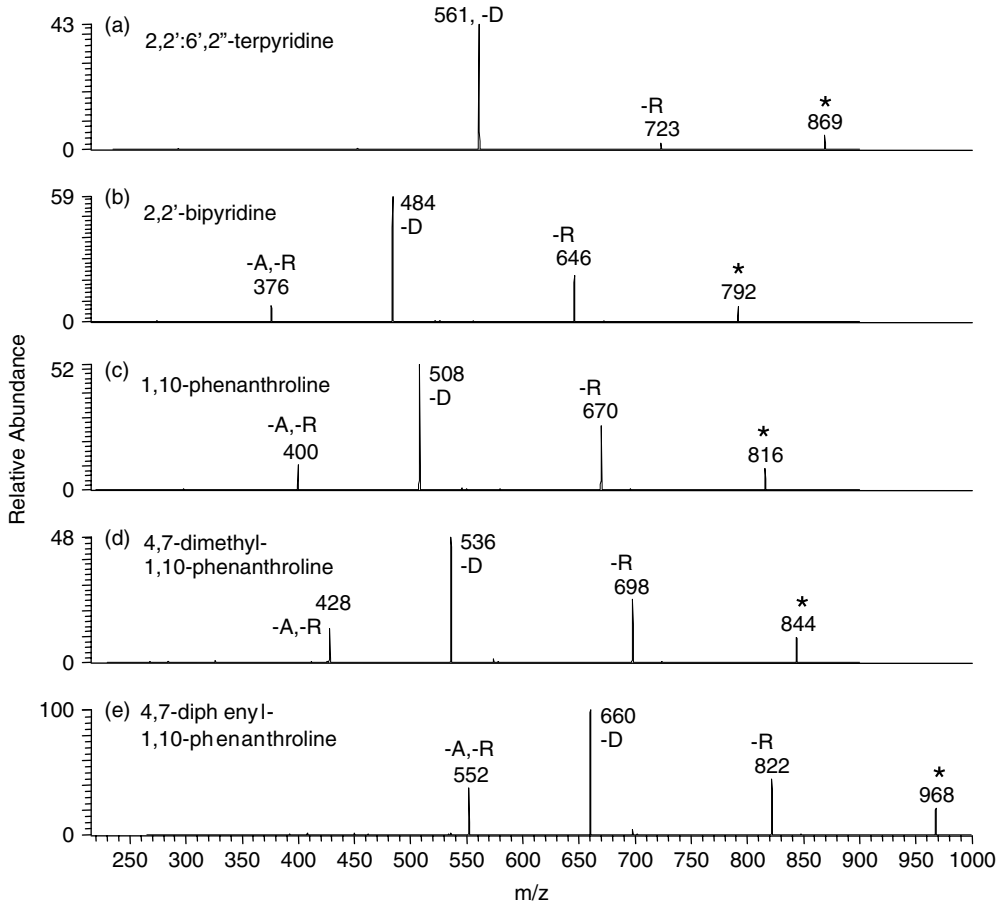

Figure 9. CID mass spectra of [Co(II) (rhoifolin − H) pyridyl ligand]+ complexes, showing relative fragment ion abundances with the variation of the auxiliary ligand. The parent ion is designated with an asterisk, the loss of the rhamnose residue is designated by −R, the loss of the disaccharide moiety is designated by −D, and the loss of the aglycon group is designated by −A (Ref. 42).

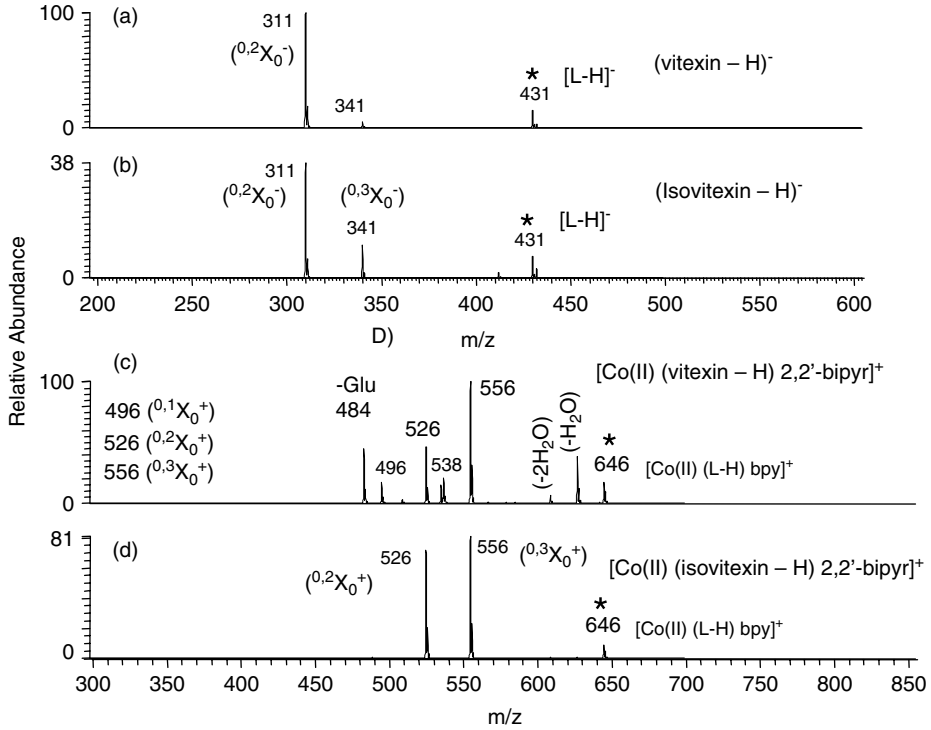

Figure 10. CID spectra for two flavonoid isomers, vitexin and isovitexin based on activation of the deprotonated species (a and b) or the [Co(II) (L − H) bpy]+ complexes (c and d). The parent ions are labeled with asterisks (Ref. 42).

DOI: 10.1002/jms

JMS

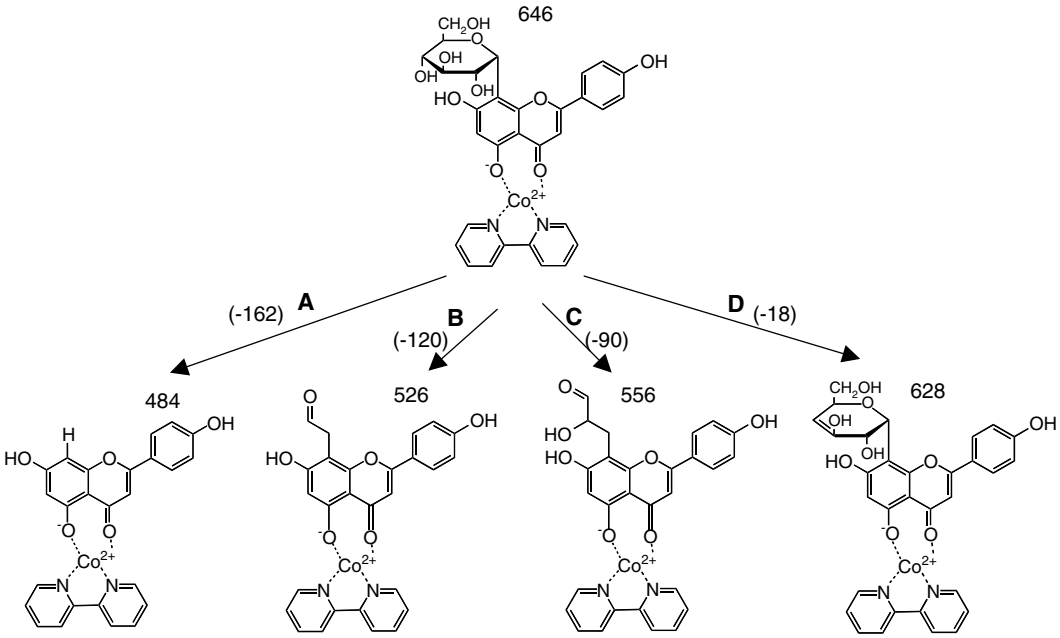

Scheme 5. CID fragmentation pathways for [Co(II) (vitexin − H) bpy]$^+$ using proposed structures of the fragment ions (Ref. 42).

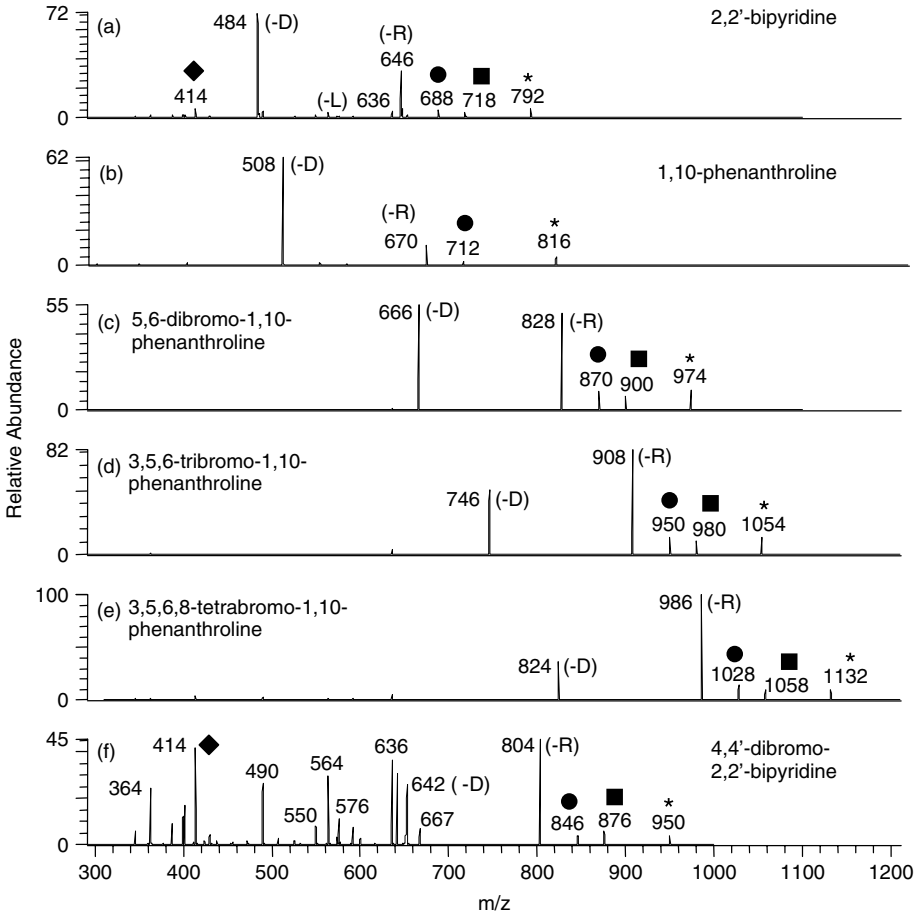

Figure 11. CID mass spectra for [Co(II) + (isorhoifolin − H) + auxiliary ligand]+ complexes containing six different auxiliary ligands (Ref. 50).

elimination of the disaccharide moiety (−D), and the loss of the aglycon and rhamnose parts (−A, −R).

A noteworthy difference between the fragmentation patterns of the flavonoid rutinosides and the neohesperidosides are two CRCs (X_1, −74 Da, and X_2, −104 Da). Moreover, the flavanone neohesperidosides are differentiated from the corresponding flavones by the characteristic loss of the aglycon moiety. Presumably, the metal/auxiliary ligand binding

DOI: 10.1002/jms

energies decrease as the substituents on the auxiliary ligand become more electron-withdrawing, thus altering the energetics of dissociation pathways, the preferred coordination sites and stabilities of the [M(II) (flavonoid − H) + auxiliary ligand]$^+$ complexes, and possibly the conformations of the complexes during activation. All these factors may contribute to the variation and resulting 'tunability' of the CID patterns.

Metal complexation also proves to be a promising strategy for differentiation of isomeric *C*- and *O*-bonded flavonoid monoglucosides for which there are five common glycosylation positions: attachment of the sugar part through an oxygen atom at position 3, 4′, or 7; or *via* a carbon atom at position 6 or 8. ESI was used to produce complexes of the type [Mg^{II} (flavonoid) (flavonoid − H)]$^+$ for 13 flavonoid monoglucosides.[43] Upon CID, the dissociation routes seen for *O*-glucosyl flavonoid complexes typically include elimination of the glucose residue, and loss of the aglycon portion. The fragmentation pathways that prove to be most characteristic of *C*-glucosyl flavonoids include dehydration and CRCs of the glucose residue, yielding losses of 90 or 120 Da. Figure 12 shows the product ion mass spectra of the Mg(II) complexes involving five isomeric flavonoids glucosides, each glycosylated at a different site. The product ion mass spectra are unique for each of the five isomers and also allow confident assignment of the glycosylation site. For example, elimination of the glucose moiety is characteristic of *O*-glucosylation, and the unusual 0,2 CRC of glucose which entails the loss of 120 Da is the dominant fragmentation pathway for the *C*-glucosyl flavonoids. In addition to identification based on *C*- or *O*-glucosylation, the site of glucosylation can be determined also from the product ion mass spectra of these metal complexes, as summarized in the flow chart in Fig. 13. The 7-*O*-glucosylation site is assigned based on the occurrence of the 0,2 CRC pathway. 3-*O*-glucosyl flavonoids only eliminate the glucose moiety upon CID, whereas the 4′-*O*-glucosyl flavonoid also dissociates by loss of the aglycon part and one entire flavonoid glucoside. The 6-*C*-glucosyl flavonoids undergo dehydration and also produce the unique fragment ion stemming from a 0,2 CRC (−120 Da) and dehydration. The 8-*C*-glucosyl flavonoids undergo a 0,3 CRC (−90 Da), as well as 0,2 cleavage of both glucose moieties from the [Mg^{II} (flavonoid) (flavonoid − H)]$^+$ complexes.

In addition to determination of the site of glycosylation, metal complexation in conjunction with MS^3 experiments allows evaluation of the specific saccharide identity (glucose, galactose, arabinose, or xylose) of isomeric monoglycosyl flavonols, flavones, and flavanones.[47] This objective was accomplished based on Mn metal complexation, with the

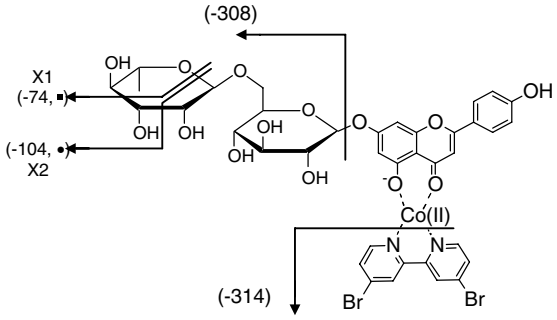

Scheme 6. CID pathways of [Co(II) + (isorhoifolin − H) + 4, 4′-dibromo-2, 2′-biypridine]$^+$ complexes (Ref. 50).

Table 1. Selected fragments observed in the CID mass spectra for Co/flavonoid/brominated ligand complexes grouped by flavonoid diglycoside class (Ref. 50)

4,4′-dibromo-2,2′-bipyridine/Co	(−R)	(−D)	(−A)	(−A, −R)	(−L)	X1	X2
Flavone neohesperidoside	√	√		√			
Flavone rutinoside	√	√			√	√	√
Flavanone neohesperidoside	√	√	√	√			
Flavanone rutinoside	√	√			√	√	√
5,6-dibromo-1,10-phenanthroline/Co	(−R)	(−D)	(−A)	(−A, −R)	(−L)	X1	X2
Flavone neohesperidoside	√	√		√			
Flavone rutinoside	√	√				√	√
Flavanone neohesperidoside		√					
Flavanone rutinoside		√					
3,5,6-tribromo-1,10-phenanthroline/Co	(−R)	(−D)	(−A)	(−A, −R)	(−L)	X1	X2
Flavone neohesperidoside	√	√		√			
Flavone rutinoside	√	√		√		√	√
Flavanone neohesperidoside	√	√	√	√			
Flavanone rutinoside	√	√		√		√	√
3,5,6,8-tetrabromo-1,10-phenanthroline/Co	(−R)	(−D)	(−A)	(−A, −R)	(−L)	X1	X2
Flavone neohesperidoside	√	√		√			
Flavone rutinoside	√	√			√	√	√
Flavanone neohesperidoside	√	√	√	√			
Flavanone rutinoside	√	√		√		√	√

(−D) indicates loss of disaccharide moiety, (−R) indicates loss of rhamnose moiety, (−L) indicates loss of ligand, (−A) indicates loss of aglycon, X1 and X2 represent the cross-ring cleavages of (−74) and (−104), respectively.

DOI: 10.1002/jms

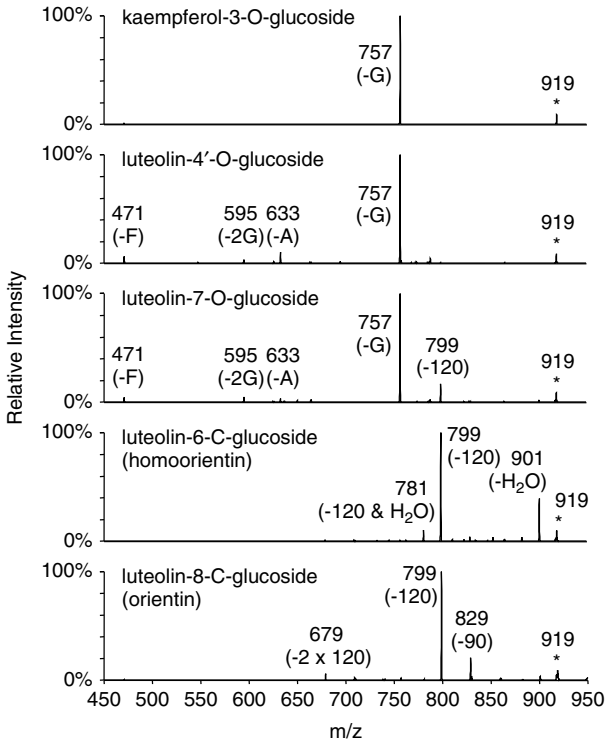

Figure 12. CID spectra of [Mg(II) (L − H) (L)]+ complexes involving isomeric monoglucosyl flavonoids glycosylated at five different positions. Fragmentation pathways are labeled as: −G, (loss of a glucose residue); −2G, (loss of two glucose residues); −A, (loss of aglycon portion); −F, (loss of one flavonoid glucoside molecule) (Ref. 43).

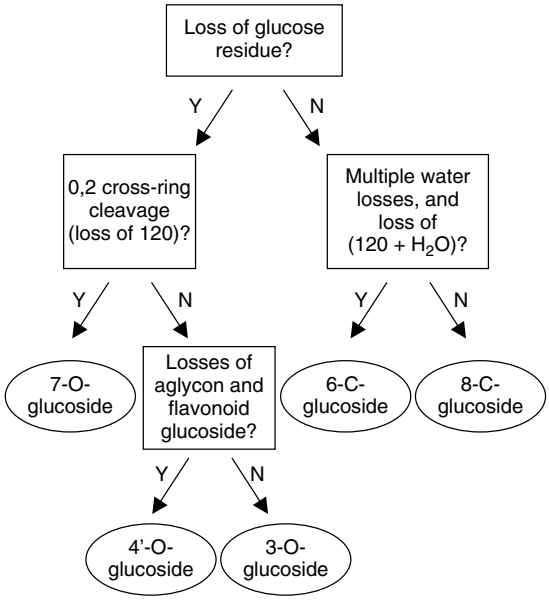

Figure 13. Determination of glycosylation site based on evaluation of fragmentation patterns of [Mg(II) flavonoid (flavonoid − H)] complexes (Ref. 43).

resulting [Mn(II) (L) (L − H)]$^+$ complexes affording the unique product ions that allow the identification of the saccharide moiety as either glucose, galactose, arabinose, or xylose. An example is shown in Fig. 14 for the differentiation of quercetin-3-*O*-glucoside and quercetin-3-*O*-galactoside in which the primary fragment ion produced during a first stage of CID of the precursor [Mn(II) (L) (L − H)]$^+$ complexes is selected for a second stage of CID (MS^3). Upon a second stage of CID, both complexes exhibit losses of the second hexose moiety and of one aglycon part, but the quercetin-3-*O*-galactoside complex also uniquely dissociates by the loss of the aglycon part plus 102 Da. This secondary loss of 102 Da is attributed to a rearrangement/cleavage of the galactose group, causing the elimination of $C_4H_6O_3$, as proposed in Scheme 7. The analogous quercetin-3-*O*-glucoside does not follow this fragmentation pathway. This Mn complexation method was utilized in a liquid chromatography/mass spectrometry (LC/MS) strategy to identify isomeric monoglycosyl flavonoids found in Fuji apples (*Malus domestica* Borkh. cv. Fuji) and red onions (*Allium cepa* L.).

A metal complexation strategy that did not incorporate auxiliary chelating ligands and instead entailed formation of 1 : 1 Ag^+: flavonoid complexes was successful for differentiation of 18 flavonoid diglycoside isomers, as well as being easily implemented for post-column LC/MS applications.[46] Analysis of the product ion mass spectra indicated that specific and consistent dissociation pathways allowed verification of the site of glycosylation, the type of disaccharide (rutinose *versus* neohesperidose), and the type of aglycon (flavonol *versus* flavone *versus* flavanone). An example of a product ion mass spectrum obtained for one of the complexes is shown in Fig. 15 for (rutin + Ag)$^+$, and the dominant fragmentation pathways are illustrated in Scheme 8. The rutin complex yields five key product ions: the loss of the aglycon moiety (m/z 417), the elimination of the rhamnose residue (m/z 573), the loss of the aglycon moiety in conjunction with dehydration (m/z 399), the loss of the aglycon residue plus 64 Da (the sugar rearrangement and cleavage process) (m/z 353), and the loss of both the aglycons and the rhamnose moieties plus one water molecule (m/z 253). By incorporating the silver complexation method into a post-column LC/MS/MS strategy, a group of flavonoids extracted from grapefruit juice were analyzed. Introducing the silver nitrate reagent after the high performance liquid chromatography (HPLC) column produced silver complexes for the eluting flavonoids. The resulting silver complexes were then detected by ESI-MS with characterization by MS/MS. An example demonstrating this approach is shown in Fig. 16 for the identification of six flavonoids in the grapefruit extract. As a counterpart to silver complexation, another metal complexation strategy that does not entail the use of auxiliary chelating ligands involves the coordination of aluminum.[45] Aluminum complexes of the type [Al^{III} (flavonoid − $H)_2$]$^+$ are generated by ESI, and this method in conjunction with CID allowed the differentiation of 18 flavonoids from among seven isomeric series.

The metal complexation methods described in this review also allowed the position of glucuronidation to be determined for flavonoid metabolites containing a single glucuronide moiety.[48,51] For example, four isomeric quercetin glucuronides (3-*O*-, 3′-*O*-, 4′-*O*-, and 7-*O*-) were

DOI: 10.1002/jms

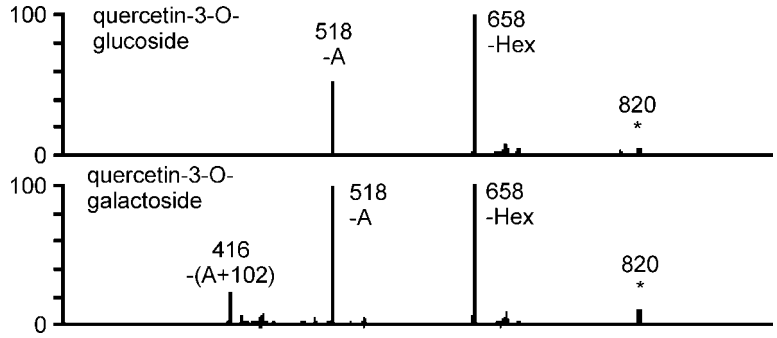

Figure 14. MS^{3+} spectra of [Mn(II) (L) (L − H)]+ complexes of two flavonoid 3-*O*-hexosides following the loss of one hexose moiety. The parent ion is denoted with an asterisk. Fragment ions are labeled as: −Hex, (loss of hexose moiety); −A, (loss of an aglycon group) (Ref. 47).

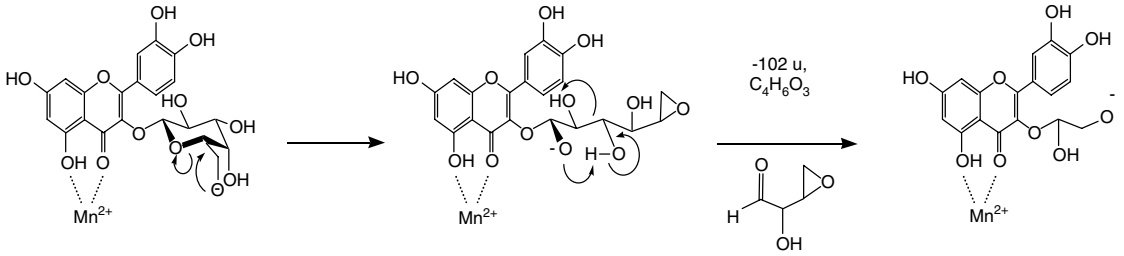

Scheme 7. Proposed mechanism for the loss of 102 Da from Mn complexes of flavonoid galactosides (hyperoside shown as example) (Ref. 47).

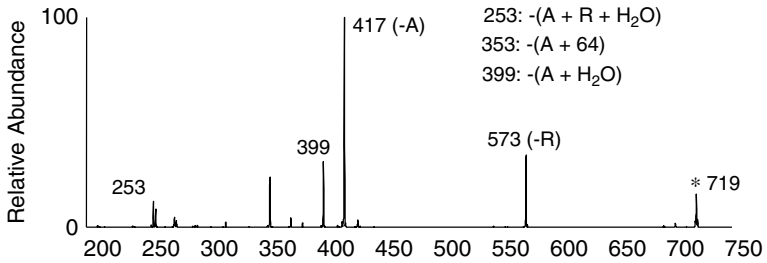

Figure 15. CID mass spectrum of the (Ag + rutin)+ complex. The parent complex ion is labeled with an asterisk. The losses are: R, rhamnose group (146); and A, aglycon moiety. The elimination of 64 Da may involve consecutive losses, i.e. the loss of water and 46 Da (a C2H6O moiety or H_2O and CO) (Ref. 46).

differentiated based on characteristic dissociation pathways, including loss of quercetin aglycon and loss of the glucuronide moiety, upon CID of the [Co(II) (flavonoid glucuronide − H) + (4,7-dimethyl-1,10-phenanthroline)]$^+$ and [Co(II) (flavonoid glucuronide − H) (4,7-diphenyl-1,10-phenanthroline)$_2$]$^+$ complexes. This strategy was adapted for LC/MS/MS to allow the determination of two naringenin glucuronides in human urine following the consumption of grapefruit juice,[48] as well as for identification of 18 flavonoid monoglucuronide metabolites synthesized using the 1A1 isozyme of human UDP-glucuronosyltransferase (UGT) with ten flavonoid aglycon substrates.[51] The specific fragmentation patterns obtained for the metal/flavonoid glucuronide complexes allowed the regioselectivity of UGT1A1 toward flavonol, flavone and flavanone substrates to be mapped. For example, it was found that flavonoids lacking a 3′-hydroxyl group were glucuronidated only at position 7, while those containing the 3′-hydroxyl group also formed 3′-*O*-glucuronides and sometimes 4′-*O*-glucuronides. This assessment was facilitated by the metal complexation ESI-MS methods described in this review.

Metal complexation strategies have also been combined with infrared multiphoton dissociation (IRMPD) to afford an extremely versatile method for the structural characterization of flavonoids.[49] IRMPD is a promising alternative to CID for dissociation of ions in the gas phase because photoactivation is not a resonant process, meaning that energy absorption by primary fragment ions formed during the activation period may result in secondary dissociation. Thus, the extent of ion dissociation can be varied by adjusting the activation time or laser power. The secondary fragments offer important structural information without the need for more elaborate MS^n strategies. For efficient IRMPD, the precursor ions must efficiently absorb infrared (IR) photons (i.e. 10.6 μm for a CO_2 laser). The use of a phosphonated auxiliary ligand provides a strong IR chromophore that allows IRMPD to be used as an alternative activation method to CID for the analysis of flavonoids. Complexes of the type

DOI: 10.1002/jms

JMS

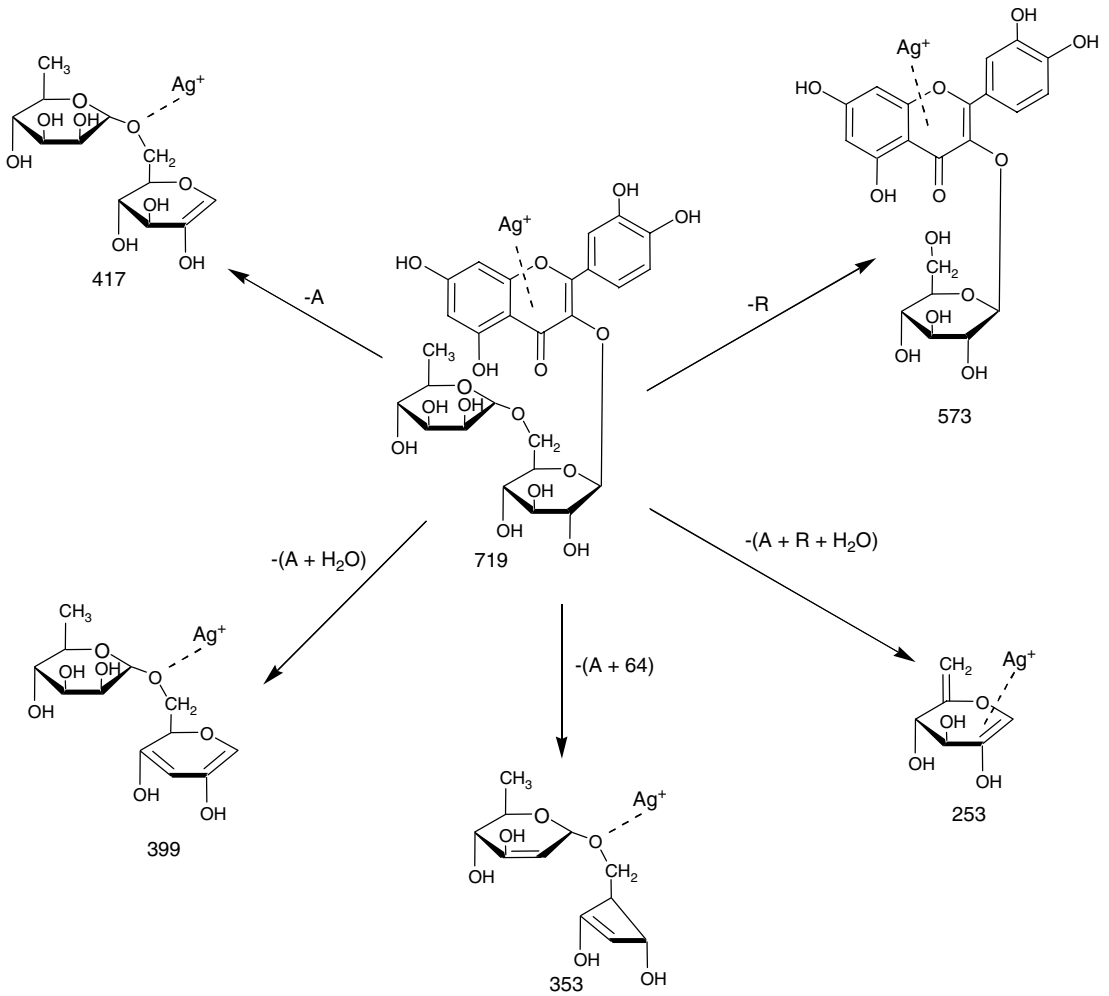

Scheme 8. Proposed CID fragmentation pathways for the [Ag + rutin]$^+$ complex. Only the *m/z* values corresponding to one isotope of the silver ion (109) are listed for simplicity. The letters A and R represent the aglycon and rhamnose residues, respectively. The elimination of 64 Da may involve consecutive losses, i.e. the loss of water and 46 Da (a C_2H_6O moiety or H_2O and CO). The dashed lines in the proposed structures indicate that the actual coordination sites of the silver ion are not known (Ref. 47).

$[M^{2+}$ (flavonoid − H) IRAL$]^+$, where IRAL is an infra-red-active ligand, are formed in solution prior to ESI, where M is a transition metal such as copper or cobalt and IRAL is a phosphonated bipyridine ligand (see Fig. 2). Examples of the resulting CID and IRMPD mass spectra are shown in Fig. 17 for the complexes containing one representative flavonoid, neodiosmin, with copper as the metal, and one of the phosphonated auxiliary ligands (IRAL-2 in Fig. 2). Upon CID, the dominant dissociation pathway entails loss of the disaccharide moiety (−D) (see Fig. 17(a)). In contrast, the analogous IRMPD mass spectrum shows a much larger array of fragment ions (Fig. 17(b)) attributed to secondary dissociation of primary product ions due to their sequential activation upon absorption of IR photons. The IRMPD mass spectra obtained for complexes containing two flavanone isomers (naringin versus narirutin) with cobalt and the two different phosphonated ligands are compared in Fig. 18. The main fragmentation pathways are ones that are characteristic of flavanones, including loss of the rhamnose residue group, loss of the disaccharide moiety, as well as the loss of both the rhamnose and aglycon parts that is diagnostic for neohesperidosides (1 → 2 disaccharides) but does not occur for rutinosides (1 → 6 disaccharides). All the product ion mass spectra in Fig. 18 show a greater array of product ions due to the secondary dissociation of the primary product ions that are activated throughout the photoirradiation period.

COLLISION-INDUCED DISSOCIATION OF FLAVONOIDS

In this section, we review a fragmentation study of a flavone triglycoside, the CID of a number of flavonoid glycosides, a study of the binding of a variety of flavonoids to a proline-rich protein using energy-resolved mass spectrometry (ERMS), and a comparison of high-energy and low-energy CID of a number of flavonoids.

Fragmentation study of a flavone triglycoside

MS/MS has been applied to the structural characterization of a tetrahydroxyflavonoid triglycoside, robinin (3,5,7,4′-tetrahydroxyflavone-3-*O*-robinoside-7-*O*-rhamnoside), which exhibited both homolytic and heterolytic dissociation.[53] The simplicity of the observed product ion mass spectra provides a vehicle for the introduction of fragmentation nomenclature applicable to triglycosides in general.

DOI: 10.1002/jms

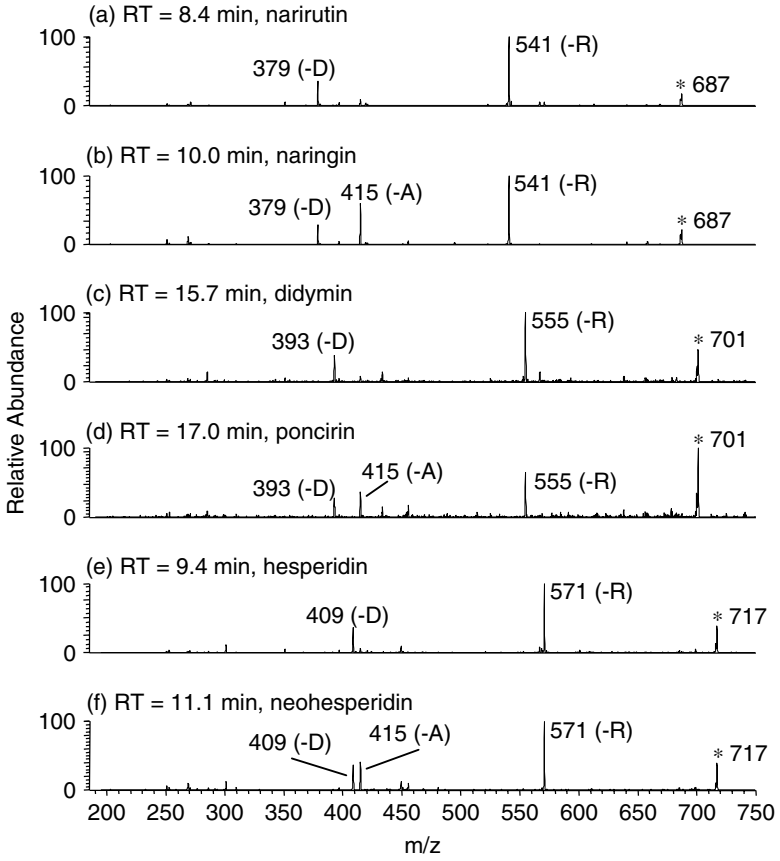

Figure 16. LC/MS/MS analysis of a grapefruit extract after post-column silver complexation, resulting in formation of (flavonoid + Ag)$^+$ ions. The selected parent ions are indicated by asterisks. The loss of the rhamnose residue is indicated by −R, the loss of the aglycon moiety is indicated by −A, and the loss of the disaccharide group is indicated by −D (Ref. 46).

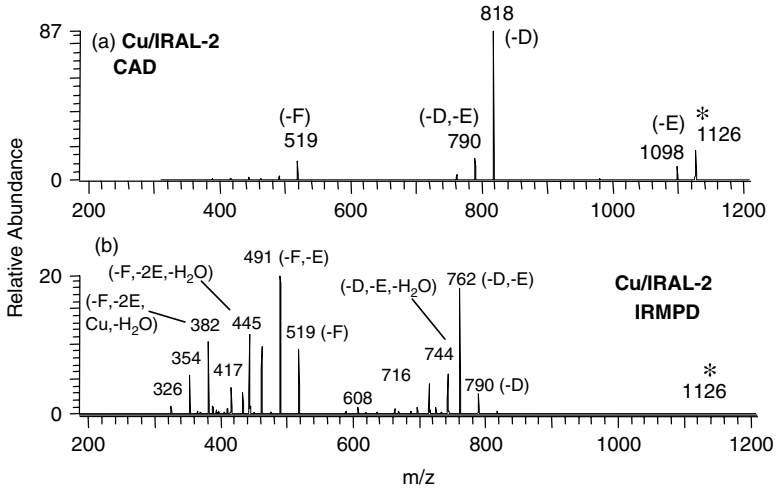

Figure 17. (a) CID and (b) IRMPD mass spectra of [Cu(II) + (neodiosmin − H) + IRAL-2]$^+$ complexes. The selected parent ions are indicated by asterisks. The loss of the rhamnose residue is indicated by −R, the loss of the aglycon moiety is indicated by −A, the loss of the flavonoid −F, the loss of ethylene is indicated by −E, and the loss of the disaccharide group is indicated by −D (Ref. 49).

The numbering scheme for substitution in flavones is shown in Scheme 9 along with the fragmentation nomenclature for carbohydrate fragmentations modified for an *O*-glycoside -*O*-diglycoside according to Li and Claeys[21] and applied to [M − H]$^-$ of robinin. In Scheme 10, the rhamnose ring bonds are numbered with a small font and ions resulting from CRCs in the sugar residue are denoted with X labels.

Robinin, the trivial name for the 3,5,7,4′-tetrahydroxyflavone triglycoside, kaempferol-3-*O*-robinoside-7-*O*-rhamnoside, is rhamnose-substituted at the 7-position and robinose-substituted at the 3-position where robinose (having the same structure as rutinose) is a 1 → 6 bonded diglycoside of glucose and rhamnose. The terminal glycoside of the diglycoside is rhamnose, hence robinin has

DOI: 10.1002/jms

JMS

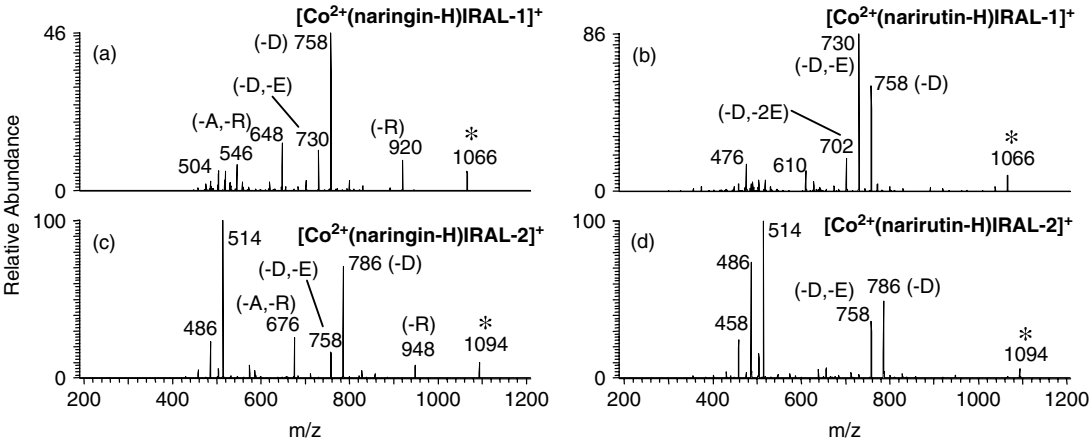

Figure 18. IRMPD mass spectra of isomeric naringin and narirutin [M(II) + (flavonoid − H) + auxiliary ligand]$^+$ complexes. The selected parent ions are indicated by asterisks. The loss of the rhamnose residue is indicated by −R, the loss of the aglycon moiety is indicated by −A, the loss of the flavonoid −F, the loss of ethylene is indicated by −E, and the loss of the disaccharide group is indicated by −D (Ref. 49).

two terminal rhamnose moieties. The structure of deprotonated robinin is given in Scheme 9 together with diagnostic fragmentations due to losses of the glycan residues.

The relatively few fragmentations observed for deprotonated robinin at a collision energy of 50 eV are depicted in Scheme 10. The deprotonated molecule, $[M - H]^-$ (m/z 739), loses the rhamnose glycan residue (146 Da) in a rearrangement reaction where the hydrogen atom from a hydroxyl group is retained[21] to form the Y_7^- ion of m/z 593. It was proposed that the rhamnose glycan residue at the 7-position is lost. The loss of the rhamnose glycan residue from the 3-position is not observed. The deprotonated molecule loses the robinose glycan (309 Da) also by scission to form the $[Y_{3,0} - H]^{-\bullet}$, a radical anion of m/z 430. It is unusual to observe only the scission reaction to form m/z 430. The Y_7^- ion of m/z 593 loses the robinose glycan (309 Da) by scission to form the $Y_7[Y_{3,0} - H]^{-\bullet}$ radical anion of m/z 284. The $[Y_{3,0} - H]^{-\bullet}$ radical anion of m/z 430 loses the rhamnose glycan residue by both rearrangement and scission to form the $[Y_7 - H][Y_{3,0} - H]^-$ ion (m/z 283) and the radical anion $Y_7[Y_{3,0} - H]^{-\bullet}$ (m/z 284), respectively. Thus, virtually the entire fragmentation process of the deprotonated molecule (m/z 739) involves two competing initial fragmentation processes where each fragment ion loses the complementary glycan residue to yield the radical anion $Y_7[Y_{3,0} - H]^{-\bullet}$ of m/z 284. Homolytic fragmentation of the $[Y_{3,0} - H]^{-\bullet}$ radical anion of m/z 430 yields the $[Y_7 - H][Y_{3,0} - H]^-$ ion (m/z 283) as shown in Scheme 10.

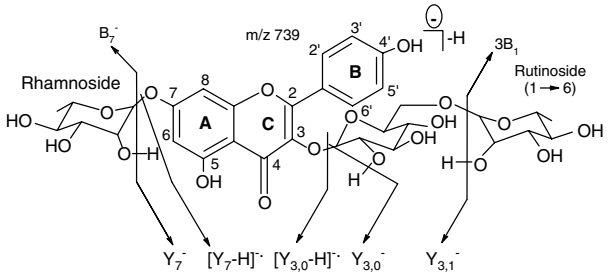

Scheme 9. Ion fragmentation nomenclature for $[M - H]^-$ of robinin, *m/z* 739 (Ref. 53).

That a significant fraction of the fragmentations of $[M - H]^-$ of robinin occurs by single-bond scission rather than by rearrangement, normally of lower activation energy, can be explained by resonance stabilization in the resulting radical anions.

Fragmentation study of flavonoid glycosides

The important analytical challenge posed by such a wide variety of structurally similar flavonoid glycoside molecules discussed above is pursued in parallel with an extensive examination of the fragmentation behavior and basic chemistry of flavonoids and flavonoid glycosides.[27–31,38,54–58] An important issue in the structural characterization of flavonoid glycosides is determination of the glycosylation site. Cuyckens and Claeys have investigated the site of glycosylation in 18 flavonoid mono -*O*-glycoside standards by CID of ESI-generated deprotonated molecules and sodium-cationized molecules.[59] A particularly interesting aspect of the conditions under which CID was carried out is the collision energy magnitude. For a discussion of the relationship between the collision energy in the laboratory frame (E_{lab}) and the center-of-mass frame (E_{cm}), and for a comparison of high-energy and low-energy CID of protonated flavonoids, refer Section Comparison of high-energy and low-energy CID of protonated flavonoids. Values of E_{cm} of <25 eV and >25 eV are considered as low- and high-energy CID, respectively. Using collision energies, E_{cm}, of *ca.* 50 eV, for CID of deprotonated molecules and sodium-cationized molecules, Cuyckens and Claeys observed that the site of glycosylation in flavonoid mono-*O*-glycosides can be determined from the ion signal intensities' ratio of radical aglycone $(Y_o\text{-}H)^{-\bullet}$ to regular aglycone (Y_o^-) ions.

Mass spectrometric differentiation of 12 common flavonoid glycosides has been reported on the basis of the product ion mass spectra, of high mass accuracy, of protonated and deprotonated molecules.[60] The flavonoid glycosides were selected as being representative of the variety of flavonoid moiety and the location of glycoside attachment in flavonoid glycosides found

DOI: 10.1002/jms

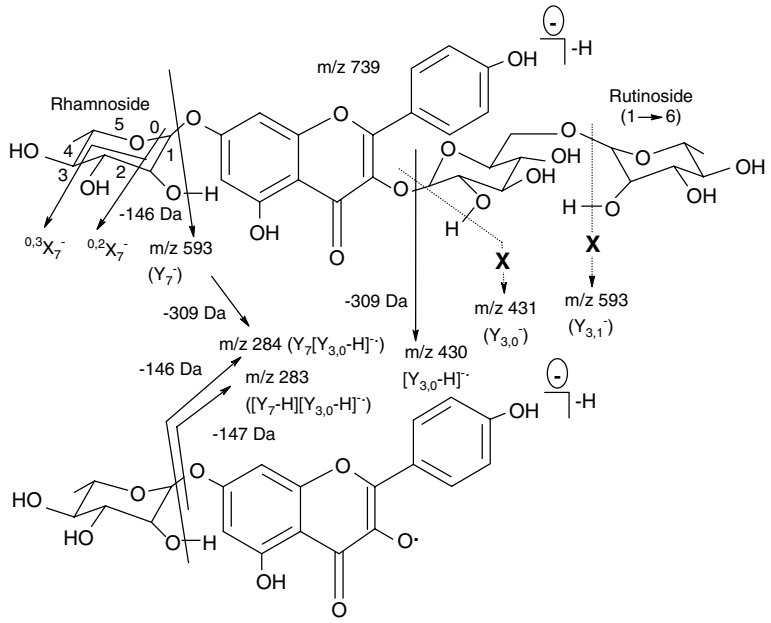

Scheme 10. Fragmentation mechanism of *m/z* 739, $[M - H]^-$, of robinin. The dashed arrows with an X superimposed represent possible fragmentations that were not observed (Ref. 53).

naturally. The compounds studied were kaempferol-3-*O*-glucoside, quercitin-3-*O*-glucoside (isoquercitrin), quercitin-3-*O*-galactoside (hyperoin), apigenin-7-*O*-glucoside, luteolin-7-*O*-glucoside, genistein-7-*O*-glucoside, naringenin-7-*O*-glucoside (prunin), luteolin-4′-*O*-glucoside, luteolin-6-*C*-glucoside (homoorientin, known also as isoorientin), apigenin-8-*C*-glucoside (vitexin), and luteolin-8-*C*-glucoside (orientin) together with the product ion mass spectrum of deprotonated kaempferol-7-*O*-glucoside. Although glucose is the most common monosaccharide in flavonoid glycosides, galactose along with rhamnose, xylose, and arabinose are not uncommon.[61,62] All isomeric ions were distinguishable on the basis of their product ion mass spectra.

For protonated 3-*O*-, 7-*O*-, and 4′-*O*-glycosides at a collision energy of 46–47 eV, homolytic cleavage of the *O*-glycosidic bond yielded aglycon Y^+ ions, whereas in deprotonated 3-*O*-, 7-*O*-, and 4′-*O*-glycosides, heterolytic, and homolytic cleavage of the *O*-glycosidic bond yielded radical aglycon $(Y_1 - H)^{-\bullet}$ and aglycon (Y_1^-) ions. In each case, fragmentation of either the glycan or the aglycon or both was observed. For 6-*C*- and 8-*C*-glycosides at a collision energy of 46–47 eV, fragmentation was restricted almost exclusively to the glycan. For luteolin-6-*C*-glucoside, the integrity of the aglycon structure is preserved at the expense of the glycan for which some 30 fragmentations were observed. Breakdown curves were determined as a function of collision energy for protonated and deprotonated luteolin-6-*C*-glucoside. An attempt was made to rationalize the product ion mass spectra derived from *C*–*O*- and *C*–*C*-luteolin glucosides in terms of computed structures that indicated significant intramolecular hydrogen bonding and rotation of the B-ring to form a coplanar luteolin structure. It was proposed that protonated and deprotonated luteolin-6-*C*-glucoside may afford examples of cooperative interactive bonding that plays a major role in directing fragmentation. In Table 2 is given a summary of the distinguishing mass spectrometric features that permitted identification of the 12 flavonoid glycosides examined. In this study, a wide variety of CRCs of the glycoside moieties was observed, such that differentiation of the flavonoid glycosides studied was facilitated by the specificity of these cleavages.

Energy-resolved mass spectrometry of peptide: flavonoid complexes

The interaction of a selection of flavonoids with synthetic segments of proline-rich peptide (PRP) has been studied by ERMS[63,64] methods established previously for tracking the energy dependence of fragmentation.[65–67] Ions of noncovalent peptide : flavonoid complexes, produced by ESI, were transmitted to an ion trap and submitted to controlled CID. The characterization of the affinity of each complex by a normalized value (DE_{50}, 'energy' required for dissociation of 50% of the irradiated complex) of the dissociation energy, reflected even small structure differences between flavonoids and highlighted the crucial role of hydrogen bonding in PRP–flavonoid interactions.

The interaction of flavonoids with proteins after nutritional uptake leads to the formation of protein–flavonoid complexes that are involved in the decrease of the gastrointestinal oxidative stress, and also in a tactile sensation in the mouth called astringency. In the particular case of red wine, flavonoids that are involved in astringency are extracted from skins and seeds of grapes during maceration and fermentation processes. Astringency is not wholly understood on a molecular scale, but it is generally accepted that this phenomenon arises when lubricating salivary proteins are precipitated under the form of protein–tannin complexes. Among salivary proteins involved in the astringency phenomenon, PRPs[68,69] are the major constituents of parotid and submandibular saliva in humans. These

DOI: 10.1002/jms

Table 2. Summary of distinguishing mass spectrometric features that permit identification of all the 12 flavonoid glycosides examined (Ref. 60)

Compound(s)	Precursor ion	Distinguishing feature(s) from product ion mass spectra
Quercitin-3-*O*-galactoside	$[M+H]^+$ isomers	3-*O*-galactoside: B^+-H_2O (m/z 145).
Quercitin-3-*O*-glucoside		3-*O*-glucoside: no m/z 145.
Quercitin-3-*O*-galactoside	$[M-H]^-$ isomers	Distinguishable by product ion mass spectra; galactoside and 3-*O*-glucoside have only two common product ions, m/z 271 ($-CH_2O$) and 255 ($-(H_2O+CO)$); no glycan fragmentation.
Quercitin-3-*O*-glucoside		
Kaempferol-3-*O*-glucoside	$[M-H]^-$	3-*O*-glu: Y^-, $(Y-H)^{-\bullet}$ ions plus m/z 255 and 227.
Kaempferol-7-*O*-glucoside	iso mers	7-*O*-glu: Y^-, $(Y-H)^{-\bullet}$ ions plus m/z 257 and 151 ($^{1,3}A^-$). Minor fragmentation of the glycan for both 3-*O*-glu and 7-*O*-glu.
7-*O*-glucosides of isomers (apigenin + genistein) plus luteolin, naringenin	$[M+H]^+$	Of the four 7-*O*-glucosides examined, only genistein exhibited extensive fragmentation of both aglycone and glycan. Refer Table 2 of Ref. 54.
Genistein-7-*O*-glucoside Luteolin-7-*O*-glucoside	$[M+H]^+$ isomers	Glycan fragmentations are strictly complementary.
Apigenin-7-*O*-glucoside Naringenin-7-*O*-glucoside	$[M+H]^+$	No glycan fragmentations.
Naringenin-7-*O*-glucoside	$[M-H]^+$	Y^- ion (m/z 271) only; no $(Y-H)^{-\bullet}$ ion.
Luteolin-7-*O*-glucoside	$[M-H]^-$ isomers	7-*O*: Y^- and $(Y-H)^{-\bullet}$ ions plus extensive aglycone fragmentation; no glycan fragmentation. C(3′) OH inhibits glycan 0,2 cleavage from $[M+H]^+$ and $[M-H]^-$. Base peak is $^{1,3}B^-$ ion.
Luteolin-4′-*O*-glucoside		4′-*O*: Y^- ion only; no $(Y-H)^{-\bullet}$ ion. Base peak is $^{1,3}B^-$ ion. $^{0,2}X^-$ ion.
7-*O*-glucosides of isomers (apigenin + genistein), (kaempferol + luteolin), naringenin	$[M-H]^-$	Distinguishable by glycan fragmentation; Refer Table 3 of Ref. 54.
Apigenin-7-*O*-glucoside	$[M-H]^-$ isomers	Apigenin-7-*O*-glu: $(Y-H)^{-\bullet}$ ion is base peak; Y^- ion is ~80% base peak.
Apigenin-8-*C*-glucoside		8-*C*-glu: $^{0,2}Y^-$ ion is base peak; $^{0,1}Y^- - 2H$ ion is ~35% base peak.
Genistein-7-*O*-glucoside		Genistein-7-*O*-glu: $(Y-H)^{-\bullet}$ ion is base peak; Y^- ion is ~80% base peak; shows $^{0,2}X^-$ ion only; no aglycone fragmentation.
Apigenin-7-*O*-glucoside	$[M+H]^+$ isomers	Apigenin-7-*O*-glu: Y^+ and $^{1,3}A^+$ ions.
Apigenin-8-*C*-glucoside		8-*C*-glu: weak Y^+ and extensive and intensive glycan fragmentations.
Genistein-7-*O*-glucoside		Genistein-7-*O*-glu: base peak, Y^+; extensive glycan fragmentation.
Luteolin-6-*C*-glucoside	$[M-H]^-$ isomers	Distinguishable by glycan fragmentation variety. Refer Table 4 of Ref. 54.
Luteolin-8-*C*-glucoside		6-*C*: $^{0,2}X^-$ and either $^{0,3}X^-$ or $^{1,4}X^-$ ions dominate.
Luteolin-6-*C*-glucoside	$[M+H]^+$ isomers	Distinguishable by glycan fragmentation variety. Refer Table 5 of Ref. 54.
Luteolin-8-*C*-glucoside		6-*C* gives wide mass range of neutral losses from glycan; $[M+H]^+$ of 8-*C* gives neutral losses of ≥96 Da only.

proteins are characterized by their unusually high proline content, and repetition of PQGPP sequence motifs. It has been suggested that PRPs act as a first line of defense against dietary polyphenols by forming complexes with them, thereby preventing them from interacting with other body components.[70] Protein–polyphenols interactions have been studied theoretically[71] and with various analytical methodologies using bovine serum albumin (BSA),[72,73] gelatin,[74,75] casein,[76,77] poly vinyl polypyrrolidone (PVPP),[78] bradykinin,[79,80] or other diverse synthetic proteins[81] as probes.

Quercetin, quercetin-3-*O*-rhamnoside, luteolin, luteolin-4′-*O*-glucoside, luteolin-7-*O*-glucoside, apigenin, apigenin-7-*O*-glucoside, apigenin-7-*O*-neohesperidoside, daidzein, daidzein-7-*O*-glucoside, naringenin, naringenin-7-*O*-neohesperidoside, (+)-catechin, (−)-epicatechin, quercetin-3-*O*-rutinoside, 7,4′-dihydroxyflavone, and dimer B3 (catechin-4 α,8-catechin), shown in Scheme 11, were each mixed in a 3 : 1 mole ratio with peptide $IB7_{14}$ (^{1}SPPGKPQGPPPQGG^{14}) immediately prior to mass analysis.

Experiments were performed with a LCQ Advantage ion trap mass spectrometer (ThermoFisher Scientific, San Jose, CA) fitted with an orthogonal ESI source. For ERMS experiments, precursor ions were isolated with a 10 Th width; ion isolation with widths of <10 Da caused internal excitation of the precursor ions. The product ion mass spectrum of the ion at m/z 1871 corresponding to $IB7_{14}$:quercetin-3-*O*-rutinoside with 1 : 4 stoichiometry, is shown in Fig. 19. All the complexes with lower stoichiometry, i.e. m/z 1566 (1 : 3), m/z 1261 (1 : 2), m/z 955 (1 : 1) were detected, together with m/z 650 (2+ ion of $IB7_{14}$) and m/z 610 (quercetin-3-*O*-7-rutinoside). Precursor ions of each stoichiometry dissociated stepwise from 1 : n

DOI: 10.1002/jms

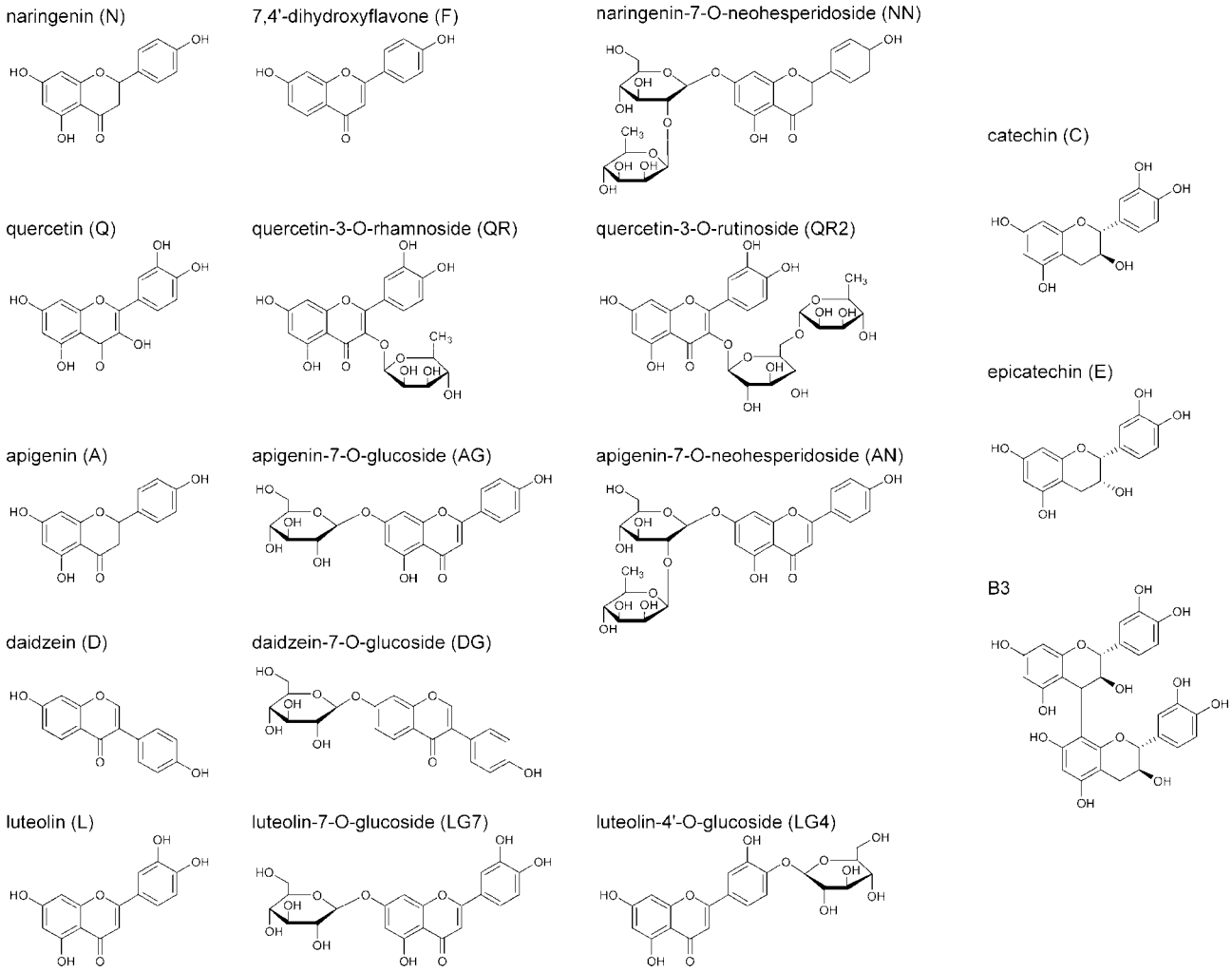

Scheme 11. Structures of flavonoids studied for their affinity towards salivary peptides (Ref. 64).

(peptide : flavonoid) stoichiometry down to 1 : 1, ending with the bare peptide. The direct loss of all bound flavonoids was not observed.

The precursor ions were activated at different percentages of normalized collision energy (NCE) in steps of 0.1% NCE for 30 ms while the q_z value was maintained at 0.25. Three breakdown curves were combined for each experiment and fitted to a Boltzmann curve (Eqn (1)).

$$y = \frac{a}{\left(1 + e^{(b-x)/c}\right)} \quad (1)$$

where a is the maximum response fixed to 1, b half the maximum response, and c is related to the slope of the breakdown curve. An example of such breakdown curves is presented in Fig. 20. The b value determined from this breakdown curve corresponds to the dissociation energy required for dissociation of 50% of the trapped complex.

DE_{50} values are obtained by monitoring the additional energy required to separate the partners of a complex transmitted to the ion trap, thus DE_{50} values represent the relative affinity of flavonoids for the peptide in the gas phase. The influence of the number of charges of the ion was examined using a longer PRP peptide as a probe (34 amino acids, further named $IB9_{34}$). As shown on Table 3 for various stoichiometries of $IB9_{34}$: naringenine-7-*O*-neohesperidoside complex, large DE_{50} differences between 3+ and 4+ charged ions are observed, indicating that the number of charges of the ion has a marked influence on DE_{50} values.

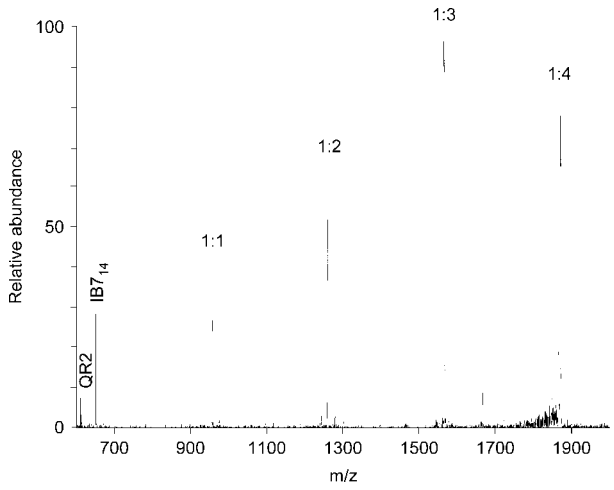

Figure 19. Product ion mass spectrum of the $IB7_{14}$: quercetin-3-*O*-rutinoside (QR2) complex. Precursor ion at *m/z* 1871 corresponds to 1 : 4 stoichiometry (Ref. 64).

DOI: 10.1002/jms

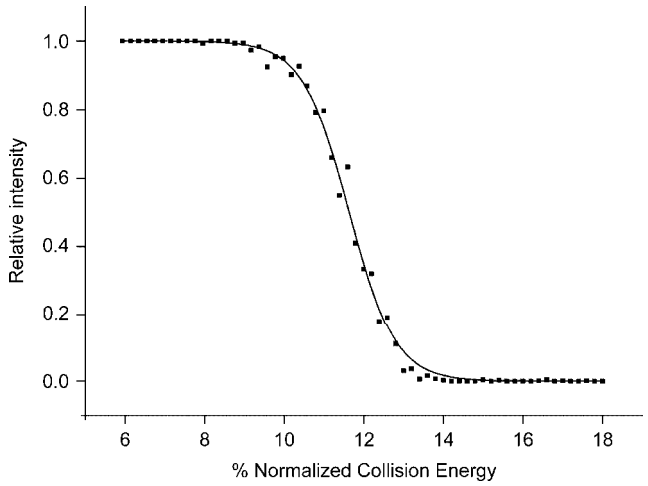

Figure 20. Breakdown curve obtained from normalized raw data (black point) fitted by a Boltzmann curve for 1 : 1 $IB7_{14}$:catechin complex (Ref. 64).

Table 3. DE_{50} of $IB9_{34}$: naringenin-7-*O*-neohesperidoside complexes of different stoichiometries with charge states 3+ and 4+. Average standard deviation for DE_{50} values was approximately 0.003 (Ref. 64)

	Charge state	
Stoichiometry	3+	4+
1 : 1	1.347	1.121
1 : 2	1.333	1.063
1 : 3	1.364	1.018
1 : 4	1.388	1.043

The lower DE_{50} values observed for charge state 4+ compared to 3+ (Table 3) may support the 'horizontal' nature of interaction, and that flavonoid glycoside molecules interact with an exposed charge site on the peptide, thus disturbing the interaction and resulting in a lower DE_{50}. However, $IB7_{14}$: catechin complexes with stoichiometries as high as 1 : 16 were observed; such a situation cannot be obtained with a peptide of 14 amino acids without stacking of flavonoids upon flavonoids already bound to the peptide. Thus, both interpretations must be considered. The observation that complexes dissociated without direct loss of a flavonoid cluster may indicate that aggregates of flavonoids are dissociated more easily by CID than are complexes involving the PRP peptide (see Table 4).

Experiments were performed in a solvent that mimicked the real conditions of interaction in wine. Complexes having a 1 : 1 peptide : flavonoid stoichiometry of 17 flavonoids (Scheme 11) with $IB7_{14}$ were characterized by ERMS; the DE_{50} values are listed in Table 4. The lowest DE_{50} is attributed to naringenin and the highest to quercetin-3-*O*-rutinoside.

Precise DE_{50} values, obtained for each $IB7_{14}$: flavonoid complex, reflect small structural differences between flavonoids (Table 4) as shown by epicatechin and catechin where the DE_{50} values differed by only 0.023; these isomers are differentiated by their stereochemistry at C3. The order of DE_{50} values may be examined for simple flavonoids to determine the influence of hydroxyl group position, presence of a ketone or rigidity of the skeleton (C2–C3 double bond). Epicatechin, catechin, luteolin and quercetin bear a hydroxyl group in position 3′ (B-ring), and their DE_{50} values (>0.744) are higher than those of flavonoids that are not 3′-hydroxylated. Comparison of DE_{50} values for daidzein and 7,4′-dihydroxyflavone shows that flavones, wherein the B-ring is linked to C2 of the flavonoid skeleton, have higher DE_{50} values than do isoflavones (B-ring is linked to C3). This conclusion is supported by the magnitudes of the DE_{50} values determined for apigenin-7-*O*-glucoside and daidzein-7-*O*-glucoside. The contribution of a C2–C3 double bond to the rigidity of the structure of the flavonoids seems not to be a crucial factor for the interaction with the peptide, at least as seen from the respective DE_{50} values for naringenin and apigenin which are lower than those for catechin and epicatechin.

Table 4. DE_{50} values for 1 : 1 $IB7_{14}$: flavonoid complexes and aggregates of two flavonoid molecules. Average standard deviation for DE_{50} values was approximately 0.003 (Ref. 64)

Flavonoid abbreviation	1 : 1 $IB7_{14}$: flavonoid complex	DE_{50} aggregate of two flavonoids
Naringenin	0.694	n.d.
Daidzein	0.713	n.d.
Apigenin	0.726	n.d.
7,4′-Dihydroxyflavone	0.734	n.d.
Quercetin	0.750	n.d.
Catechin	0.794	n.d.
Luteolin	0.797	n.d.
Epicatechin	0.817	0.611
Daidzein-7-*O*-glucoside	0.827	0.638
Luteolin-4′-*O*-glucoside	0.830	0.598
Apigenine-7-*O*-glucoside	0.840	0.641
Luteolin-7-*O*-glucoside	0.841	0.663
Quercetin-3-*O*-rhamnoside	0.872	0.455
Apigenin-7-*O*-neohesperidoside	0.907	0.631
B3	0.936	0.510
Naringenin-7-*O*-neohesperidoside	0.955	0.488
Quercetin-3-*O*-rutinoside	0.991	0.483

The results of this study led to a relative affinity scale in the gas phase for a flavonoid and a peptide that is related to salivary proteins; this scale has the potential to probe the astringency phenomenon. In agreement with DE_{50} values, sensorial analysis related to astringency describes epicatechin as being more effective than catechin in binding with salivary proteins.[82,83] It is known that oligomerization of catechin and epicatechin monomers increases astringency,[84–86] and it was observed here that B3 has a higher affinity for $IB7_{14}$ than does catechin. Simon *et al.*[87] have shown that B3 binds to the hydrophilic side of $IB7_{14}$, suggesting that the stability of the complex is governed by hydrogen bonds; this conclusion is supported by the observation that flavonoids having the highest number of hydroxyl groups display the highest DE_{50} values.

DOI: 10.1002/jms

Comparison of high-energy and low-energy CID of protonated flavonoids

Product ion mass spectra of a series of nine protonated flavonoids have been observed by ESI combined with quadrupole/time-of-flight (ESI QTOF), and matrix-assisted laser desorption ionization (MALDI) combined either with quadrupole ion trap (MALDI QIT) tandem mass spectrometry, or time-of-flight tandem mass spectrometry (MALDI TOF ReTOF).[58] The compounds examined were 3,6-, 3,2′-, and 3,3′-dihydroxyflavone, apigenin (5,7,4′-trihydroxyflavone), luteolin (5,7,3′,4′-tetrahydroxyflavone), apigenin-7-*O*-glucoside, hesperidin (5,7,3′-trihydroxy-4′-methoxyflavanone), daidzein (7,4′-dihydroxyisoflavone), and rutin (quercitin-3-*O*-rutinoside) where quercitin is 3,5,7,3′,4′-pentahydroxyflavone; sodium-cationized rutin was also examined.

The energy in the center-of-mass system, E_{cm}, is related to the laboratory energy, E_{lab}, as in Eqn (2):[88,89]

$$E_{cm} = E_{lab}\left(\frac{m_T}{m_P + m_T}\right) \quad (2)$$

where m_T and m_P are the target and projectile masses, respectively; normally, $m_T \ll m_P$ such that $E_{cm} \ll E_{lab}$. The center-of-mass energy in an ion/neutral collision represents the maximum kinetic energy that can be transferred to internal energy in the ion; hence, only those dissociative pathways of activation energy $<E_{cm}$ can be accessed. The center-of-mass energies in ESI QTOF and MALDI QIT are similar (1–4 eV) and their product ion mass spectra are virtually identical. In the MALDI TOF ReTOF instrument, wherein ions are accelerated to 20 keV, center-of-mass energies range from 126 to 309 eV for sodium-cationized rutin to protonated dihydroxyflavones, respectively. Due to the high center-of-mass energies available with the MALDI TOF ReTOF instrument, product ion mass spectra become simplified with increasing precursor mass/charge ratio so as to be of limited structural value. Electronic excitation of the protonated (and sodium-cationized) species examined may offer an explanation for the simple product ion mass spectra observed here particularly for glycosylated flavonoids.

Experiments were performed on a Q TOF II mass spectrometer (Micromass, Manchester, UK) equipped with a Z-spray ES source; this instrument is referred to as an ESI QTOF tandem mass spectrometer. Positive ion MALDI mass spectra were acquired on an AXIMA QIT-TOF (Shimadzu Biotech, Manchester, UK); this instrument is referred to as a MALDI QIT tandem mass spectrometer. Positive ion mass spectra in the MS and MS/MS modes of operation were acquired on an Axima TOF/ReTOF instrument (Shimadzu Biotech, Manchester, UK).[90] ReTOF refers to the curved field reflectron (CFR) that permits efficient collection of all fragment ions, including those produced from metastable decay as well as CID occurring in the collision cell. This instrument is referred to as a MALDI TOF ReTOF tandem mass spectrometer.

CID of a protonated methoxylated trihydroxyflavone, hesperidin

Hesperidin (5,7,3′-trihydroxy-4′-methoxyflavanone) differs from apigenin (5,7,3′-trihydroxyflavone) in two respects; the former is methoxylated at the 4′-position whereas apigenin is not, and the C(2)–C(3) ethylenic bond in apigenin has been hydrogenated in hesperidin. The product ion mass spectra of protonated hesperidin, m/z 303, as observed from ESI QTOF and MALDI TOF ReTOF are shown in Fig. 21. The base peak m/z 153 in the product ion mass spectrum of Fig. 21(a), obtained by ESI under conditions of $E_{cm} = 3.5$ eV and of high mass resolution with a QTOF instrument, is the $^{1,3}A^+$ species whereas the m/z 177 product ion is the $^{1,4}B^+ - 2H$ species formed by the loss of the A-ring moiety $C_6H_6O_3$. Product ions of m/z 145 and 117 are possibly formed by 0,3 C-ring scission; the resulting $^{0,3}B^+$ ion (m/z 167) is not observed as it dissociates immediately by loss of H_2O and of ($H_2O + CO$) to yield m/z 145 and 117, respectively.

The product ion mass spectrum obtained by MALDI TOF ReTOF and shown in Fig. 21(b), for which $E_{cm} = 260.6$ eV, is striking in that the two major product ions, m/z 176 and 152, are radical cations and correspond to the two major product ions observed under ESI conditions less a hydrogen atom in each case. It was proposed that the elemental compositions for m/z 176 and 152 are $C_{10}H_8O_3^{+\bullet}$ and $C_7H_4O_4^{+\bullet}$, respectively. In each product ion mass spectrum is observed at low ion signal intensity m/z 285 due to the loss of H_2O. Hesperidin affords the sole example where product ions formed through collisions of high center-of-mass energy ions have resembled those formed through collisions of low center-of-mass energy ions. The high center-of-mass energy in the MALDI TOF ReTOF instrument is manifested in the observation of a series of hydrocarbon ions of the form $C_3H_x^+$ ($x = 1$–6), $C_4H_x^+$ ($x = 1$–6), $C_5H_x^+$ ($x = 1$–8), and $C_6H_x^+$ ($x = 2$–8). The elemental composition of protonated hesperidin is $C_{16}H_{14}O_6^+$; as the C : H ratio in the precursor ion is <1, formation of the above series of hydrocarbon product ions having C : H ratios of >1 requires substantial rearrangements of the precursor ion. Such rearrangements are possible in CID processes where $E_{cm} = 260.6$ eV.

CID of a protonated trihydroxyflavone, apigenin

The product ion mass spectra of protonated apigenin, 5,7,3′-trihydroxyflavone, m/z 271, as observed from ESI QTOF and MALDI TOF ReTOF are shown in Fig. 22. The uppermost product ion mass spectrum, that was obtained under conditions of $E_{cm} = 3.9$ eV and of high mass resolution with a QTOF instrument, affords a classic tandem mass spectrometric example of a protonated (or deprotonated) flavonoid. In such cases, product ions are formed by CRCs of the C-ring (Scheme 2) and by opening of the C-ring followed by successive fragmentations in which small, stable molecules are lost. In Fig. 22(a), the two major peaks at m/z 153 and 119 are identified as $^{1,3}A^+$ and $^{1,3}B^+$, respectively; they are complementary products of retro-Diels–Alder reactions (CRC). The product ions of m/z 163 and 145 are identified as the $^{0,4}B^+$ and $^{0,4}B^+$-H_2O species, respectively. The remaining product ions of m/z 253, 243, 229, 225, 203, 197, 187, and 169 are due, respectively, to C-ring opening (RO) followed by losses of H_2O, CO, C_2H_2O, ($H_2O + CO$), ($C_2H_2O + C_2H_2$), ($H_2O + 2CO$), 3CO, and ($H_2O + 3CO$). The product ion mass spectrum obtained by MALDI QIT (Fig. 22(b)) is remarkably similar to that

DOI: 10.1002/jms

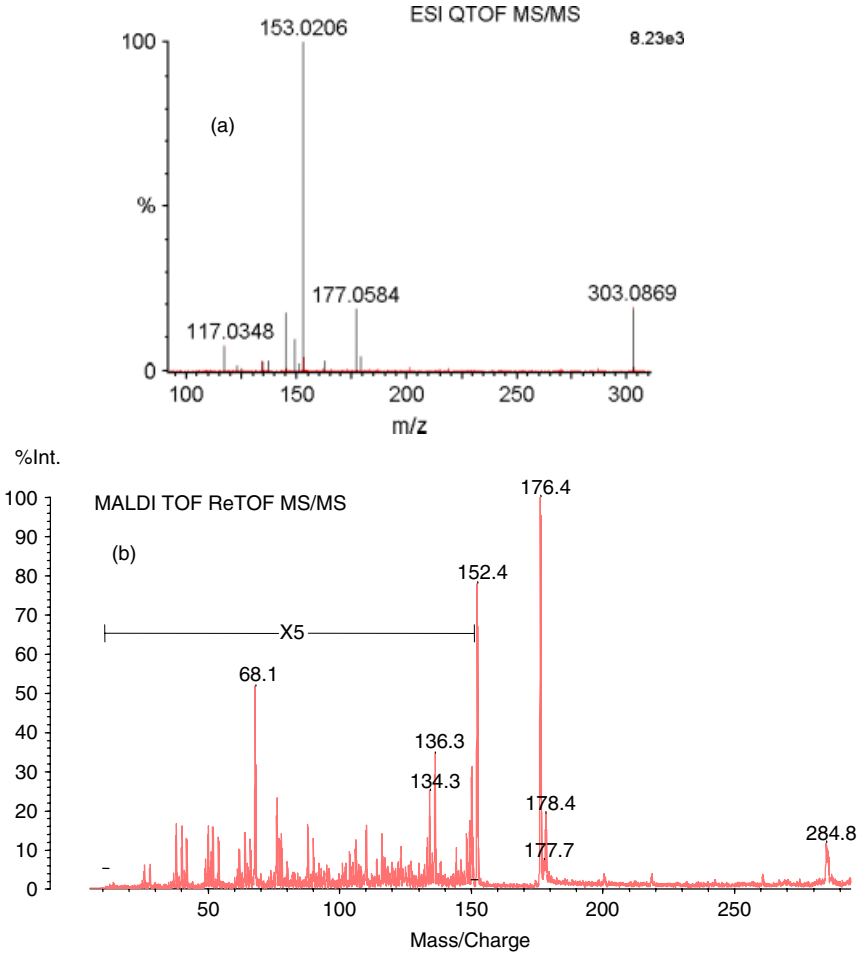

Figure 21. Product ion mass spectra of protonated hesperidin (5,7,3′-trihydroxy-4′-methoxyflavanone) *m/z* 303. (a) Observed with ESI QTOF; (b) MALDI TOF ReTOF (Ref. 58 .

of Fig. 22(a) with respect to both product ion species and relative ion signal intensities.

The product ion mass spectrum obtained by MALDI TOF ReTOF at $E_{cm} = 290.1$ eV and shown in Fig. 22(c) differs markedly from those of Fig. 22(a), (b). The ion of m/z 245 corresponds to the loss of an oxygen atom from protonated apigenin while that of m/z 166 corresponds to the loss of 105 Da from the precursor ion. However, 2,3 (or 1,2) cleavage in a flavone involves scission of an ethylenic bond plus a single C–C bond while 2,3 cleavage in daidzein involves scission of but two single C–C bonds. Thus, the identification of m/z 166 as the $^{0,4}B^+ - 3H^\bullet$ ion, formed by the loss of the A-ring fragment $C_6HO_2^\bullet$, may be of greater probability than that of the $^{1,2}A^+$ ion formed by the loss of the B-ring fragment $C_7H_5O^\bullet$. The identity of m/z 84.8 is not clear; however, as C_7H^+ and $C_5H_9O^+$ are unlikely elemental compositions, it is possible that the elemental composition is $C_4H_5O_2^+$. Once more, a series of hydrocarbon ions of the form $C_3H_x^+$ ($x = 1$–5), $C_4H_x^+$ ($x = 3$–9), $C_5H_x^+$ ($x = 4$–10), and $C_6H_x^+$ ($x = 5$–11) was observed.

CID of a protonated di-O-glycosylated pentahydroxyflavone, rutin (quercitin-3-O-rutinoside)

Rutin (quercitin-3-*O*-rutinoside) is a pentahydroxyflavone (quercitin) to which a diglycoside (glucose-rhamnose) has been substituted in the 3-position such that there is an –*O*–linkage between the flavonoid and the diglycoside. An opportunity was afforded to investigate both protonated and sodium-cationized rutin with the above mass spectrometric instruments.

The product ion mass spectra of protonated rutin, m/z 611, as observed from ESI QTOF and MALDI TOF ReTOF and shown in Fig. 23 are relatively simple. In Fig. 23(a) obtained by ESI QTOF with $E_{cm} = 1.8$ eV, the base peak, m/z 303, is the Y_o^+ species that corresponds to loss of the diglycoside (308 Da); the Y_1^+ species observed at m/z 465 corresponds to the loss of a single glycoside (146 Da). The absence of product ions in the range $465 \leq m/z \leq 611$ indicates that fragmentation of the rhamnose moiety does not occur with $E_{cm} = 1.8$ eV; however, fragmentation of the glucose moiety is observed in the range $303 \leq m/z \leq 465$. The product ion mass spectrum shown in Fig. 24(b) as observed from MALDI TOF ReTOF with $E_{cm} = 130$ eV is also relatively simple. The center-of-mass energy has been dissipated in fragmentations of the diglycoside moiety. The base peak, m/z 335, of Fig. 23(b) may correspond to the $Y_o^+ + CH_3OH$ species. The radical cations in Fig. 23(b) at m/z 482 and 468 correspond to losses of 129 and 143 Da, respectively. It was proposed that m/z 482 is due to loss of (Rha $-$ OH$^\bullet$) and m/z 468 is due to loss of (Rha $- 3H^\bullet$). The features at m/z 182.5 and 603.4 may be due to ring-opened and hydrogenated glycoside radical cation and the loss of $8H^\bullet$, respectively.

DOI: 10.1002/jms

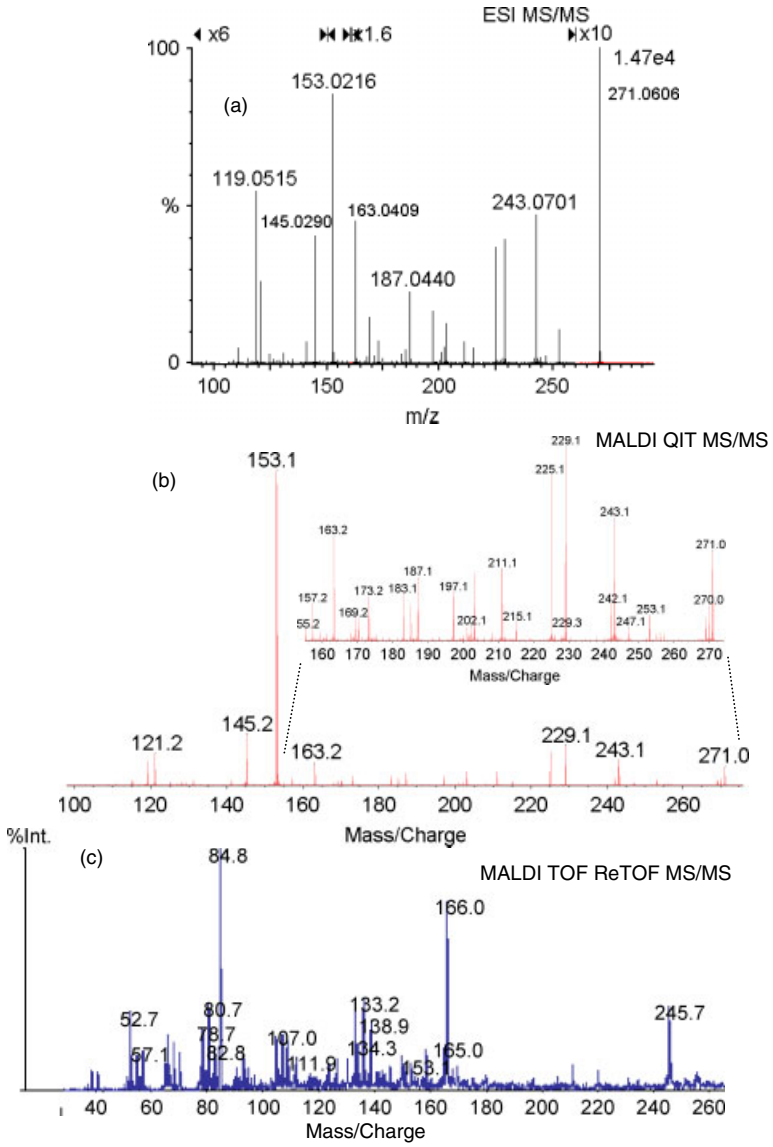

Figure 22. Product ion mass spectra of protonated apigenin (5,7,3′-trihydroxyflavanone) *m/z* 271. (a) Observed with ESI-TOF; (b) MALDI QIT, (c) MALDI TOF (Ref. 58).

The product ion mass spectra of sodium-cationized rutin, *m/z* 633, as observed from ESI QTOF and MALDI TOF ReTOF and shown in Fig. 24 are again relatively simple. In Fig. 24(a), obtained by ESI QTOF with E_{cm} = 1.8 eV, the base peak of *m/z* 331 is the sodium-cationized diglycoside (with the loss of 302 Da) and is accompanied by ion signals of relatively low intensity due to the Y_o^+ and Y_1^+ species. Again, the MALDI QIT product ion mass spectrum (not shown) resembles closely that observed with the ESI QTOF instrument. The base peak in the relatively simple product ion mass spectrum obtained by MALDI TOF ReTOF, with E_{cm} = 125.6 eV and shown in Fig. 24(b) is *m/z* 363 that appears to be sodium-cationized diglycoside plus CH_3OH, (Digly + CH_3OH + Na^+). The product ions of *m/z* 504.7 and 357.7 in Fig. 24(b) are the sodium-cationized analogues of *m/z* 482.7 and 335.3 in Fig. 23(b).

In summary, product ion mass spectra of nonglycosylated flavonoids observed with MALDI TOF ReTOF at high center-of-mass energies do not reflect the competing fragmentation processes observed at low (1–4 eV) center-of-mass energies. Despite the low C : H ratio (<1) in nonglycosylated flavonoids, CID at high E_{cm} values tends to produce hydrocarbon ions of low mass/charge ratio with C : H >1 together with product ions corresponding to the loss of specific hydrocarbon neutrals.

As the mass of the projectile or precursor ion is increased, with concomitant reduction in E_{cm} to 260.6 eV, product ion mass spectra observed with MALDI TOF ReTOF become simpler in that the mass spectra show two or three dominant product ions. The product ion mass spectrum (not shown) of protonated apigenin-7-*O*-glucoside is dominated by the base peak of *m/z* 289.2, proposed as the $Y^+ + H_2O$ species. It is, indeed, curious that with E_{cm} = 183.1 eV, a single fragmentation pathway would be so dominant under these energy-rich conditions.

Naíve expectations of the manifestation of increasing center-of-mass energy in CID are increases in both the number of product ion species and their ion signal intensities. Such expectations are based on the increase in vibrational energy that is expected to be deposited in the projectile ion

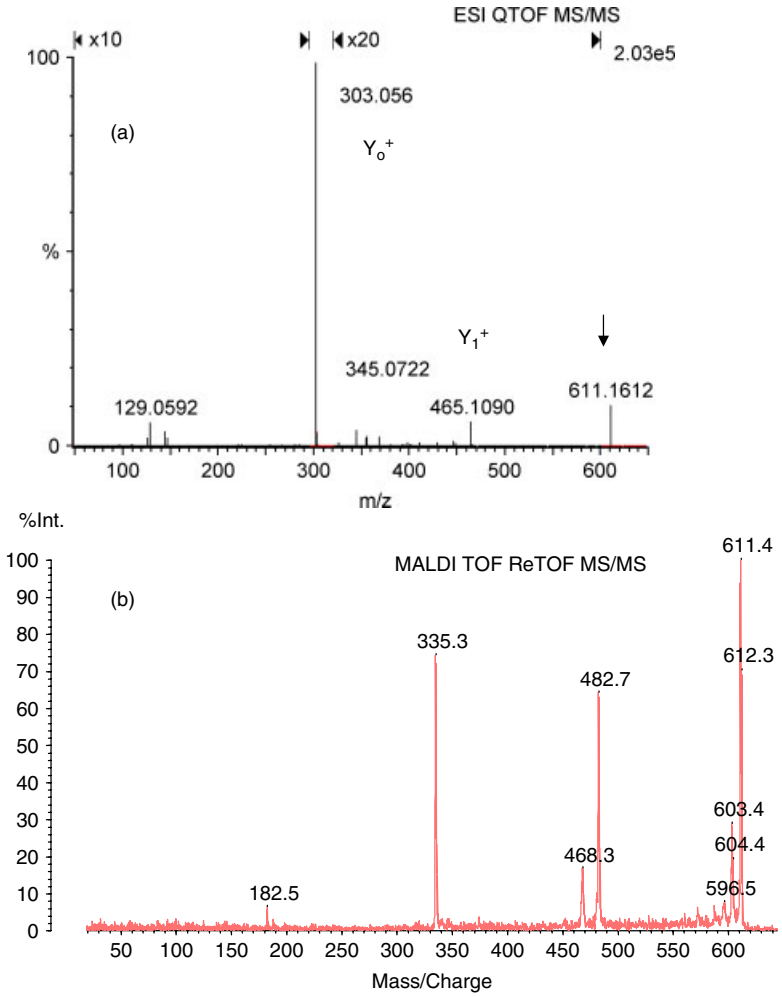

Figure 23. Product ion mass spectra of protonated rutin, *m/z* 611. (a) observed with ESI QTOF and (b) MALDI TOF ReTOF (Ref. 58).

with increasing center-of-mass energy. Thus, the simplification of product ion mass spectra observed must be due to another influence that leads to excitation of the projectile ion with increasing center-of-mass energy but with limited enhancement of projectile ion vibrational energy. In this case, transfer of electronic energy may be considered. Electronic excitation of the protonated species examined may well offer an explanation for the simple product ion mass spectra observed, particularly in Figs 23 and 24.

CHEMICAL COMPUTATIONS

Three *ab initio* studies are noteworthy: (1) Meyer[91] carried out a study of flavone and the flavylium ion to determine the structures and barriers to internal rotation, (2) with respect to the anti-HIV activities of hydroxyflavones, Zhang[92] reported their total energies, atomic charges, dipole moments, multipole moments, molecular orbital compositions, and orbital energies, and (3) conformational analyses of flavone (2-phenyl-4H-benzopyran-4-one) and related compounds have been carried out by Czismadia and coworkers[93] using quantum chemical calculations. In addition, Codorniu-Herna'ndez *et al*.[94] have carried out MO-calculations on the effects of solvation on the structures of flavonoids.

The advent of powerful personal computers has made possible a wide range of computations of molecules and ions that include molecular shape and energies (preferably minimized) of formation, ionization, protonation, etc. The results of such computations have become common features of articles based on MS. Three such examples are discussed in this review. First, possible structures for the [Co(II) + (flavonoid − H) + 2, 2-bipyridine] complexes, shown in Fig. 4, have been computed, and energy-minimized structures for five flavonoids calculated from molecular dynamics simulations are shown in Fig. 5. Second, the computational difficulties of treating ion dissociation when one of the products is a singlet diradical is discussed in this section with reference to the dissociation of deprotonated 3-hydroxyflavone. Third, an attempt to rationalize product ion mass spectra with ^{13}C chemical shifts is described. However, the NMR ^{13}C and ^{1}H shift data were obtained for neutral molecules, thus, it was necessary to adjust the experimental NMR shifts to values appropriate for protonated and deprotonated molecules. To this end, atomic charges for carbon atoms in the neutral, protonated, and deprotonated hydroxyflavone molecules were computed; the linear relationship between computed atomic charges and experimental ^{13}C-chemical shifts permitted the determination of pseudo-^{13}C-chemical shifts for protonated and deprotonated hydroxyflavone molecules (refer NMR spectroscopy below).

DOI: 10.1002/jms

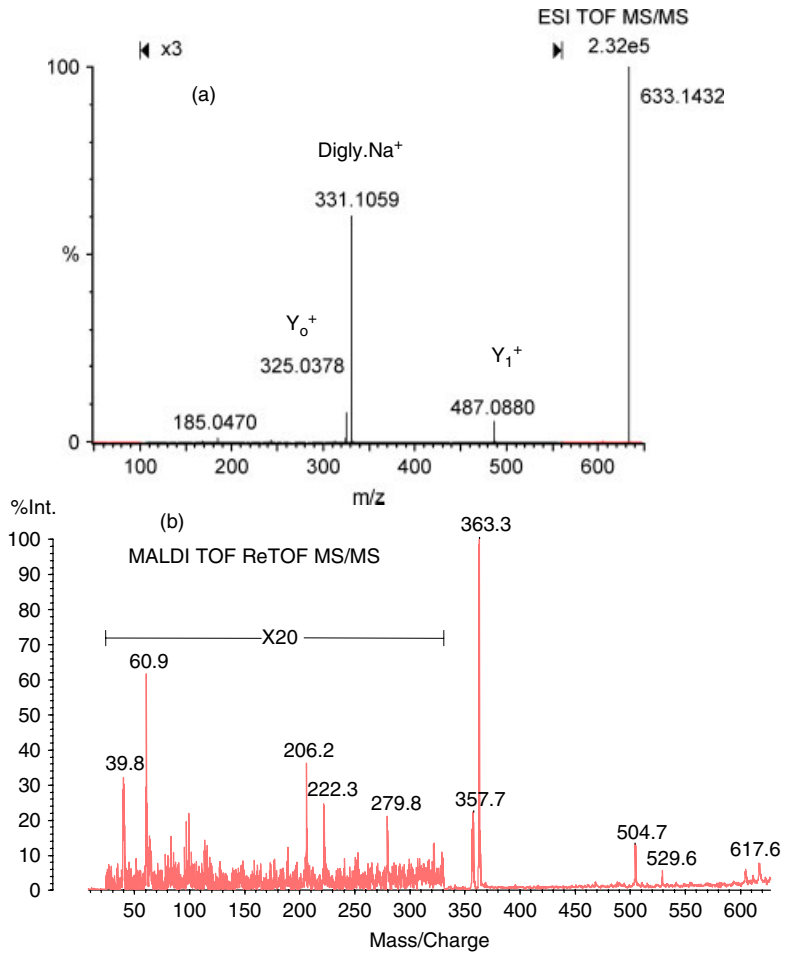

Figure 24. Product ion mass spectra of sodiated rutin, *m/z* 633. (a) observed with ESI-QTOF and (b) MALDI TOF ReTOF (Ref. 58).

Much of the reported tandem mass spectrometric experimental work is accompanied by proposed mechanisms for the formation of product ions; yet the basis for these fragmentation mechanisms is often merely chemical intuition as no chemical computations are carried out. An attempt has been made to rectify this situation through the computation of all probable C-ring fragmentations and successive fragmentations of primary product ions of deprotonated 3-hydroxyflavone.[95]

In a CID study of protonated and deprotonated molecules of 3-, 5-, 6-, 7-, 2′-, 3′- and 4′-hydroxyflavone, it was observed that the ratio, γ, of the propensities for CRC to RO varied by a factor of 660, that is, from 0.014 : 1 (for deprotonated 3-hydroxyflavone) to 9.27 : 1 (for deprotonated 5-hydroxyflavone).[57] Hydroxylation in the C-ring at C(3) leads to a special case for both protonated and deprotonated molecules where the C(2)–C(3) bond becomes highly polarized as shown by the ^{13}C-chemical shift changes in Fig. 4 in Ref. 57. In deprotonated 3-hydroxyflavone, the bond order of the highly polarized C(2)–C(3) bond (see Table 9 of Ref. 57) is reduced to the lowest value of 1.26 which militates against a retro-Diels–Alder reaction (CRC) such that RO dominates; the γ value is reduced to 0.014 : 1. Thus, deprotonated 3-hydroxyflavone exhibited the highest ion signal intensity for fragmentation following RO relative to that for CRC.

The objectives were (1) to compute the energy states of successive generations of product ions formed by RO and subsequent fragmentation of deprotonated molecules of 3-hydroxyflavone and observed by MS/MS, (2) to compute the energy states of product ions formed by retro-Diels–Alder reactions, (3) to identify those pathways of lowest activation energy, and (4) to compare the energetics of RO and retro-Diels–Alder reactions.

All bond energies for the a_0–a_4 cleavage approximation reactions were calculated by the CBS-4M (complete basis set 4M) method[96] using Gaussian 03[97] on model compounds participating in model reactions. A bond dissociation energy (BDE) can, in principle, be calculated by comparing the energies of the radical fragment and the intact molecule. However, reliable BDEs for the breaking of one bond in a large molecule cannot be obtained by a routine 'model chemistry' method, because the energy of a diradical cannot be calculated reliably by such methods. 'Model chemistry' is a term coined by John Pople to denote a calculation based on a straightforward application of an algorithm.[98] Let us consider the BDE of cyclohexane shown in Scheme 12:

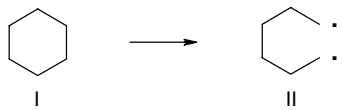

Scheme 12. Bond dissociation in cyclohexane (I) to yield a diradical (II) (Ref. 95).

In order to obtain the BDE of the CC bond in cyclohexane (I), the energies of both I (*EI*) and of the hexane-1,2-diyl radical II (*EII*) are needed. *EI* is obtained readily by a good model chemistry method, but not *EII*, because such methods are based on the assumption that the electrons in the molecule are paired in molecular orbitals. However, in II, there are two molecular orbitals, each of which has one electron; these unpaired electrons have opposite spin and II is a singlet diradical. As model chemistries for singlet diradicals are in the development stage,[99–103] the standard, tested method of handling singlet diradicals is the complete active space self-consistent-field method, CASSCF.[104] However, as CASSCF is time-consuming and requires judgment in its application, it was circumvented by using 'model molecules' with the expectation of obtaining approximate BDEs. Two examples are shown in Scheme 13. Reaction **I** → **II**, which involves a diradical, is approximated by model reaction **I′** → **II′**, which involves two radicals. The strengths of the bonds being broken in these two reactions should be very similar taking into account the possibility that reactants and products may have significantly different strain. Similarly, reaction **III** → **IV**, which involves a diradical, is approximated by model reaction **III′** → **IVa′** + **IVb′**.

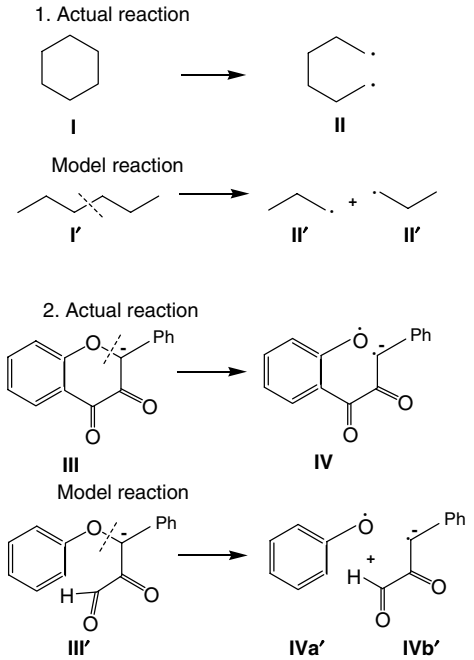

Scheme 13. Two examples of actual reactions that have a diradical product ion together with the substituted model reactions that have two radical product ions (Ref. 95).

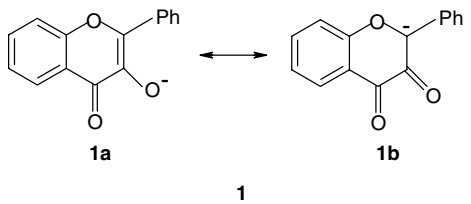

Scheme 14. Anion **1,** deprotonated 3-hydroxyflavone, as a resonance hybrid of the canonical structures **1a** and **1b** (Ref. 95).

Anion **1**, deprotonated 3-hydroxyflavone, is shown in Scheme 14 as a resonance hybrid of the canonical structures **1a** and **1b**; the **1b** representation was used because it lends itself better to depicting cleavage of the five nonbenzenoid bonds (three C–C and two C–O) in the heterocyclic ring when all of them are shown as single bonds.

The magnitudes of the barriers, that is, the bond energies, to homolytic cleavage of the nonbenzenoid bonds of **1** were estimated; the results are summarized in Fig. 25.

The reactions used to estimate these bond energies are set out below. The CC bond shared between the benzene and the heterocyclic rings may be regarded as inviolate compared to the other five bonds, because of the great stability of the benzene nucleus. In Fig. 25, the cleavages a_0–a_4 of the C-ring bonds 0–4 give diradicals B_0–B_4. In order to avoid the quite impractical calculations needed to handle diradicals reliably and directly, each of these reactions was approximated by a process that gave two monoradicals. Bond energies are calculated from the approximation reactions as the energy of products minus the energy of reactants (refer Scheme 15). Using the surrogate structure $\mathbf{A_0}$, the approximated cleavage a_0 was computed as follows:

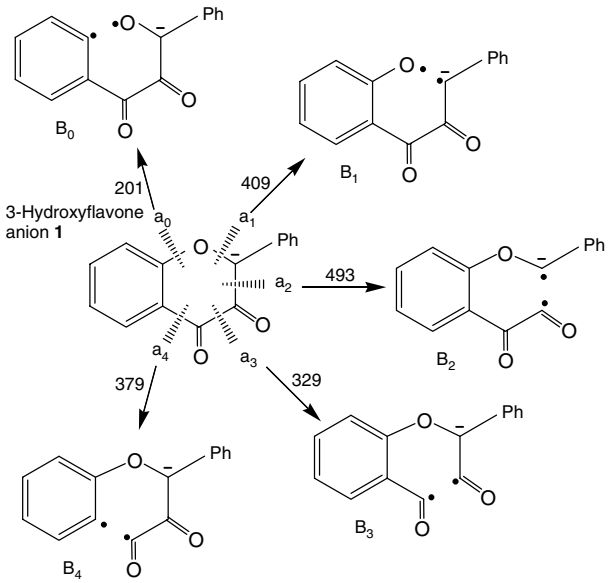

Figure 25. 3-Hydroxyflavone anion. Bonds 0–4 (see Scheme 1) are broken homolytically by reactions a_0–a_4 to form diradicals B_0–B_4. The numbers (379, etc.) indicate the estimated (given in the text) bond energies, in kJ mol^{-1}. The benzenoid bond shared with the heterocyclic ring is assumed to remain intact (given in the text) (Ref. 95).

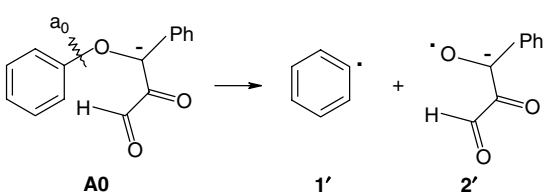

Scheme 15. Model reaction of the surrogate structure $\mathbf{A_0}$ (Ref. 95).

DOI: 10.1002/jms

Bond energies for the a_0-a_4 cleavage approximation reactions were calculated by the CBS-4M (complete basis set 4M) method using Gaussian 03. While this method has a mean square absolute deviation of 14 kJ mol^{-1} on a standard set of molecules; it is somewhat less accurate for these calculations because the 'model structures' used in the approximation reactions are not precisely the ones involved in cleavages in the 3-hydroxyflavone anion **1.** A reasonable estimate of the mean square absolute deviation is *ca*. 30 kJ mol^{-1}. The CBS-4M energies used here are those designated CBS_4 (0 K) in the Gaussian output. For simple bond breaking these energies yield bond energies that match well those in standard tables; for example, the calculated bond energies for $CH_3CH_2-CH_2CH_3$ and CH_3-CH_3 are 366 and 372 kJ mol^{-1}, respectively, while the literature values are 368 and 377 kJ mol^{-1}.[105]

$$\text{Bond dissociation energy (BDE) for } \mathbf{a_0=(1' + 2') - A0}$$
$$= [-231.158466 - 571.499467] - [-802.734523]$$
$$= -802.657933 + 802.734523 = 0.076590 = 201.1 \text{ kJ mol}^{-1} \quad (3)$$

The CBS-4M energies are in atomic units (hartrees) and the reaction energy was converted to kJ mol^{-1} by multiplying with 2626.

The bond strength of bond 0 in the C-ring of the 3-hydroxyflavone anion **1** is, at 201.1 kJ mol^{-1}, the weakest of all the C-ring bonds (Fig. 25). Thus, it was assumed that C-RO occurs by a_0 cleavage to form $\mathbf{B}_0$ and that subsequent fragmentation occurs principally by competing cleavages of $\mathbf{B}_0$. In comparison, the energy of activation for the RDA reaction of **1** $\longrightarrow$ **2 + 3** has a value of 289 kJ mol^{-1}. Because the cleavage $\mathbf{a}_0$ of least energy is but 70% of the RDA reaction of lowest energy of activation, CID of the 3-hydroxyflavone anion **1** will favor markedly RO to CRC leading to a ratio of $\ll 1$ for γ that is in good agreement with experiment where $\gamma = 0.014 : 1$. The most probable RDA reaction involves 1,3 cleavage and this finding is supported by observation of the $^{1,3}B^-$ ion of m/z 117.

NUCLEAR MAGNETIC RESONANCE SPECTROSCOPY

There has been considerable activity in the application of NMR spectroscopy to the structural identification of flavonoids, principally through the utilization of instruments wherein NMR is coupled with LC. A range of flavonoids either have been examined directly or extracted from plants and characterized subsequently by ^{13}C and ^{1}H NMR.[106–111] Wawer and Zielinska[112] have reported the ^{1}H and ^{13}C NMR spectra for a number of flavonoids in dimethyl sulphoxide (DMSO) in addition to the cross-polarization magic angle spinning (CP/MAS) solid-state ^{13}C NMR spectra; among the compounds examined was chrysin (5,7-dihydroxyflavone).

NMR spectroscopy has been combined with FAB/MS/MS (fast atom bombardment/tandem mass spectrometry)[113]; with HPLC/MS for the structural characterization of flavonoids and flavonoid -*O*-glycosides[114,115]; with HPLC-UV (ultraviolet absorbance)-SPE (solid phase extraction)-MS for the identification of flavonoids taxifolin, aromadendrin, eriodictyol, naringenin, and apigenin present in Greek oregano[116]; HPLC/MS for the identification of quercitin and quercetin glycosides in *Hypericum perforatum* L.[114]; HPLC/MS for the identification of quercetin glycosides in apple peel[115]; and with HPLC-UV-MS for the on-line structural investigation of isoflavones and isoflavanones.[117] In addition, ^{13}C NMR spectra have been obtained for a number of flavonoids,[112] and both ^{13}C and ^{1}H NMR spectra have been reported for acylated derivatives of apigenin-7-*O*-glucoside.[118] Recently, Park *et al*.[119] published the NMR ^{1}H and ^{13}C chemical shifts for flavone and 19 substituted flavones among which was 7,8,4′-trihydroxyflavone. Traldi and coworkers have developed a fast and effective analytical method for metabolomic fingerprinting of plant extracts.[120] In this method, they employed ESI-MS and ^{1}H NMR techniques together with statistical analyses of the acquired data. Shahat *et al*. have reported on the characterization of unknown flavonoids of the herb *Farsetia aegyptia Tirra* (Crucifereae) using LC/UV-DAD (photodiode array detection) and LC/ESI-MS in both positive and negative ion modes.[121] They obtained NMR data that permitted structural elucidation of the new flavonoid, isorhamnetin 3-*O*-α-L-arabinoside 7-*O*-[β-D-glucosyl-[1 $\rightarrow$ 2]-α-L-rhamnoside.

In NMR spectroscopy, the magnetic field experienced at the nucleus of an atom is less than that of the applied magnetic field because electrons around the nucleus shield it from the applied field; the difference between the applied magnetic field and the field at the nucleus is termed the *nuclear shielding*. The chemical shift, that is defined as the nuclear shielding/applied magnetic field, is a function of the nucleus and its environment; it is measured relative to a reference compound. For two bonded or adjacent carbon atoms, the chemical shifts reflect the environment of both atoms and are indicative of the order (and thus the strength) of the connecting bond. The environment of a ^{13}C nucleus can also be affected in an inductive, through-space (field effect), or resonance-based manner by substituents that are bonded to its carbon framework. These effects, which become apparent when ^{13}C substituent chemical shift analyses are performed,[122] cause the associated chemical shifts to vary in a systematic and predictable manner.

Rationalization of ^{13}C-chemical shifts with product ion mass spectra

^{13}C-chemical shifts of carbon atoms are required for the prediction of product ion mass spectra of ions subjected to CID. During the development of MS, libraries of electron ionization mass spectra were accumulated so as to assist in the identification of molecules; such libraries have been used extensively with instruments in which gas chromatography is combined with mass spectrometry, (GC/MS). However, in the main, flavonoids are not readily susceptible to examination using GC/MS. In ESI/MS/MS, the precursor ion is normally either the protonated molecule or the deprotonated molecule that undergoes CID to yield a product ion mass spectrum; unfortunately, libraries of such mass spectra do not exist unless one has been accumulated in-house. An alternate approach is to use NMR in order to predict where

DOI: 10.1002/jms

a given protonated or deprotonated flavonoid molecule may dissociate. However, NMR data such as ^{13}C and ^{1}H chemical shifts are not normally available for gaseous ions.

A method has been described for the estimation of ^{13}C chemical shifts in ions; such shifts are described as pseudo-^{13}C-chemical shifts.[57] The method involves computation of atomic charges for each carbon atom in neutral, protonated, and deprotonated molecules and relating atomic charges for molecules with experimental ^{13}C chemical shifts for carbon atoms. The essentially linear relationship between atomic charges and experimental ^{13}C chemical shifts in neutral monohydroxyflavones, together with computed atomic charges for carbon atoms in protonated and deprotonated molecules, can be applied to obtain pseudo-^{13}C-chemical shifts in protonated and deprotonated molecules. The pseudo ^{13}C-chemical shifts in ions have been applied, in turn, to the rationalization of the relative propensities for competing CRC and RO fragmentations observed in product ion mass spectra of protonated and deprotonated monohydroxyflavone molecules. For convenience, the pseudo-^{13}C-chemical shifts in protonated molecules can be expressed relative to pseudo-^{13}C-chemical shifts in protonated flavone, while those for deprotonated molecules can be expressed relative to NMR ^{13}C-chemical shifts in flavone.

The gap between NMR spectroscopy and MS has been bridged by chemical computations using the semiempirical PM3 method. The clear advantage of chemical computations is that it is possible to examine both charged species and neutral species.

The pseudo-^{13}C-chemical shifts obtained were applied to the rationalization of product ion mass spectra of protonated and deprotonated molecules of flavone and 3-, 5-, 6-, 7-, 2′-, 3′ -, and 4′ -hydroxyflavones, where product ion formation is due to either CRC of the C-ring (retro-Diels–Alder reaction) or to cleavage of a C-ring bond followed by loss of either a small neutral molecule or a radical. The total product ion abundance ratio of C-ring cross-cleavage to C-ring bond cleavage, γ, varied by a factor of 660 for deprotonated monohydroxyflavones, i.e. from 0.014 : 1 to 9.27 : 1. The magnitude of γ, which is dependent on the relative bond orders within the C-ring of the protonated and deprotonated molecules of monohydroxyflavones, can be rationalized on the basis of the magnitudes of the ^{13}C- and ^{1}H-chemical shifts as determined by NMR spectroscopy.

Charge density versus ^{13}C chemical shifts

In Scheme 16 are shown (a) the calculated Mulliken charges for flavone[93] and (b) the ^{13}C chemical shifts for flavone

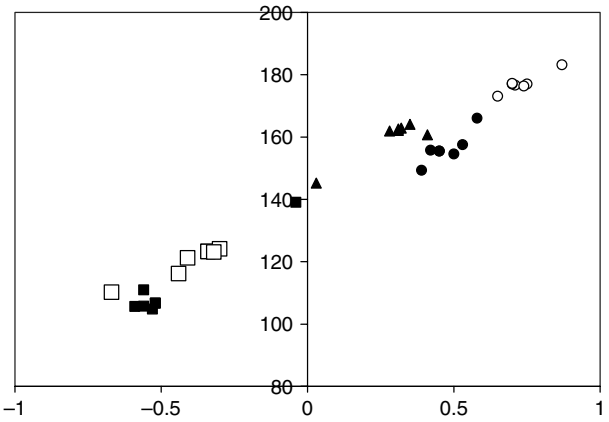

Figure 26. A plot of the experimental ^{13}C chemical shift *versus* the computed ESP charge for each of the C-ring atoms C(2) (▲), C(3) (■), C(4) (○), C(10) (□), and C(9) (●) in each of the neutral 3-, 5-, 6-, 7-, 8-, 2′-, 3′-, and 4′-hydroxyflavones (Ref. 57).

observed experimentally. The degree of shielding by electron density at each carbon correlates very well with the ^{13}C chemical shifts. In order to relate the ^{13}C chemical shift data to the variation of the tandem mass spectrometric parameter γ, let us compare the C-ring experimental ^{13}C chemical shift values with the PM3-method computed values for the ESP charges on the C- ring atoms for neutral 3-, 5-, 6-, 7-, 8-, 2′-, 3′-, and 4′-hydroxyflavones. In Fig. 26 are plotted the ^{13}C chemical shifts for each of the C-ring atoms C(2), C(3), C(4), C(10), and C(9) *versus* the computed ESP charges for these carbon atoms in each of the seven monohydroxy-flavones. The data points in Fig. 26 fall on or are close to a line of slope = 51 ppm/charge thus there is an approximate linear relationship between experimental ^{13}C chemical shift and computed ESP charge.

Figure 26 shows that for, say, the C(4) atom, where the triangular data points are found in the top right hand corner, the experimental and computed data vary slightly according to the position of substitution of the hydroxyl group. There are some exceptions to this general observation: the outliers for C(2) and C(3) were observed (and computed) in each case from 3-hydroxyflavone while that for C(10) was observed from 5-hydroxyflavone. Within the dataset for each C-ring carbon atom, two points were observed to have the same values with the result that while there are seven data points in each set, only six are apparent in Fig. 26; in each case, a carbon atom in 3′-hydroxyflavone has a value identical with a carbon atom in another hydroxyflavone.

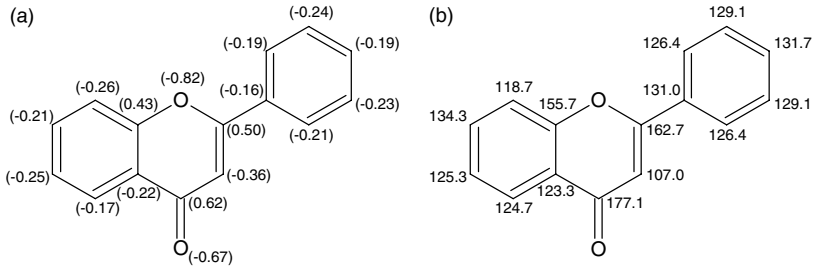

Scheme 16. (a) Calculated Mulliken charges for flavone (Ref. 92) and (b) observed ^{13}C NMR chemical shifts for flavone (Ref. 57).

DOI: 10.1002/jms

Because the computed charge density values show a roughly linear relationship with experimental ^{13}C chemical shifts, an examination can be made of the variation of computed charge density values for neutral, protonated, and deprotonated monohydroxyflavones.

In Fig. 27 are shown the computed charge density (or atomic charge) values for 5-, 6-, 7-, 8-, 2′-, 3′-, and 4′-hydroxyflavones. All the changes in magnitude of computed atomic charge in going either from neutral to protonated state or from neutral to deprotonated state are small, generally less than 0.2 atomic charges; however, a change of such magnitude is significant because the corresponding ^{13}C chemical shift difference is some 10 ppm. Generally, the computed charge density value of a carbon atom in a molecule does not change polarity upon either protonation or deprotonation; however, C(2) and C(3) in 3-hydroxyflavone, as shown in Fig. 28, exhibit both reversal in computed charge density polarity upon either protonation or deprotonation and somewhat greater variations than 0.2 atomic charges.

For neutral 3-hydroxyflavone, the charge difference between C(2) and C(3) is 0.03-(−0.04) = 0.07. When the linearity between ^{13}C chemical shift values and the computed PM3-method values for the ESP charges is assumed, where the slope is 51 ppm/charge, the difference between ^{13}C chemical shift values is predicted as 0.07 charges × 51 ppm/charge = 3.6 ppm whereas the experimental value from NMR is 145.2−139.1 = 6.1 ppm. For 5-, 6-, 7-, 2′, and 4′-hydroxyflavones, the computed charge differences between C(2) and C(3) correspond to predicted differences between ^{13}C chemical shift values of 47.9, 44.4, 40.8, 49.7, and 43.3 ppm compared with experimental values of 58.4, 56.3, 55.2, and 58.1 ppm, respectively. Due to the reversal in polarity of the atomic charges upon either protonation or deprotonation for C(2) and C(3) in 3-hydroxyflavone (Fig. 28), the charge difference between C(2) and C(3) in protonated 3-hydroxyflavone is given by the atomic charge of C(2) less that of C(3), −0.24-(0.20) = −0.44, while that in deprotonated 3-hydroxyflavone is given as −0.58−0.46 = −1.04.

Prediction of protonated and deprotonated chemical shifts for comparison with γ

It is convenient to express the ^{13}C chemical shifts (δ) for C-ring atoms in neutral monohydroxyflavones relative to those of flavone, that is, as $\Delta\delta_{monohyd} = \delta_{monohyd} - \delta_{flavone}$. Prior to this operation, the ^{13}C chemical shifts for flavone are expressed relative to those for chromone, that is, as $\Delta\delta_{flavone} = \delta_{flavone} - \delta_{chromone}$. The results of these operations are shown in Table S1 of the supporting electronic information section. For example, δC(2) in flavone is 162.6 ppm while δC(2) in chromone is 156.9 ppm, thus $\Delta\delta_{flavone} = \delta_{flavone} - \delta_{chromone}$ for C(2) in flavone is 162.6−156.9 = 5.7 ppm (Table S1). Similarly, δC(2) in 7-hydroxyflavone is 161.9 ppm while δC(2) in flavone is 162.6 ppm, thus $\Delta\delta_{7-OH} = \delta_{7-OHflavone} - \delta_{flavone}$ for C(2) in 7-hydroxyflavone is 161.9−162.6 = −0.7 ppm (Table S1). In the last three rows in Table S1 are given the averages of the relative differences for each of the A-, B-, and C-rings. The value of Table S1 is that it affords an opportunity for correcting the computed values of relative chemical shifts in protonated and deprotonated monohydroxyflavones that were obtained using the average linear dependence of ^{13}C chemical shift with atomic charge shown in Fig. 26.

For protonated monohydroxyflavones, the ^{13}C chemical shifts are expressed relative to those of protonated flavone and are shown in Table S2. For example, δC(2) in flavone is 162.6 ppm and the change in ESP charge upon protonation, that is, final charge – initial charge, is 0.13−0.28 = −0.15 charges; this change in charge equates to a decrease in δC(2) in flavone of −7.65 ppm such that δC(2) in protonated flavone is 162.6−7.65 = 154.95 ppm. Similarly, δC(2) in neutral 7-hydroxyflavone is 161.9 ppm and the change in ESP charge upon protonation is 0.14−0.28 = −0.14 charges; this change in charge equates to a decrease in δC(2) in 7-hydroxyflavone

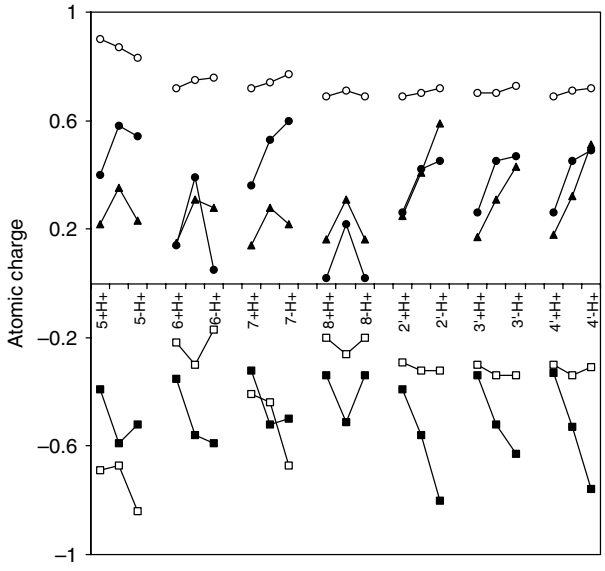

Figure 27. Computed charge density values for protonated, neutral, and deprotonated 5-, 6-, 7-, 8-, 2′-, 3′-, and 4′-hydroxyflavones (Ref. 57).

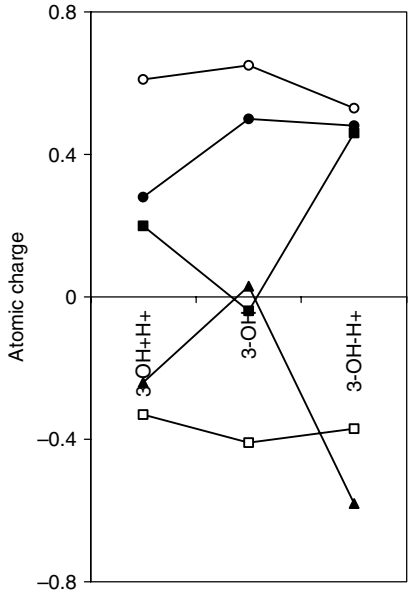

Figure 28. Computed charge density values for protonated, neutral, and deprotonated 3-hydroxyflavone. C(2) (▲), C(3) (■), C(4) (○), C(10) (□), and C(9) (●) (Ref. 57).

DOI: 10.1002/jms

upon protonation of −7.14 ppm such that δC(2) in protonated 7-hydroxyflavone is 161.9–7.14 = 154.76 ppm. Thus δC(2) in protonated 7-hydroxyflavone relative to δC(2) in protonated flavone, ($\Delta\delta C(2)_{7-OHflavoneH^+} = \delta C(2)_{7-OHflavoneH^+} - \delta C(2)_{flavoneH^+}$) is 154.76–154.95 = −0.19 ppm. Isomer-specific departure from the ideal linear dependence of ^{13}C chemical shift with atomic charge (Fig. 26) is corrected for. The corrected values for ^{13}C chemical shift differences are shown in Table S3. The net effect of this correction procedure, Eqn (4), is that, using C(2) in protonated 7-hydroxyflavone as an example:

$$\Delta\delta C(2)_{corr} = [2\delta_{7-OH} - 2\delta_{flavone} + (\Delta charge_{7-OH} - \Delta charge_{flavone}) \times 51 \text{ ppm/charge}] \quad (4)$$

With respect to the computed ^{13}C chemical shifts for C-ring atoms in deprotonated monohydroxyflavones, the point of reference must be changed because flavone cannot be deprotonated by loss of a hydroxyl hydrogen atom. In this case, the computed ^{13}C chemical shifts are expressed relative to those for neutral flavone.

The correction for isomer-specific departure from the ideal linear dependence of ^{13}C chemical shift with atomic charge (Fig. 27) is the same as for protonated species; the difference between the chemical shifts for neutral 7-hydroxyflavone and neutral flavone, −0.7 ppm, is added to the above value of $\Delta\delta C(2)_{7-OH-H}{}^{+} = -3.76$ ppm to obtain $\Delta\delta C(2)_{corr} = -4.46$ ppm. The corrected values for ^{13}C chemical shift differences are shown in Table S3. The net effect of this correction procedure, Eqn (5), is that, using C(2) in protonated 7-hydroxyflavone as an example:

$$\Delta\delta C(2)_{corr} = [\delta_{7-OH} - \delta_{flavone} + (\Delta charge_{7-OH} \times 51 \text{ ppm/charge})] \quad (5)$$

where $\Delta charge_{7-OH}$ refers to the ESP charge on C(2) in deprotonated 7-hydroxy-flavone less that on C(2) in the neutral molecule.

Compound-specific relation of ^{13}C chemical shifts to γ

In protonated monohydroxyflavones, hydroxylation of carbon atoms in the A- and B-rings exerts a significant, but minor influence on the C(2), C(3), and C(4) ^{13}C chemical shift changes (relative to protonated flavone), as shown diagrammatically in Fig. 29 and, therefore, on electron densities. For the B-ring, this is likely because rotation around C(2)-C(1′) (diphenyl bridge) reduces the resonance between the B- and C-rings. Crystal structures of a number of neutral hydroxyflavones[123–127] show that the O–C(2)–C(1′)–C(2′) dihedral angle (B-ring twist) is between 5 and −10°, moving the A, C and B-ring system out of planarity and, therefore, disrupting resonance between the rings. The computed values of the B-ring twist dihedral angles are shown in Fig. 29. Extended conjugation from ring A into ring C is terminated at C(4) which limits the effect of A-ring hydroxylation on C(2) and C(3). Thus, changes in C-ring electron density are small for protonated 5-, 6-, 2′-, and 4′-hydroxyflavone such that the γ values are essentially constant at ∼2 : 1. Increased electron density at C(10) in protonated 7-hydroxyflavone is accompanied by enhanced 1,4 CRC that may account for an increase in the γ value to 5.12 : 1. The diminution of the γ value to 0.77 : 1 in protonated 3′-hydroxyflavone is not readily explained. Hydroxylation in the C-ring at C(3), that is, protonated 3′-hydroxyflavone, is a special case; the ^{13}C chemical shift changes reveal that the C(2)–C(3) bond becomes highly polarized such that enhanced RO leads to a reduced γ value to 1.42 : 1.

In deprotonated monohydroxyflavones, 3-, 2′-, and 4′-hydroxylation leads to resonance structures wherein the bond order of the C(2)–C(3) bond is reduced. In each case, the B-ring twist is approximately 0° indicating a near planar arrangement of the A, B, and C-rings. Hydroxylation in the C-ring at C(3) leads to another special case where, again, the C(2)–C(3) bond becomes highly polarized as shown by the ^{13}C chemical shift changes in Fig. 29. The C(2)–C(3) bond order is reduced to the lowest value of 1.26 which militates against a retro-Diels–Alder reaction (CRC) such that RO dominates; the γ value is reduced to 0.014 : 1. Increased electron density at C(10) upon deprotonation of the A-ring hydroxyl substituent at C(5) contributes to a diminished C(3)–C(4) bond order that, along with resonance within the $^{-}$O–C(5)=C(10)–C(4) = O system, will facilitate 1,3 and 0,3 CRCs at the expense of RO; the observed γ value is 9.27 : 1. As the location of hydroxylation is changed from 2′- to 3′- to 4′- in deprotonated monohydroxyflavones, the electron densities at both C(2) and C(3) are increased leading to an increase in γ values from 0.70 : 1 to 1.61 : 1 to 7.69 : 1, respectively.

Deprotonation of the A-ring hydroxyl substituents at C(6) and C(7) results in increased electron densities at C(9) and C(10), respectively. In the former case, the accompanying electron density decrease at C(10) brings about a weakening of both the C(2)–C(3) and C(4)–C(10) bonds, thus facilitating RO (and militating against CRC) to yield γ = 0.019 : 1. In the latter case, the increased electron density at C(10) combined with resonance in the –O–C(7) = C(6)–C(5) = C(10)–C(4) = O system leads to weakening and strengthening of the O–C(2) and C(2)–C(3) bonds, respectively. The net result is that the propensity of the C-ring for CRC *versus* RO fragmentations in deprotonated 7-hydroxyflavone (γ = 0.17 : 1) is intermediate between those of deprotonated 5- and 6-hydroxyflavones.

Predictive model

An approach has been described whereby the monohydroxyflavone ^{13}C chemical shifts have been assigned and compared to those of flavone for the development of a predictive tool for the ^{13}C NMR of polyhydroxylated flavonols and their glycosylated analogues.[128] This tool, which relies on the cumulative chemical shift differences between a test set of shifts (i.e. the monohydroxyflavonols) and a baseline set of shifts (i.e. flavone), has been used to predict polyhydroxyl flavonoid chemical shifts. The predicted ^{13}C chemical shifts were then compared to the measured ^{13}C chemical shifts of the polyhydroxyflavones and to previously reported polyhydroxyflavone ^{13}C chemical shifts as a test for accuracy in this approach. The ^{1}H and ^{13}C NMR data of flavone, the monohydroxyflavonols (3-, 5-, 6-, 7-, 2′-, 3′- and 4′-hydroxyflavone),

DOI: 10.1002/jms

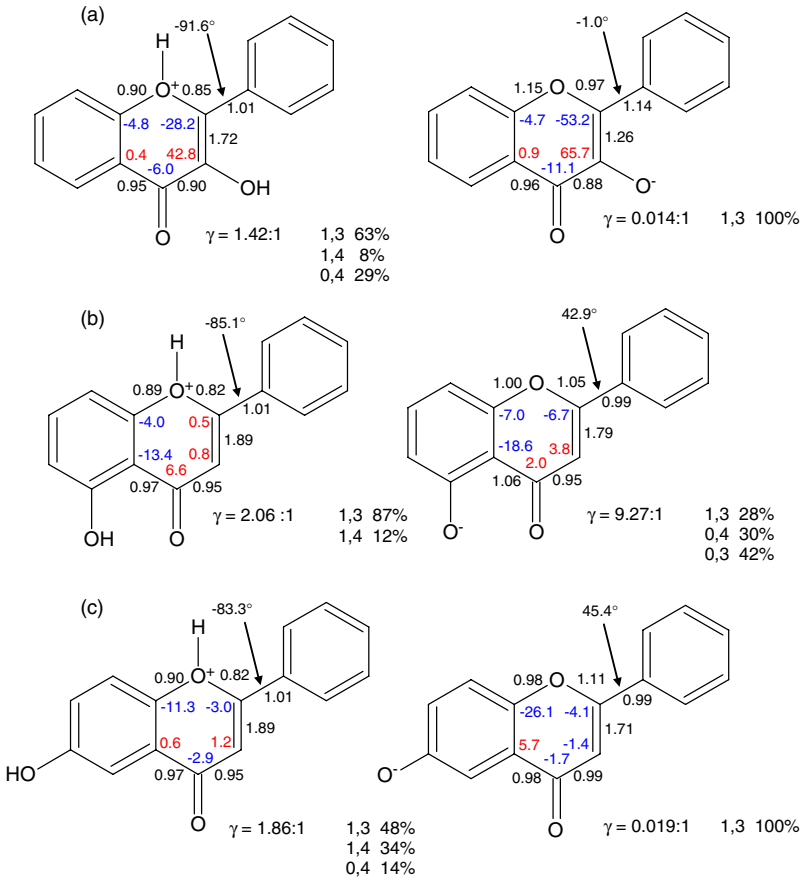

Figure 29. Structures of protonated and deprotonated monohydroxyflavones showing exterior to the C-ring computed bond orders of C-ring atoms and, interior to the C-ring, ^{13}C chemical shift changes as given in Tables S2 and S3. A positive ^{13}C chemical shift change reflects a decrease in electron density relative to flavone. The computed dihedral angle O–C(2)–C(1′)–C(2′) is shown in each structure. Also shown are the respective γ values and the populations (%) of predominant cross-ring cleavage fragmentation pathways observed. (a) 3- (b) 5- (c) 6-hydroxyflavone (Ref. 57).

selected polyhydroxylated flavonoids (3,2′-, 3,3′-, 3,4′-, 2′, 3′-, and 3,6-dihydroxyflavone, apigenin (5,7,4′-trihydroxyflavone) luteolin (5,7,3′,4′-tetrahydroxyflavone)), and glycosylated flavonoids (luteolin-8*C*-*β*-D-glucoside (orientin), luteolin-6*C*-*β*-D-glucoside (homoorientin), and apigenin-8*C*-*β*-D-glucoside (vitexin)), for which the structures are shown in Fig. 1 are presented here along with an assessment of this simple approach for predicting flavonoid ^{13}C chemical shifts.

It was reported that, for the monohydroxyflavones, ^{13}C chemical shift differences can be used to assess the impact of hydroxylation with regards to the modification of the flavone electronics and structure. These shift differences may be measured for the polyhydroxyflavones (Eqn (6)) or may be predicted by summing the chemical shift differences between the constituent monohydroxyflavones and flavone (Eqn (7)):

$$\Delta\delta_{\text{measured}} = (\delta_{\text{phf}} - \delta_{\text{flavone}}) \quad (6)$$

$$\Delta\delta_{\text{predicted}} = \Sigma[(\delta_{\text{mhf1}} - \delta_{\text{flavone}}) + (\delta_{\text{mhf2}} - \delta_{\text{flavone}})\ldots] \quad (7)$$

$$\Delta = \Delta\delta_{\text{measured}} - \Delta\delta_{\text{predicted}} \quad (8)$$

where 'mhf 1' and 'mhf 2' are monohydroxyflavones and 'phf' is the corresponding polyhydroxyflavone.

For illustration, let us consider the value of Δ from Eqn (8) for C2 from 3,2′-dihydroxyflavone. According to Eqn (6), $\Delta\delta_{\text{measured}} = 147.6 - 162.6 = -15.0$ ppm as shown in Table S4. In accordance with Eqn (7), $\Delta\delta_{\text{predicted}}$(C2 from 3,2′-dihydroxyflavone) = $\Sigma[(^{13}\text{C}$ shift for C2 in 3-hydroxyflavone $- ^{13}$C shift for C2 in flavone) + (^{13}C shift for C2 in 2′-hydroxyflavone $- ^{13}$C shift for C2 in flavone)]. Using the appropriate values, $\Delta\delta_{\text{predicted}}$(C2 from 3,2′-dihydroxyflavone) = $\Sigma[(145.2 - 162.6) + (160.7 - 162.6)] = [(-17.4) + (-1.9)] = -19.3$ pm. Thus $\Delta = -15.0 - (-19.3) = 4.3$ ppm, as shown in Table S4.

The glycosylated polyhydroxyflavone NMR spectra were analyzed by comparing their ^{13}C chemical shifts to flavone (Eqn (9)). These chemical shift differences, $\Delta\delta_{\text{g}}$, were then compared against the nonglycosylated analogues, $\Delta\delta_{\text{phf}}$ (Eqns (10), (11)), to reveal the impact of glycosylation on polyhydroxyflavone electrostatics (Table S4):

$$\Delta\delta_{\text{g}} = \delta_{\text{glycosylated polyhydroxyflavone}} - \delta_{\text{flavone}} \quad (9)$$

$$\Delta\delta_{\text{phf}} = \delta_{\text{polyhydroxyflavone}} - \delta_{\text{flavone}} \quad (10)$$

$$\Delta_{\text{g}} = \Delta\delta_{\text{g}} - \Delta\delta_{\text{phf}} \quad (11)$$

where 'g' and 'phf' have identical hydroxyl-substitution patterns.

Many of the nuclei within vitexin, orientin, and homoorientin yield small δ_{g} values, particularly those of the B- and

C-rings ($\delta_g \leq 0.2$ ppm). In these situations, the factors that influence the chemical shifts, electronics, and structure for each compound and its aglycan analogue are equivalent, and their local structures and electrostatics are likely similar. By extrapolation, one can assume that the overriding influences of polyhydroxyl substitution on flavone electrostatics, would be expected to occur in the glycosylated analogues. Hence, it may be presumed that the structure and electronics of the B- and C-rings of homoorientin and its C6-glucoside analogue, luteolin, are similar because their ^{13}C chemical shifts are equivalent. Thus, the B- and C-rings of homoorientin are not at all influenced by glycosylation.

Vitexin, orientin, and homoorientin are all examples of A-ring glycosylated flavonoids, and it is these resonances that are affected to the greatest extent. Overall, glycosylation is expected to contribute in an additive way to the chemical shift positions (and electrostatics) of ^{13}C and ^{1}H nuclei in much the same manner as additional hydroxyl substituents affect the electrostatics of each monohydroxyflavone. In each of the glycosylated flavonoids, the ^{13}C resonances at the site of substitution are shifted downfield significantly (C_{ipso}; $\Delta = 10.2$ to 10.9 ppm). The remaining A-ring carbon nuclei and C-ring C9 nucleus are shielded with respect to the nonglycosylated analogues ($\Delta_g = -0.4$ to -1.7 ppm). Thus, additional electron density is drawn into the A-ring in response to electron withdrawal at the site of glucopyranose substitution. These chemical shift differences are not apparent in C6-substituted homoorientin and must, therefore, be indicative of indirect and/or direct through-space interactions between the C8-substituted glycosyl subunit and rings B and C. Hydrogen bonding between the glycosyl unit and B-ring is not possible for vitexin so that additional deshielding of the H2′/H6′, C1′, and C2′/C6′ nuclei may occur either as a result of their proximity to the glucopyranose ring or as a result of interaction with O1 on the C-ring.

^{1}H and ^{13}C NMR data have been recorded for flavone, selected monohydroxy-, dihydroxy-, trihydroxy-, and tetrahydroxyflavones, as well as three glycosylated flavones (luteolin-6C-β-D-glucoside, luteolin-8C-β-D-glucoside, and apigenin-8C-β-D-glucoside). The ^{13}C chemical shifts of flavone can be grouped to the A-, B-, or C-rings and perturbations in these shifts upon hydroxylation and glycosylation are readily identifiable. For the hydroxylated flavones, the ^{13}C NMR assignments and number of hydroxyl substituents can be estimated based simply on inspection and comparison of the ^{13}C chemical shifts relative to those of flavone. There should be at least 1 $\Delta\delta$ value above +27.4 ppm for each hydroxyl group and 2 $\Delta\delta$ values above 16.5 ppm for each 1,2-diol. Because the measured polyhydroxyflavone chemical shift differences and predicted values are in close agreement and because the measured chemical shift differences will match closely to one set *only* of predicted chemical shift differences, the ^{13}C assignments of the polyhydroxyflavones may be identified immediately without the need for a rigorous gradient heteronuclear multiple bond coherence (gHMBC)-based assignment strategy. The number and location of flavone glycosyl substituents may also be predicted based solely on a ^{13}C chemical shift analysis since glycosylation was found to deshield the ^{13}C nuclei at the site of substitution (causing a 10.2 ppm upfield shift) without significantly affecting the remaining chemical shifts.

The accuracy of this tool was assessed by comparing the reported ^{13}C chemical shifts of several di- and trihydroxylated flavones[15,129–131] to their predicted values (Tables S5 and S6, respectively). The measured and predicted ^{13}C chemical shifts of the dihydroxyflavones were in close agreement ($\leq \pm 0.4$ ppm). The predicted ^{13}C chemical shifts differed from the reported ^{13}C chemical shifts when two or more hydroxyl substituents were able either to participate in hydrogen bonding with one another (i.e. 3′,4′-dihydroxyflavone, Table S5) or to affect strongly the environment of a single ^{13}C nucleus. This latter behavior was most apparent when two hydroxyl groups occupied positions that were meta to one another on ring A or ring C. Thus, a 5,7-dihydroxy substitution pattern, as in apigenin and luteolin, can be recognized by an average deviation of -2.1 ppm at C6 and of 2.7 ppm at C8 from the predicted value and a 2′,4″-dihydroxy substitution pattern could be recognized by deviations of 0.9 ppm at C1′, -0.4 ppm at C3′, and 1.9 ppm at C5′ from the predicted values. Chemical shift deviations of similar magnitude were consistent amongst each of the dihydroxyflavones suggesting that these could be treated as correction factors for the predicted values, although this approach was not taken. The reported and predicted chemical shifts of 3,7,3′-, and 3,7,4′-trihydroxyflavone (Table S6) were consistent and exhibited differences of >0.4 ppm at only 4 of 30 ^{13}C nuclei, while those of 3,6,3′-, and 3,6,4′-trihydroxyflavone were not inconsistent with those observed for 3,6-dihydroxyflavone. Thus, on the whole, the predicted and measured chemical shifts of the trihydroxyflavones are in good agreement.

From Table S5, it was proposed that a deviation of >4 ppm between the measured and predicted ^{13}C chemical shifts indicated either an incorrect assignment or an incorrectly reported ^{13}C chemical shift. In the case of 6,4′-dihydroxyflavone, there were four chemical shifts whose predicted and reported values differed by more than ±3.9 ppm: $\Delta C3 = 3.9$ ppm; $\Delta C5 = -4.0$ ppm; $\Delta C6 = -5.6$ ppm; and $\Delta C9 = 5.6$ ppm (Table S5). When the assignments of C3 and C5 were switched for one another and those of C6 and C9 were switched similarly, then the chemical shift deviations of these nuclei fell within $< \pm 0.3$ ppm. Thus, the reported chemical shifts for C3, C5, C6, and C9 in 6,4′-dihydroxyflavone are incorrect. For 3,7,4′-trihydroxyflavone, there was a deviation (Δ of -10.0 ppm between the reported and predicted C1′ ^{13}C chemical shifts (Table S6). It was proposed that the reported C1′ chemical shift (112.1 ppm) should have been given as 121.1 ppm, which is in line with similarly substituted flavones, and would yield a more reasonable chemical shift deviation of -1.0 ppm.

Overall, the polyhydroxy- and glycosylated flavone chemical shifts and, by proxy, their structure and electronics are *fully predictable*. The power of such a tool is apparent for predicting the NMR of flavonoids and identifying unknown flavonoids from novel sources. For example, a search using SciFinder[132] revealed that ^{13}C NMR spectra of only 11 of 28 commercially available dihydroxyflavones

DOI: 10.1002/jms

have been recorded and analyzed. Using the proposed strategy proposed, ^{13}C NMR data for the remaining 17 flavonoids can be predicted. The ^{13}C chemical shifts for 8-hydroxyflavone, which does not occur in nature, have been predicted using this model.[133] The ^{13}C chemical shifts can also be predicted for polyhydroxylated flavonoids for which NMR spectra have not been observed, for rapid assessment of unassigned flavonoids NMR spectra and for verifying previously reported ^{13}C chemical shifts of flavonoids. The prediction of these values is of importance because it allows quick and facile assessment of flavonoid structure and electronics, which can be important for determining their behavior in laboratory, environmental, and *in vivo* settings.

OTHER RESEARCH AREAS

Despite the enormous importance of LC to the overall efficiency of the detection and identification of flavonoids from natural sources, there is little evidence of systematic examination of the optimization of LC conditions for MS/MS. An exception is the study of the effects of eluent on the ionization efficiencies of flavonoids by ion spray (IS), atmospheric pressure chemical ionization (APCI), and atmospheric pressure photoionization mass spectrometry (APPI).[134] Nine different eluent compositions were found to have a great effect on the ionization efficiency; the optimal ionization conditions were achieved in positive ion IS and APCI using 0.4% formic acid (pH 2.3) as a buffer, and in negative ion IS and APCI using ammonium acetate buffer (pH 4.0). For APPI, the eluent of choice appeared to be a mixture of organic solvent and 5 mM aqueous ammonium acetate. The results show that negative ion IS with an eluent system consisting of acidic ammonium acetate buffer provides the best conditions for detection of flavonoids by MS.

The pK_a values of flavonoids are of importance because they determine the order of deprotonation of the hydroxyl substituents. While computational programs exist for the calculation of pK_a values, experimental verification is desirable. Such experimental verification of dissociation constants of flavonoids using capillary electrophoresis has been reported.[135] While for catechin and epicatechin, the first ionizable OH group occurs in the B-ring and the second ionizable group in the A-ring; in flavonols the order is reversed.

CONCLUSIONS

MS/MS continues to be a powerful technique for the analysis of flavonoids in conjunction with chromatographic techniques, particularly, LC. Metal complexation strategies that can be implemented easily post-column, that is, following LC elution, have met with great success in the LC/MS differentiation of flavonoid diglycoside isomers. A variant of metal complexation is the addition of ligands to the metal complex in order to extend the range of differentiation. In particular, the addition of a chromophoric ligand enhances the application of IRMPD for the differentiation of isomers. Analytical chemistry is vital to the analysis of flavonoids in plant extracts and, thus, to the optimization of the beneficial effects of the Mediterranean diet. The astringency of red wine, an important yet somewhat controversial component of this diet, has been examined in the context of the variation of the binding affinity of flavonoids to proline-rich proteins.

The gas-phase ion chemistry of flavonoids is an active area of research particularly when combined with accurate mass measurement. Yet often in fragmentation studies, attention is focused on the constancy of experimental conditions rather than on the variation of the collision energy in the center-of-mass frame, E_{cm}. It is the magnitude of E_{cm} that determines the dissociation channels that may be observed. An example has been discussed where the value of E_{cm} was varied by a factor of ~100 to illustrate the wide variety of accompanying ion fragmentation behavior. The enhanced application of a variety of *ab initio* and chemical computation methods to the study of flavonoids is applauded. The results of computations of ion and molecular structures have been shown together with computations of atomic charges and ion fragmentation.

Rarely does MS alone, even MS^n, provide an unambiguous structure and it becomes necessary to combine MS with spectroscopic techniques such as UV and NMR for structure determination. The application of LC, where the eluent is split between MS and NMR, constitutes a powerful combination for the determination of molecular structure but this technique has not yet been applied significantly to flavonoids (as distinct from the NMR examination of pure compounds). The combination of MS with NMR reveals an uneasy interface of two solitudes because the practitioners of each technique are rarely comfortable in their understanding of the other. In such collaborations, the reliance of MS practitioners upon NMR practitioners is almost total, and vice versa. A threefold attempt has been made to facilitate comprehension of NMR on the part of the MS practitioner: (1) a simple predictive tool, which can be applied using a spreadsheet, may now be applied to the calculation of accurate ^{13}C NMR spectra for all flavonoids, methoxyflavones, and flavonoid glycosides for the rapid assessment of ^{13}C NMR spectra, and for assigning substitution patterns in newly isolated flavonoids; (2) chemical computation of atomic charge can bridge the gap between neutral and protonated (or deprotonated) molecules such that pseudo-^{13}C chemical shifts may be estimated for protonated (or deprotonated) molecules; and (3) product ion mass spectra of flavonoids may be rationalized with ^{13}C NMR spectra.

Supporting Information

Supporting information may be found in the online version of this article.

Acknowledgements

JSB acknowledges the financial support from The Welch Foundation (F1155) and NIH (NIH RO1 GM63512). REM acknowledges the financial support from each of the Natural Sciences and Engineering Research Council of Canada (Discovery Grants Program), the Canada Foundation for Innovation, the Ontario Research & Development Challenge Fund, and Trent University.

JMS

REFERENCES

1. Bohm BA. *Introduction to the Flavonoids*. Harwood Academic: Australia, 1998.
2. Sjostrom E. *Wood Chemistry Fundamentals and Applications*. Academic Press: New York, London, 1981.
3. Bate-Smith EC. In *Wood Extractives and their Significance to the Pulp and Paper Industries*, W. E. Hillis (ed). Academic Press: New York, London, 1962; 133.
4. Harborne JB, Grayer RJ. In *The Flavonoids: Advances in Research Since 1986*, J. B. Harborne (ed). Chapman & Hall: London, 1994; 589.
5. Beck V, Unterrieder E, Krenn L, Kubelka W, Jungbauer A. Comparison of hormonal activity (estrogen, androgen and progestin) of standardized plant extracts for large scale use in hormone replacement therapy. *Journal of Steroid Biochemistry and Molecular Biology* 2003; **84**: 259.
6. Boue SM, Wiese TE, Nehls S, Burow ME, Elliott S, Carter-Wientjes CH, Shih BY, McLachlan JA, Cleveland TE. Evaluation of the estrogenic effects of legume extracts containing phytoestrogens. *Journal of Agricultural and Food Chemistry* 2003; **51**: 2193.
7. Shirley BW. Flavonoid biosynthesis: 'new' functions for an 'old' pathway. *Trends in Plant Science* 1996; **1**: 377.
8. Fritz KL, Seppanen CM, Kurzer MS, Csallany AS. The *in vivo* antioxidant activity of soybean isoflavones in human subjects. *Nutrition Research* 2003; **23**: 479.
9. Dixon RA, Steel CL. Flavonoids and isoflavonoids – a gold mine for metabolic engineering. *Trends in Plant Science* 1999; **4**: 394.
10. Gerhauser C, Klimo K, Heiss E, Neumann I, Gamal-Eldeen A, Knauft J, Liu GY, Sitthimonchai S, Frank N. Mechanism-based in vitro screening of potential cancer chemopreventive agents. *Mutation Research* 2003; **523**: 163.
11. Packer L, Rimach G, Virgili F. Antioxidant activity and biologic properties of a procyanidin-rich extract from pine (*pinus maritima*) bark, pycnogenol. *Free Radical Biology and Medicine* 1999; **27**: 704.
12. Yao LH, Jiang YM, Shi J, Tomás-Barberán FA, Datta N, Singanusong R, Chen SS. Flavonoids in food and their health benefits. *Plant Foods for Human Nutrition* 2004; **59**: 113.
13. Chung KT, Wong TY, Wei CI, Huang YW, Lin Y. Tannins and human health: a review. *Critical Reviews in Food Science and Nutrition* 1998; **38**: 421.
14. Baron-Menguy C, Bocquet A, Guihot A-L, Chappard D, Amiot M-J, Andriantsitohaina R, Loufrani L, Henrion D. Effects of red wine polyphenols on postischemic neovascularization model in rats: low doses are proangiogenic, high doses anti-angiogenic. *FASEB (Federation of American Societies Experimental Biology) Journal* 2007; **21**: 3511, DOI: 10.1096/fj.06-7782com.
15. Aviram M, Fuhrman B. Wine flavonoids protect against LDL oxidation and atherosclerosis. *Annals of the New York Academy of Sciences* 2002; **957**: 146.
16. Cuyckens F, Claeys M. Mass spectrometry in the structural analysis of flavonoids. *Journal of Mass Spectrometry* 2004; **39**: 1, erratum 2004; **39**: 461.
17. Ma YL, Li QM, Van den Heuvel H, Claeys M. Characterization of flavone and flavonol aglycones by collision-induced dissociation tandem mass spectrometry. *Rapid Communications in Mass Spectrometry* 1997; **11**: 1357.
18. Domon B, Costello C. A systematic nomenclature for carbohydrate fragmentations in FAB-MS/MS spectra of glycoconjugates. *Glycoconjugate Journal* 1988; **5**: 397.
19. Cuyckens F, Ma YL, Pocsfalvi G, Claeys M. Tandem mass spectral strategies for the structural characterization of flavonoid glycosides. *Analusis* 2000; **28**: 888.
20. Li QM, van den Heuvel H, Dillen L, Claeys M. Differentiation of 6-C- and 8-C- glycosidic flavonoids by positive ion fast atom bombardment and tandem mass spectrometry. *Biological Mass Spectrometry* 1992; **21**: 213.
21. Li QM, Claeys M. Characterization and differentiation of diglycosyl flavonoids by positive fast atom bombardment and tandem mass spectrometry. *Biological Mass Spectrometry* 1994; **23**: 406.
22. Cuyckens F, Shahat AA, Pieters L, Claeys M. Direct stereochemical assignment of hexose and pentose residues in flavonoid O-glycosides by fast atom bombardment and electrospray ionization mass spectrometry. *Journal of Mass Spectrometry* 2002; **37**: 1272.
23. Cuyckens F, Rozenburg R, Hoffmann E, Claeys M. Structure characterization of flavonoid O-diglycosides by positive and negative nano-electrospray ionization ion trap mass spectrometry. *Journal of Mass Spectrometry* 2001; **36**: 1203.
24. Ma Y-L, Cuyckens F, Van den Heuvel H, Claeys M. Mass spectrometric methods for the characterisation and differentiation of isomeric O-diglycosyl flavonoids. *Phytochemical Analysis* 2001; **12**: 159.
25. Ma Y-L, Van den Heuvel H, Claeys M. Characterization of 3-methoxyflavones using fast-atom bombardment and collision-induced dissociation tandem mass spectrometry. *Rapid Communications in Mass Spectrometry* 1999; **13**: 1932.
26. Ma Y-L, Vedernikova I, Van den Heuvel H, Claeys M. Internal glucose residue loss in protonated O-diglycosyl flavonoids upon low-energy collision-induced dissociation. *Journal of the American Society for Mass Spectrometry* 2000; **11**: 136.
27. Hughes RJ, Croley TR, Metcalfe CD, March RE. A tandem mass spectrometric study of selected characteristic flavonoids. *International Journal of Mass Spectrometry* 2001; **210/211**: 371.
28. Waridel P, Wolfender J-L, Ndjoko K, Hobby KR, Major HJ, Hostettmann K. Evaluation of quadrupole time-of-flight tandem mass spectrometry and ion-trap multiple-stage mass spectrometry for the differentiation of C-glycosidic flavonoid isomers. *Journal of Chromatography A* 2001; **926**: 29.
29. Hvattum E, Ekeberg D. Study of the collision-induced radical cleavage of flavonoid glycosides using negative electrospray ionization tandem quadrupole mass spectrometry. *Journal of Mass Spectrometry* 2003; **38**: 43.
30. Justesen U. Collision-induced fragmentation of deprotonated methoyxlated flavonoids, obtained by electrospray ionization mass spectrometry. *Journal of Mass Spectrometry* 2001; **36**: 169.
31. Fabre N, Rustan I, de Hoffmann E, Quetin-Leclercq J. Determination of flavone, flavonol, and flavanone aglycones by negative ion liquid chromatography electrospray ion trap mass spectrometry. *Journal of the American Society for Mass Spectrometry* 2001; **12**: 707.
32. Ferreres F, Llorach R, Gil-Izquierdo A. Characterization of the interglycosidic linkage in di-, tri-, tetra- and pentaglycosylated flavonoids and differentiation of positional isomers by liquid chromatography/electrospray ionization tandem mass spectrometry. *Journal of Mass Spectrometry* 2004; **39**: 312.
33. Ablajan K, Abliz Z, Shang X-Y, He J-M, Zhang R-P, Shi J-G. Structural characterization of flavonol 3,7-di-*O*-glycosides and determination of the glycosylation position by using negative ion electrospray ionization tandem mass spectrometry. *Journal of Mass Spectrometry* 2006; **41**: 352.
34. Kang J, Hick LA, Price WE. A fragmentation study of isoflavones in negative electrospray ionization by MS^n ion trap mass spectrometry and triple quadrupole mass spectrometry. *Rapid Communications in Mass Spectrometry* 2007; **21**: 857.
35. Zhao Y, Wang L, Bao Y, Li C. A sensitive method for the detection and quantification of ginkgo flavonols from plasma. *Rapid Communications in Mass Spectrometry* 2007; **21**: 971.
36. Geng P, Zhang R, Aisa HA, He J, Qu K, Zhu H, Abliz Z. Fast profiling of the integral metabolism of flavonols in the active fraction of *Gossypium herbaceam* L. using liquid chromatography/multi-stage tandem mass spectrometry. *Rapid Communications in Mass Spectrometry* 2007; **21**: 1877.
37. Hvattum E. Determination of phenolic compounds in rose hip (*Rosa canina*) using liquid chromatography coupled to

electrospray ionisation tandem mass spectrometry and diode-array detection. *Rapid Communications in Mass Spectrometry* 2002; **16**: 655.
38. March RE, Miao X-S, Metcalfe CD, Stobiecki M, Marczak L. A fragmentation study of an isoflavone glycoside, genistein-7-O-glucoside, using electrospray quadrupole time-of-flight mass spectrometry at high mass resolution. *International Journal of Mass Spectrometry* 2004; **232**: 171.
39. Satterfield M, Brodbelt J. Enhanced detection of flavonoids by metal complexation and electrospray ionization-mass spectrometry. *Analytical Chemistry* 2000; **72**: 5898.
40. Satterfield M, Brodbelt JS. Structural characterization of flavonoid glycosides by collisionally activated dissociation of metal complexes. *Journal of the American Society for Mass Spectrometry* 2001; **12**: 537.
41. Zhang J, Brodbelt JS. Structural characterization and isomer differentiation of chalcones by electrospray ionization tandem mass spectrometry. *Journal of Mass Spectrometry* 2003; **38**: 555.
42. Pikulski M, Brodbelt JS. Differentiation of flavonoid glycoside isomers by using metal complexation and electrospray ionization mass spectrometry. *Journal of the American Society for Mass Spectrometry* 2003; **14**: 1437.
43. Davis B, Brodbelt JS. Determination of the glycosylation site of flavonoid monoglucosides by metal complexation and tandem mass spectrometry. *Journal of the American Society for Mass Spectrometry* 2004; **15**: 1287.
44. Zhang J, Wang J, Brodbelt JS. Threshold dissociation and molecular modeling of transition metal complexes of flavonoids. *Journal of the American Society for Mass Spectrometry* 2005; **16**: 139.
45. Zhang J, Wang J, Brodbelt JS. Characterization of flavonoids by aluminum complexation and collisional activated dissociation. *Journal of Mass Spectrometry* 2005; **40**: 350.
46. Zhang J, Brodbelt JS. Silver complexation and tandem mass spectrometry for differentiation of isomeric flavonoid diglycosides. *Analytical Chemistry* 2005; **77**: 1761.
47. Davis B, Brodbelt JS. LC-MS^n methods for saccharide characterization of monoglycosyl flavonoids using post-column manganese complexation. *Analytical Chemistry* 2005; **77**: 1883.
48. Davis BD, Needs P, Kroon P, Brodbelt JS. Identification of isomeric flavonoid glucuronides in urine and plasma by metal complexation and liquid chromatography/tandem mass spectrometry. *Journal of Mass Spectrometry* 2006; **41**: 911.
49. Pikulski M, Wilson J, Aguilar A, Brodbelt JS. Amplification of infrared multiphoton dissociation efficiency in a quadruple ion trap by using IR-active ligands. *Analytical Chemistry* 2006; **78**: 8512.
50. Pikulski M, Aguilar A, Brodbelt JS. Tunable transition metal-ligand systems for enhanced elucidation of flavonoid diglycosides by electrospray ionization mass spectrometry. *Journal of the American Society for Mass Spectrometry* 2007; **18**: 422.
51. Davis BD, Brodbelt JS. Regioselectivity of human UDP-glucuronsyltransferase 1A1 in the synthesis of flavonoid glucuronides determined by metal complexation and tandem mass spectrometry. *Journal of the American Society for Mass Spectrometry* 2008; **19**: 246.
52. Clowers BH, Hill HH Jr. Influence of cation adduction on the separation characteristics of flavonoid diglycoside isomers using dual gate-ion mobility-quadrupole ion trap mass spectrometry. *Journal of Mass Spectrometry* 2006; **41**: 339.
53. March RE, Miao X-S, Metcalfe CD. A fragmentation study of a flavone triglycoside, kaempferol-3-O robinoside-7-O-rhamnoside. *Rapid Communications in Mass Spectrometry* 2004; **18**: 931.
54. Croley TR, Hughes RJ, Metcalfe CD, March RE. Observation of apigenin anionic oligomers in the gas phase. *Rapid Communications in Mass Spectrometry* 2000; **14**: 1494.
55. Croley TR, Hughes RJ, Hao C, Metcalfe CD, March RE. Observation of Na+-bound oligomers of quercetin in the gas phase. *Rapid Communications in Mass Spectrometry* 2000; **14**: 2154.
56. March RE, Miao X-S. A fragmentation study of kaempferol using electrospray quadrupole time-of-flight mass spectrometry at high mass resolution. *International Journal of Mass Spectrometry* 2004; **231**: 157.
57. Burns DC, Ellis DA, Li H, Lewars EG, March RE. A combined NMR and computational study of monohydroxyflavones applied to product ion mass spectra. *Rapid Communications in Mass Spectrometry* 2007; **21**: 437.
58. March RE, Li H, Belgacem O, Papanastasiou D. High-energy and low-energy collision-induced dissociation of protonated flavonoids generated by MALDI and by electrospray ionization. *International Journal of Mass Spectrometry* 2007; **262**: 51.
59. Cuyckens F, Claeys M. Determination of the glycosylation site in flavonoid mono-O-glycosides by collision-induced dissociation of electrospray-generated deprotonated and sodiated molecules. *Journal of Mass Spectrometry* 2005; **40**: 364.
60. March RE, Lewars EG, Stadey CJ, Miao X-S, Zhao X, Metcalfe CD. A comparison of flavonoid glycosides by electrospray tandem mass spectrometry. *International Journal of Mass Spectrometry* 2006; **248**: 61.
61. Iwashina T. The structure and distribution of the flavonoids in plants. *Journal of Plant Research* 2000; **113**: 287.
62. Markham KR. *Techniques of Flavonoid Identification*. Academic Press: London, 1982.
63. Plet B. Doctoral Thesis, La spectrométrie de masse dans l'étude de l'interaction entre proteins de la salive humaine et polyphénols,' Université Bordeaux 1, March 2007.
64. Plet B, Schmitter J-M. Private communication.
65. Hart KJ, McLuckey SA. Relative dissociation energy measurements using ion trap collisional activation. *Journal of the American Society for Mass Spectrometry* 1994; **5**: 250.
66. Colorado A, Brodbelt J. An empirical approach to estimation of critical energies by using a quadrupole ion trap. *Journal of the American Society for Mass Spectrometry* 1996; **7**: 1116.
67. Crowe MC, Brodbelt JS. Evaluation of noncovalent interactions between peptides and polyether compounds via energy-variable collisionally activated dissociation. *Journal of the American Society for Mass Spectrometry* 2003; **14**: 1148.
68. Baxter NJ, Lilley TH, Haslam E, Williamson MP. Multiple interactions between polyphenols and a salivary proline-rich protein repeat result in complexation and precipitation. *Biochemistry* 1997; **36**: 5566.
69. Charlton AJ, Baxter NJ, Khan ML, Moir AJG, Haslam E, Davies AP, Williamson MP. Polyphenol/peptide binding and precipitation. *Journal of Agricultural and Food Chemistry* 2002; **50**: 593.
70. Shimada T. Salivary proteins as a defense against dietary tannins. *Journal of Chemical Ecology* 2006; **32**: 1149.
71. Codorniu-Herna'ndez E, Mesa-Ibirico A, Montero-Cabrera LA, Marti'nez-Luzardo F, Borrmann T, Stohrer W-D. Theoretical study of flavonoids and proline interactions. Aqueous and gas phases. *Journal of Molecular Structure (Theochem)* 2003; **623**: 63.
72. Chen Y, Hagerman AE. Characterization of soluble non-covalent complexes between bovine serum albumin and beta-1,2,3,4,6-penta-O-galloyl-D-glucopyranose by MALDI-TOF MS. *Journal of Agricultural and Food Chemistry* 2004; **52**: 4008.
73. Papadopoulou A, Green RJ, Frazier RA. Interaction of flavonoids with bovine serum albumin: a fluorescence quenching study. *Journal of Agricultural and Food Chemistry* 2005; **53**: 158.
74. Edelmann A, Lendl B. Toward the optical tongue: flow-through sensing of tanninprotein interactions based on FTIR spectroscopy. *Journal of the American Chemical Society* 2002; **124**: 14741.

75. Llaudy MC, Canals R, Canals JM, Rozes N, Arola L, Zamora F. New method for evaluating astringency in red wine. *Journal of Agricultural and Food Chemistry* 2004; **52**: 742.
76. Jobstl E, Howse JR, Fairclough JPA, Williamson MP. Noncovalent cross-linking of casein by epigallocatechin gallate characterized by single molecule force microscopy. *Journal of Agricultural and Food Chemistry* 2006; **54**: 4077.
77. Jobstl E, O'Connell J, Fairclough JPA, Williamson MP. Molecular model for astringency produced by polyphenol/protein interactions. *Biomacromolecules* 2004; **5**: 942.
78. Laborde B, Moine-Ledoux V, Richard T, Saucier C, Dubourdieu D, Monti JP. PVPP polyphenol complexes: a molecular approach. *Journal of Agricultural and Food Chemistry* 2006; **54**: 4383.
79. Richard T, Lefeuvre D, Descendit A, Quideau S, Monti JP. Recognition characters in peptide-polyphenol complex formation. *Biochimica et Biophysica Acta* 2006; **1760**: 951.
80. Verge S, Richard T, Moreau S, Richelme-David S, Vercauteren J, Prome J-C, Monti JP. First observation of noncovalent complexes for a tannin-protein interaction model investigated by electrospray ionisation mass spectroscopy. *Tetrahedron Letters* 2002; **43**: 2363.
81. Sarni-Manchado P, Cheynier V. Study of non-covalent complexation between catechin derivatives and peptides by electrospray ionization mass spectrometry. *Journal of Mass Spectrometry* 2002; **37**: 609.
82. Thorngate JH, Noble AC. Sensory evaluation of bitterness and astringency of 3R(−)-epicatechin and 3S(+)-catechin. *Journal of the Science of Food and Agriculture* 1995; **67**: 531.
83. Kallithraka S, Bakker J, Clifford MN. Evaluation of bitterness and astringency of (+)-catechin and (−)-epicatechin in red wine and in model solution. *Journal of Sensory Studies* 1997; **12**: 25.
84. Vidal S, Francis L, Kwiatkowski M, Gawel R, Waters EJ, Guyot S, Marnet N, Cheynier V. The mouth-feel properties of grape and apple proanthocyanidins in a wine-like medium. *Journal of the Science of Food and Agriculture* 2003; **83**: 564.
85. Preys S, Mazerolles G, Courcoux P, Samson A, Fischer U, Hanafi M, Bertrand D, Cheynier V. Relationship between polyphenolic composition and some sensory properties in red wines using multiway analyses. *Analytica Chimica Acta* 2006; **563**: 126.
86. Vidal S, Francis L, Noble A, Kwiatkowski M, Cheynier V, Waters E. Taste and mouth-feel properties of different types of tannin-like polyphenolic compounds and anthocyanins in wine. *Analytica Chimica Acta* 2004; **513**: 57.
87. Simon C, Barathieu K, Laguerre M, Schmitter JM, Fouquet E, Pianet I, Dufourc EJ. Three-dimensional structure and dynamics of wine tannin-saliva protein complexes. A multitechnique approach. *Biochemistry* 2003; **42**: 10385.
88. Fowles. *Analytical Mechanics*. Holt, Rinehart & Winston: Toronto, 1962; 148.
89. RDLevine GR, Berstein RB. *Molecular Reaction Dynamics and Chemical Reactivity*. Oxford University Press: New York, 1987; 36.
90. Belgacem O, Bowdler A, Brookhouse I, Brancia FL, Raptakis E. Dissociation of biomolecules using a ultraviolet matrix-assisted laser desorption/ionisation time-of-flight/curved field reflectron tandem mass spectrometer equipped with a differential-pumped collision cell. *Rapid Communications in Mass Spectrometry* 2006; **20**: 1653.
91. Meyer M. Ab initio study of flavonoids. *International Journal of Quantum Chemistry* 2000; **76**: 724.
92. Zhang Y. Ab initio study on the anti-HIV activities of hydroxylflavones. *Chinese Journal of Structural Chemistry* 2005; **24**: 462.
93. Mantas A, Derety E, Ferretti FH, Estrada M, Czismadia IG. Ab initio conformational analysis of flavone and related compounds. *Journal of Molecular Structure (Theochem)* 2000; **504**: 77.
94. Codorniu-Herna'ndez E, Mesa-Ibirico A, Montero-Cabrera LA, Marti'nez-Luzardo F, Stohrer W-D. MO-calculations on the solvation effects on the structure of natural flavonoids in aqueous and acetone phases. *Journal of Molecular Structure (Theochem)* 2005; **715**: 227.
95. Lewars EG, March RE. Fragmentation of 3-hydroxyflavone; a computational and mass spectrometric study. *Rapid Communications in Mass Spectrometry* 2007; **21**: 1669.
96. Montgomery JA Jr, Frisch MJ, Ochterski JW, Petersson GA. A complete basis set model chemistry. VII. Use of the minimum population localization method. *Journal of Chemical Physics* 2000; **112**: 6532.
97. Frisch MJ, Trucks GW, Schlegel HB, Scuseria GE, Robb MA, Cheeseman JR, Montgomery JA Jr, Vreven T, Kudin KN, Burant JC, Millam JM, Lyengar SS, Tomasi J, Barone V, Mennucci B, Cossi M, Scalmani G, Rega N, Petersson GA, Nakatsuji H, Hada M, Ehara M, Toyota K, Fukuda R, Hasegawa J, Ishida M, Nakajima T, Honda Y, Kitao O, Nakai H, Klene M, Li X, Knox JE, Hratchian HP, Cross JB, Adamo C, Jaramillo J, Gomperts R, Stratmann RE, Yazyev O, Austin AJ, Cammi R, Pomelli C, Ochterski JW, Ayala PY, Morokuma K, Voth GA, Salvador P, Dannenberg JJ, Zakrzewski VG, Dapprich S, Daniels AD, Strain MC, Farkas O, Malick DK, Rabuck AD, Raghavachari K, Foresman JB, Ortiz JV, Cui Q, Baboul AG, Clifford S, Cioslowski J, Stefanov BB, Liu G, Liashenko A, Piskorz P, Komaromi I, Martin RL, Fox DJ, Keith T, Al-Laham MA, Peng CY, Nanayakkara A, Challacombe M, Gill PMW, Johnson B, Chen W, Wong MW, Gonzalez C, Pople. *Gaussian 03, Revision B.05*. Gaussian: Pittsburgh, 2003.
98. JAPople JA. Molecular orbital methods in organic chemistry. *Accounts of Chemical Research* 1970; **3**: 217.
99. Shao Y, Head-Gordon M, Krylov AI. The spin−flip approach within time-dependent density functional theory: theory and applications to diradicals. *Journal of Chemical Physics* 2003; **118**: 4807.
100. Gräfenstein J, Kraka E, Filatov M, Cremer D. Can unrestricted density-functional theory describe open shell singlet biradicals? *International Journal of Molecular Sciences* 2002; **3**: 360.
101. Cremer D, Filatov M, Polo V, Kraka E, Shaik S. Implicit and explicit coverage of multi-reference effects by density functional theory. *International Journal of Molecular Sciences* 2002; **3**: 604.
102. Gräfenstein J, Cremer D. On the diagnostic value of S[sup 2] in Kohn-Sham density functional theory. *Molecular Physics* 2001; **99**: 981.
103. Gräfenstein J, Hjerpe AM, Kraka E, Cremer D. An accurate description of the bergman reaction using restricted and unrestricted DFT: stability test, spin density, and on-top pair density. *Journal of Physical Chemistry A* 2000; **104**: 1748.
104. Foresman JB, Frisch A. *Exploring Chemistry with Electronic Structure Methods*, 2nd ed, Chapter 4. Gaussian: Pittsburgh, 1996.
105. Blanksby SJ, Ellison GB. Bond dissociation energies of organic molecules. *Accounts of Chemical Research* 2003; **36**: 255, Table 2.
106. Budzianowski J, Morozowska M, Wesolowska M. Lipophilic flavones of Primula veris L. from field cultivation and in vitro cultures. *Phytochemistry* 2005; **66**: 1033.
107. Blasko G, Xun L, Cordell GA. Studies in the Thymelaeaceae, V. 2′-hydroxyflavone from *Daphnopsis sellowiana*: isolation and synthesis. *Journal of Natural Products* 1988; **51**: 60.
108. Kim H, Moon BH, Ahn JH, Lim Y. Complete NMR signal assignments of flavonol derivatives. *Magnetic Resonance in Chemistry* 2006; **44**: 188.
109. Biekofsky RR, Buschi CA, Pomilio AB. Conformational analysis of 5,6,7-trisubstituted flavones: ^{13}C NMR and molecular mechanics study. *Magnetic Resonance in Chemistry* 1991; **29**: 569.
110. Aksnes DW, Standnes A, Andersen OM. Complete assignment of the ^{1}H and ^{13}C NMR spectra of flavone and its A-ring hydroxyl derivatives. *Magnetic Resonance in Chemistry* 1996; **24**: 820.

111. Zhou X, Peng J, Fan G, Wu Y. Isolation and purification of flavonoid glycosides from *Trollius ledebouri* using high-speed counter-current chromatography by stepwise increasing the flow-rate of the mobile phase. *Journal of Chromatography A* 2005; **1092**: 216.
112. Wawer I, Zielinska A. ^{13}C CP/MAS NMR studies of flavonoids. *Magnetic Resonance in Chemistry* 2001; **39**: 374.
113. Borges C, Martinho P, Martins A, Rauter AP, Almoster Ferreira MA. Structural characterisation of flavonoids and flavonoid-*O*-glycosides extracted from *Genista tenera* by fast-atom bombardment tandem mass spectrometry. *Rapid Communications in Mass Spectrometry* 2001; **15**: 1760.
114. Hansen SH, Jensen AG, Cornett C, Bjørnsdottir I, Taylor S, Wright B, Wilson ID. High-performance liquid chromatography on-line coupled to high-field NMR and mass spectrometry for structure elucidation of constituents of *Hypericum perforatum* L. *Analytical Chemistry* 1999; **71**: 5235.
115. Lommen A, Godejohann M, Venema DP, Hollman PCH, Spraul M. Application of directly coupled HPLC-NMR-MS to the identification and confirmation of quercetin glycosides and phloretin glycosides in apple peel. *Analytical Chemistry* 2000; **72**: 1793.
116. Exarchou V, Godejohann M, van Beek TA, Gerothanassis IP, Vervoort J. LC-UV-solid-phase extraction-NMR-MS combined with a cryogenic flow probe and its application to the identification of compounds present in Greek oregano. *Analytical Chemistry* 2003; **75**: 6288.
117. Wolfender J-L, Ndjoko K, Hostettmann K. Liquid chromatography with ultraviolet absorbance–mass spectrometric detection and with nuclear magnetic resonance spectroscopy: a powerful combination for the on-line structural investigation of plant metabolites. *Journal of Chromatography A* 2003; **1000**: 437.
118. Švehlíková V, Bennett RN, Mellon FA, Needs PW, Piacente S, Kroom PA, Bao Y. Isolation, identification and stability of acylated derivatives of apigenin-7-O-glucoside from chamomile (Chamomilla recutita [L.] Rauschert). *Phytochemistry* 2004; **65**: 2323.
119. Park Y, Moon BH, Lee E, Lee Y, Yoon Y, Ahn JH, Lim Y. ^{1}H and ^{13}C-NMR data of hydroxyflavone derivatives. *Magnetic Resonance in Chemistry* 2007; **45**: 674.
120. Mattoli L, Cangi F, Maidecchi A, Ghiara C, Ragazzi E, Tubaro M, Stella L, Tisato F, Traldi P. Metabolomic fingerprinting of plant extracts. *Journal of Mass Spectrometry* 2006; **41**: 1534.
121. Shahat AA, Cuyckens F, Wang W, Abdel-Shafeek KA, Husseiny HA, Apers S, Van Miert S, Pieters L, Vlietinck AJ, Claeys M. Structural characterization of flavonol di-O-glycosides from *Farsetia aegyptia* by electrospray ionization and collision-induced dissociation mass spectrometry. *Rapid Communications in Mass Spectrometry* 2005; **19**: 2172.
122. Ewing DF. ^{13}C substitutive effects in mono-substituted benzenes. *Magnetic Resonance in Chemistry* 1979; **12**: 499.
123. Seetharman J, Rajan SS. Structure of 2′-hydroxyflavone. *Zeitschrift fur Kristallograhie* 1995; **210**: 104.
124. Seetharman J, Rajan SS. Structure of 6-hydroxyflavone. *Acta Crystallographica* 1992; **C48**: 1714.
125. Shoja M. 5-Hydroxyflavone. *Acta Crystallographica* 1990; **C46**: 517.
126. Shoja M, Yen MW, Peterson L. The crystal structure of 6-hydroxyflavone, $C_{15}H_{10}O_3$. *Zeitschrift fur Kristallograhie* 1998; **213**: 729.
127. Kumar S, Ramanathan T, Subramanian K, Steiner T. Crystal and molecular structure of 7-hydroxyflavone monohydrate, $C_{14}H_{10}O_3 \cdot H_2O$. *Journal of Chemical Crystallography* 1998; **28**: 931.
128. Burns DC, Ellis DA, March RE. A predictive tool for assessing ^{13}C NMR chemical shifts of flavonoids. *Magnetic Resonance in Chemistry* 2007; **45**: 835.
129. Ibrahim A-L, Abul-Hajj YJ. Microbiological transformation of chromone, chromanone, and ring A hydroxyflavones. *Journal of Natural Products* 1990; **53**: 1471.
130. Moon B-H, Lee Y, Ahn J-H, Lim Y. Complete assignment of ^{1}H and ^{13}C NMR data of dihydroxyflavone derivatives. *Magnetic Resonance in Chemistry* 2006; **44**: 99.
131. Park Y, Lee Y-U, Kim H, Lee Y, Yoon Y-A, Moon B, Chong Y, Ahn J-H, Shim Y-H, Lim Y. NMR data of flavone derivatives and their anti-oxidative activities. *Bulletin of the Korean Chemical Society* 2006; **27**: 1537.
132. https://scifinder.cas.org. Last accessed in [2007].
133. March RE, Burns DC, Ellis DA. Empirically-predicted ^{13}C NMR chemical shifts for 8-hydroxyflavone starting from 7,8,4′-trihydroxyflavone and 7,8-dihydroxyflavone. *Magnetic Resonance in Chemistry* 2008; **46**: 680.
134. Rauha JP, Vuorela H, Kostiainen R. Effect of eluent on the ionization efficiency of flavonoids by ion spray, atmospheric pressure chemical ionization, and atmospheric pressure photoionization mass spectrometry. *Journal of Mass Spectrometry* 2001; **36**: 1269.
135. Herrero-Martínez J-M, Sanmartin M, Rosés M, Bosch E, Ràfols C. Determination of dissociation constants of flavonoids by capillary electrophoresis. *Electrophoresis* 2005; **26**: 1886.

DOI: 10.1002/jms